A MICROMECHANICAL APPROACH TO THE BEHAVIOUR OF SINGLE WOOD FIBERS AND WOOD FRACTURE AT CELLULAR LEVEL

Marjan SEDIGHI GILANI

M.Sc. in Civil Engineering, Marine Structures, University of Tehran, Iran
et de nationalité iranienne

EPFL
ÉCOLE POLYTECHNIQUE
FÉDÉRALE DE LAUSANNE

Lausanne, EPFL
2006

Abstract

Mechanical and fracture behaviors of wood are defined by the morphology and mechanical properties of wood fibers and their bonding medium. Parallel orientation of wood fibers makes them the most influential microstructural elements from the mechanical point of view. On the other hand, in wood fracture, the difference between the properties of fiber and bonding medium (which make weak cleavage plates) plays a more important role. Experiments show that the mechanical behavior of a single wood fiber under axial tension is complex, although the cause of this complexity has still not been clearly understood. In this thesis, in order to explain the mechanism underlying the mechanical behavior of wood fibers and the fracture of wood specimens at fiber level, a micromechanical approach has been used.

Confocal laser scanning microscopy was used to investigate the pattern of the distribution of microfibrils in different wood fibers. It was shown that the microfibril angle within a single fiber is non-uniform and this non-uniformity in radial walls of earlywood fibers, which contain the bordered pits, is higher than tangential walls of earlywood fibers and also higher than in latewood fibers.

Tensile and cyclic tensile tests on single spruce fibers were carried out and their non-linear and force-history dependent behaviors under axial tension were shown. It was found that the fiber behavior is affected by the range of microfibril angle non-uniformities and other defects. After a certain force limit, wood fiber undergoes irreversible strains and the elastic limit of the fiber increases in the tensile loading. To explain these results, a model based on the assumption of helical and non-uniform distribution of cellulose microfibrils in the fiber and damage of the hemicellulose and lignin matrix after yielding, was proposed. The model indicated that multi-damage and evolution of microfibrils in the damages segments are the main governing mechanisms of the tensile behavior of wood fiber.

Difficulties of considering the porous and heterogeneous microstructure of wood in a continuum-based fracture model, led us to develop a mixed lattice-continuum model. The three-dimensional geometry of lattice, composed of different beam elements which represent the bonding medium and alternation of earlywood and latewood fibers, enabled us to

detect the propagation of cracks in both cross sections and longitudinal sections at the fiber level. Model showed that in Mode I fracture, parallel to the fibers, the location of the developed crack and the resulting stress-strain curves have a good agreement with the experimental evidence.

Résumé

Les comportements mécaniques et la rupture du bois sont définis par la morphologie et les propriétés mécaniques des fibres de bois et leur medium de liaison. Le parallélisme des fibres de bois fait de ces dernières les éléments les plus influents du point de vue mécanique. D'un autre côté, en ce qui concerne la rupture du bois, la différence entre les propriétés des fibres et leur medium de liaison (celui-ci étant responsable des plaques de fendage) joue un rôle plus important. Les expériences montrent que le comportement d'une fibre unique de bois sous traction uniaxiale est complexe, de plus son origine reste encore relativement incomprise. Dans le cadre de cette thèse, une approche micromécanique a été utilisée afin d'expliquer le mécanisme sous-jacent du comportement mécanique des fibres de bois et de la rupture d'échantillons de bois à l'échelle de la fibre.

La microscopie confocale à balayage laser a été utilisée pour étudier le motif de distribution des microfibrilles de diverses fibres de bois. Il a été montré que l'angle des microfibrilles pour une fibre unique n'est pas uniforme. De plus, cette non-uniformité dans les parois radiales de fibres de bois de printemps, comprennent des ponctuations auréolées, est plus importante que dans les fibres de bois d'été et que dans les parois tangentielles des fibres de bois de printemps.

Des tests de traction ainsi que des tests de tractions cycliques sur des fibres isolées de sapin ont été entrepris et leur comportement non-linéaire ainsi que leur dépendance de l'histoire des déformations ont pu être démontrés. Il a également été montré que le comportement d'une fibre est affecté par la gamme de distributions non-uniformes des angles de microfibrilles ainsi que par d'autres effets annexes. Au-delà d'une certaine force limite, les fibres subissent des déformations irréversibles et la limite élastique de la fibre augmente en traction uniaxiale. Afin d'expliquer ces résultats, un modèle basé sur une distribution hélicoïdale et non-uniforme de la cellulose des microfibrilles dans la fibre ainsi que sur les endommagements de l'hémicellulose et de la lignine après le seuil d'écoulement, a été proposé. Le modèle indique que de multiples endommagements accompagnés d'une évolution des microfibrilles dans les segments endommagés sont les principaux mécanismes gouvernant le comportement en traction des fibres de bois.

Les difficultés concernant la porosité et l'hétérogénéité de la microstructure du bois pour un modèle de rupture en milieu continu nous ont conduits à développer un modèle couplé d'une approche en milieu continu et d'un réseau. La géométrie tridimensionnelle du réseau, ce dernier étant composé de différents rayons représentant le medium de liaison et l'alternance entre fibres de bois de printemps et d'été, nous a permis de détecter la propagation de fissures sur les sections transverse et longitudinale à l'échelle de la fibre. Le modèle montre, pour la rupture en Mode I, parallèle aux fibres, que la localisation des fissures de même que les courbes de contrainte-déformation sont en accord avec les évidences expérimentales.

Mots-clés : fibre de bois, angle de microfibrilles, approche micromécanique, rupture, réseau, modèle couplé.

Acknowledgment

This thesis is the outcome of a wonderful four years experience at the constructions materials laboratory (LMC) in Ecole Polytechnique Fédéral de Lausanne (EPFL). I would like to express my deep gratitude to a number of people that I had the chance to meet during this period.

I am deeply thankful to Doctor P. Navi, the director of my thesis, who introduced me to the astonishing world of the wood science. I thank him for his availability, his continues support and guidance and his patience in reading and correcting my articles and thesis manuscript.

I sincerely thank Professor K. Scrivener, head of the constructions materials laboratory for giving me the opportunity to carry out this research in her laboratory and for her support.

I would like to acknowledge Professor P. Morlier, Professor A. Mortensenm and Professor P. Niemz, who honored me by accepting to review and evaluate this thesis and Professor H.J. Mathieu for accepting to be the president of my PhD thesis jury.

I thank Dr. H. Sunderland for her guidance in working with CLSM and also for her encouragement and friendship. I also thank Mr. P. Vulliemin, our ingenious technician, for the design and implementation of the tensile testing mini-press, Mr. D. Anguish who patiently helped me with my early experiences in UNIX system and Mr. M. Mahzari for being always available to answer my questions on FEM.

My outmost gratitude goes to all my colleagues and friends in constructions materials laboratory for providing a dynamic and amicable environment. I warmly thank Tibor for the time he spent to edit the English of this thesis, Amor, Cyrille, Frédéric, Nicola, Patrick, and Shashank for our insightful discussions and Mercedes, Ines, Julien, Prakash, Xinyu, Emmanuel, Michel, Philippe, Lionel, Vanessa, Janine, Laurence, Hélène, Séverine, Mohsen, Rodrigo, Andreas, Aude, Christophe, Gwenn, Silvia and Antonino for the great time we spent together.

I would like to express my deepest gratitude to my family. I thank Arash, for his care, encouragement and love and I am grateful to my parents, Mahine and Naser and my two

amiable sisters that all achievements in my life would be impossible without their sympathy and support.

Contents

List of figures

Lift of tables

Chapter 1 Introduction

1.1 Background

Wood has been an important construction material since humans began building shelters. Even today, the unique properties of wood such as lightness and strength, renewability, environmental benefits, abundance and versatility make it prevalent as a construction material and as a material resource for paper and wood particle-based industries.

The problem in using this bio-polymeric composite is the complexity of its physical and mechanical properties. This complexity originates from different sources such as the parallel oriented form of the wood fibers, heterogeneity in the structure from micro to macro level and variation of properties of constituents with humidity and temperature changes.

Mechanical and fracture behaviors of wood are defined by the morphology and mechanical properties of its structural elements at micro-level, wood fibers and their bonding medium. Parallel orientation of wood fibers and their higher mechanical properties comparing to the bonding medium, make the fibers the most influential microstructural elements from the mechanical point of view. On the other hand, the difference between the properties of fiber and the bonding medium, by making the weak planes, plays more important role in wood fracture.

Dominant influences of mechanical properties and morphology of wood fiber on both mechanical and fracture behaviors of wood, make it the subject of interest for many scientific researchers working in different domains: fibers anatomy, chemistry, physics and mechanics, for the last fifty years. Wood fibers have different morphologies and properties, even in one wood specimen: earlywood and latewood, juvenile and mature wood, normal and compression wood fibers. The multilayer walls of wood fibers composed of cellulose crystalline chains (microfibril), which are helically located in a matrix of hemicellulose and lignin. Formation and properties of these constituents define the mechanical properties of wood fibers. The angle between the orientation of cellulose microfibrils and the longitudinal axis of wood fiber, microfibril angle, as well as pits, cross-field zones and defects in the fiber structure have important influences on the mechanical properties of wood fibers. Because of the

important role of the orientation of microfibrils, studies about microfibril angle and its probable variation have always been an important research subject. However, the definitive pattern of microfibrils distribution in a wood fiber, in spite of much improvement of experimental facilities is still unclear.

The existing mechanical models can explain the behavior of wood fiber only in the elastic zone, although the experiments show that the behavior of different single wood fibers under tensile test is complex, with different slope of stress-strain curves after yielding. In spite of a number of mechanical tests on single wood fibers, the mechanism of their complex tensile behavior has not been properly understood and the causes of this complexity are rarely discussed. The problem is that observation of what underlies the structural evolution of small single wood fibers in tensile test by means of microscopy is not yet possible. Consequently, modeling tools should be coupled with experiments to explain, using a *micromechanical approach,* the mechanism underlying the wood fibers behavior in tension.

The fracture of wood, similar to its mechanical behavior, is influenced by its porous fibrous structure and different heterogeneities at different levels. For a long time, these influences have been studied by implementing different methods like fracture tests, microscopic observation of fractured surface and modeling. Different experimental results indicated the predominant influences of lower mechanical properties of the bonding medium compared to the fibers, alternation of earlywood and latewood fibers with different characteristics and other heterogeneities like rays and fiber defects on wood fracture. In the modeling domain, despite the significant progress in computing power, application of fracture mechanics to wood fracture still remains a difficult problem. The continuum-based fracture models have not been successful in confirming the major observed phenomena in microscopic studies and experiments, as introducing the porous structure and heterogeneities of wood to them is still difficult. In contrast to continuum-based fracture model, the potential of morphology-based model, i.e. *lattice-model* to consider the heterogeneous and porous nature of wood, makes it an appropriate approach to study the wood fracture at fiber level.

1.2 Objectives of the study

The main aim of this thesis is to study and explain the tensile behavior of single wood fibers as the main structural elements of wood together with the fracture behavior of small wood specimens at fiber level. For this purpose, a research program with two following main parts was designed to:

(1) Investigate the behavior of single wood fibers under axial tension, in relation to their microstructural heterogeneities.

(2) Investigate the fracture parallel to the fibers of wood at the fiber level, considering its porous and heterogeneous structure.

The main objectives in the first part are the analysis of the behaviors of different single wood fibers under tension, in relation to the type and morphology of the fibers and modeling these observed behaviors. For this purpose, gaining more insight into the microstructure and anatomy of single fibers is the first step. Variation of local microfibril angle, by changing the local properties of a single wood fiber, could dominate its effective properties and behavior. Consequently a detailed study for understanding the pattern of distribution of microfibrils in different zones of a wood fiber is the other objective.

In the second part, the objective is to investigate the fracture behavior parallel to the fibers of a small wood specimen at the fiber level. The developed model for this purpose should be able to consider the fibrous porous structure of wood with different heterogeneities like seasonal alternation of wood fibers and defects.

The applied methodology in both parts is a combined experimental and modeling approach.

1.3 Thesis content

In the chart given in Figure 1-1, the different chapters of this thesis are illustrated. The study is divided into two main parts. The main focus in the first part, which includes chapters 3, 4 and 5, is to investigate (experiment and modeling) the mechanical behavior of single wood fibers under axial tension. In the second part of the study, which includes chapters 6 and 7, the process of wood fracture at fiber level is investigated.

Chapter 1: this chapter is an introduction to the study.

Chapter 2: in this chapter a short introduction to the microstructure of wood and wood fibers is presented.

Chapter 3: the results of a detailed study about microfibril angle and extend and pattern of its variation in different single wood fibers are presented. In this study, the measured local microfibril angles in different parts of earlywood, latewood and compression wood fibers are compared to the existing results in literature.

Chapter 4: first the process of preparing the samples of single wood fibers for tensile tests and method to perform the tensile tests on these samples are explained and then the results obtained from tensile tests and cyclic tensile tests for different fibers are demonstrated. Stress-strain curves of fibers with different types are compared and the effect of microfibril angle variation on the fiber behavior is discussed.
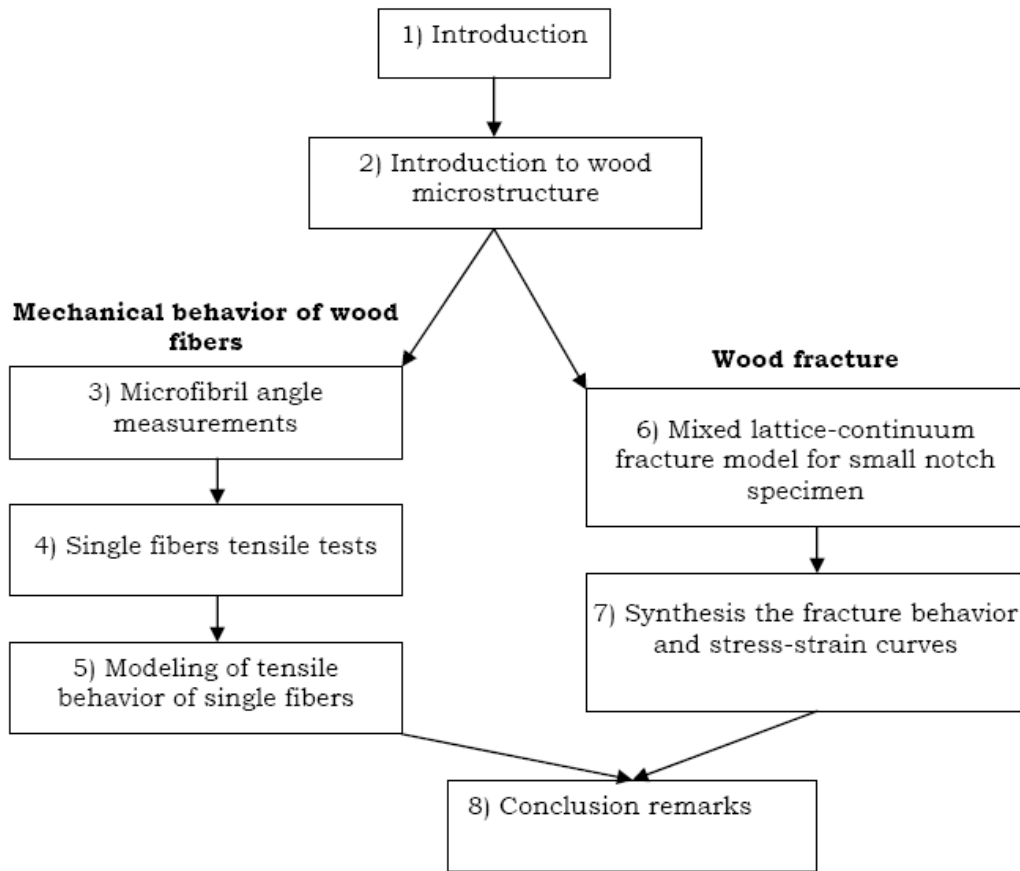
Figure 1-1 Illustration of thesis structure

Chapter 5: the developed model to explain the experimental observations in tensile tests and cyclic tensile tests is presented. Using this model, the effect of within fiber non-uniformities of microfibril angle on damage initiation is explained and different mechanisms, which might underlie the wood fibers behavior after the yield point, are discussed.

Chapter 6: the assumptions and requirements for developing a three-dimensional mixed lattice-continuum model to investigate the wood fracture at fiber level are explained. The goal is modeling the parallel to the fibers fracture in a small wood specimen in direct tension fracture test while the geometry represents the wood microstructure. To this end, by introducing the most dominant features of wood microstructure to model, the closest geometry to wood morphology with the minimum number of elements is constructed.

Chapter 7: the results of simulating the fracture in a small wood specimen in direct tension fracture test by using the developed model are presented. The obtained stress-deformation curve and the crack pattern which are presented in this chapter are compared to the experimental results gain from literature.

Chapter 8: finally, the general conclusion derived from this research work and suggestions for future work are given in chapter 8.

Chapter 2   A short introduction to wood and wood fibers microstructure

2.1 Stem anatomy

In Figure 2-1 a typical cross section of a tree stem is shown. Pith is the primary tissue at the center of the stem cylinder. In the darker portion of the stem which is called heartwood, cells are dead even in a live tree while in the outer lighter colored portion which is called sapwood they are partly alive.

Heartwood and sapwood together make the wood (Xylem). Cambium is a narrow layer of cells located between the wood and inner bark, which is capable of producing the wood cells.
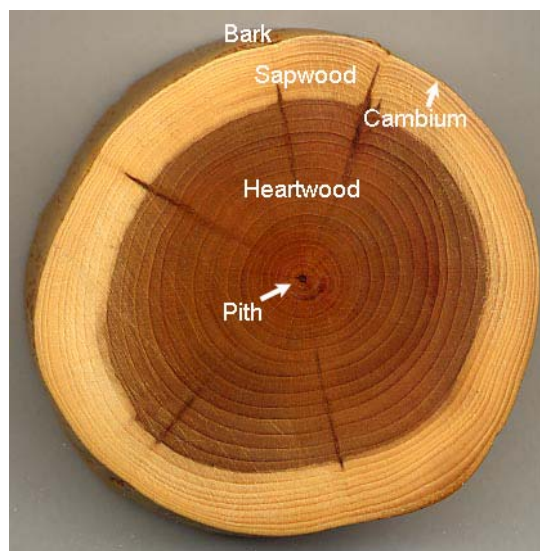
Figure 2-1 cross section of a tree trunk[1]

---

[1] Photo was picked from Wikipedia, the free online encyclopedia http://wikipedia.org/ .

2.1.1 Wood juvenility and maturity

In the first years of growth, the tree produces juvenile wood, a zone of wood extending outward from the pith. Later, wood characteristics are improved until they become relatively constant and make mature wood. Juvenile wood is characterized by thin cell walls, short tracheids with large lumens and lower strength and stiffness compared to mature wood (Macdonald and Hubert 2002). In Figure 2-2 the schematic locations of juvenile and mature wood in the tree stem are shown.
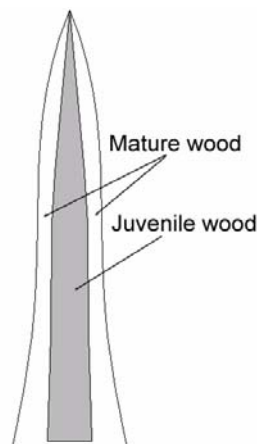
Figure 2-2 Schematic representation of juvenile and mature wood locations in tree stem

2.1.2 Growth rings

During each growing season a new layer of wood (growth from cambium) is formed over the tree stem, which is called a growth ring. Wood layers produced in spring and summer have different colors and densities which let the growth rings be recognized even without a microscope (see Figure 2-3). Produced wood fibers in spring and summer —i.e., earlywood and latewood fibers have many microstructural differences which are reviewed in section 2.3.2.
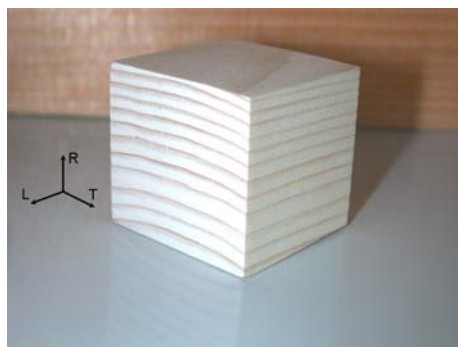
Figure 2-3 Alternation of earlywood (lighter color) and latewood (darker color) on a spruce cubic sample; R, T and L are the radial, tangential and longitudinal directions, respectively

2.2 Wood classification

Trees are classified into two main groups, softwoods (narrow leaf trees) and hardwoods (broad leaf trees). The major difference between the anatomy of hardwoods and softwoods is the lack of vessels in softwood. Vessels are created to conduct the fluid in the tree trunk. In softwood, the longitudinal tracheids perform the role of conducting the fluid (Wangaard 1979). In Figure 2-4 the cross sectional views of two hardwood and softwood specimens are shown.
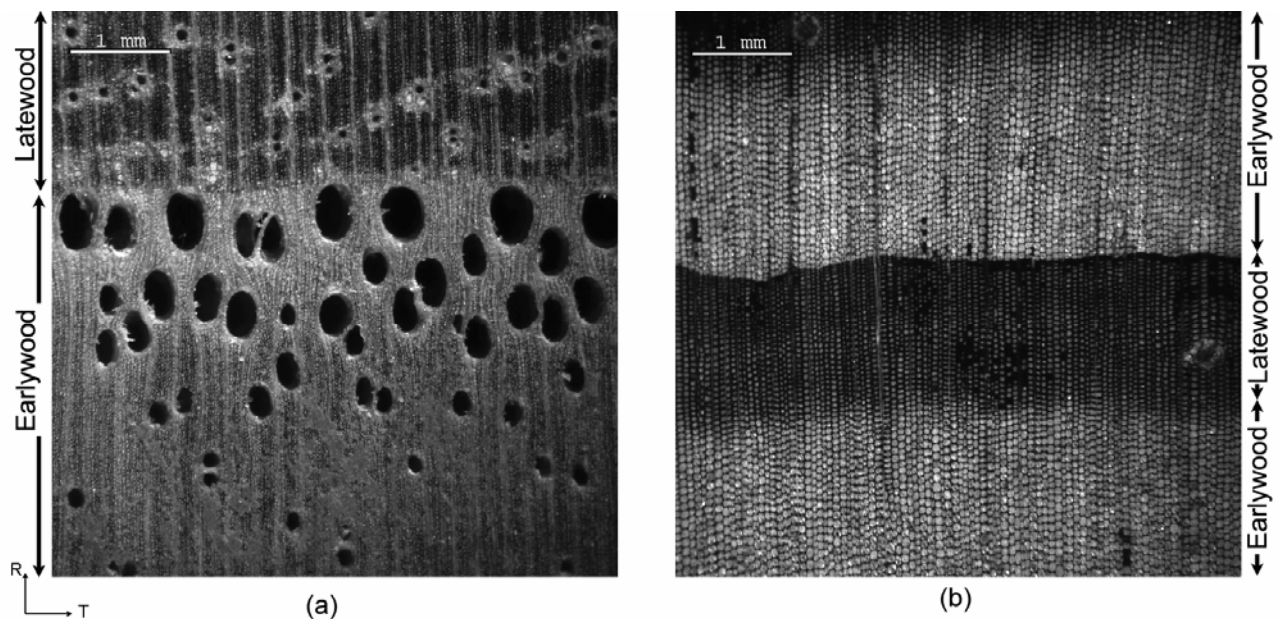
Figure 2-4 Structural differences between hardwood and softwood; (a) visible longitudinal vessels in oak (hardwood) are larger in earlywood than latewood, (b) alternation of earlywood and latewood tracheids in spruce (softwood)

In this thesis, because of the simpler structure of softwood comparing to hardwood, only softwood and softwood tracheids were used and everywhere the term of *wood fiber* is used, it is referenced to wood tracheid.

2.3 Softwood microstructure

The two main types of cells in softwood are fibers and transversal parenchyma which stores the food. Structure and properties of these elements highly affect the mechanical properties of wood. Wood fibers are the tubular cells, with a length of between 0.5-4 mm and diameter of between 20-50 μm. *Lumen* is the space or void enclosed by the walls of a fiber. In this part some microstructural aspects of softwood fibers such as their multilayer formation, chemical constituents, and structural differences between earlywood and latewood fibers, pits and rays are reviewed.

2.3.1 Layers and constituents of wood fiber wall

Figure 2-5 illustrates the layered structure of a softwood fiber. Wood fiber wall has generally one primary layer (P layer) and a set of secondary layers (S_1, S_2 and S_3 layers). Each fiber is separated from its neighbors by an intercellular substance called middle lamellae. As middle lamellae are difficult to distinguish from the primary wall layers, sometime the term *compound middle lamellae* is used for the zone between the secondary walls of neighbor fibers.

The first layer in the secondary wall, adjacent to compound middle lamella, is S1. S2 is the central and thickest secondary wall layer which makes up about 70-80% of the wall thickness (Fengel and Stoll 1973) and S_3 is the thinnest layer adjacent to the fiber lumen.

1 S_3 layer
2 S_2 layer
3 S_1 layer
4 Primary wall
5 Middle lamella
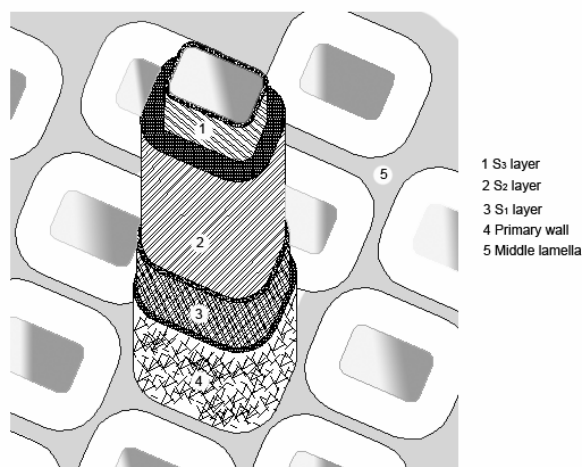
Figure 2-5 Wood fiber wall layers architecture

Each layer of wood fiber wall consists of cellulose crystalline chains (microfibril) which are located in a matrix of hemicellulose and lignin. The volume fractions of different chemical constituents which are different in different wall layers are presented in Table 2-1 (Fengel 1969).

Cell wall layers	Chemical constituents %		
	Cellulose	Hemicellulose	Lignin
Compound middle lamellae	12.5	25.5	62.0
Secondary wall, S_1	34.5	35.5	30.0
Secondary wall, S_2+ S_3	55.7	14.3	30.0

Table 2-1 Percentage of different chemical constituents in different layers of wood fiber wall

The microfibrils width varies from 10 to 30 nm. The angle between the cellulose microfibrils and the fiber longitudinal axis is called the fiber *microfibril angle* (*MFA*). Cellulose microfibrils act as the reinforcing elements of the cell wall structure and deviation of their orientation from the fiber longitudinal axis highly affects the mechanical properties of whole wood fiber. For a long time, it has been considered that the MFA has a random distribution in

primary wall of wood fibers and ordered helical distributions in secondary walls. It was also assumed that MFAs are constant in S_2 layer (10-50° in different earlywood and latewood fibers), crossed in S_1 layer (-80 to 80) and with two or more principal orientations in S_3 layer (-70 to 70°) (Wangaard 1979) (see Figure 2-6).
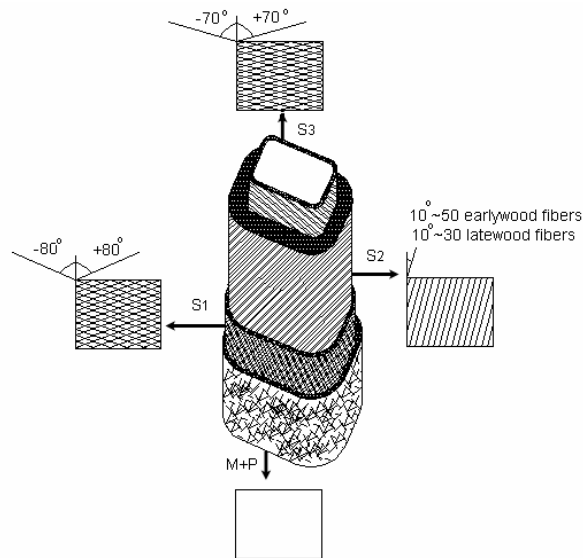
Figure 2-6 schematic diagram of the MFA distribution in different wall layers

From a mechanical point of view, as the S_2 layer is the thickest layer of the wood fiber wall, its MFA is more important than other MFAs and has the most important role in the mechanical properties of whole wood fiber. Microfibrils in the S_2 layer have usually a Z spiral orientation form (see Figure 2-7) and the S spiral orientation of microfibril has been rarely reported (Khalili, Nilsson et al. 2001).
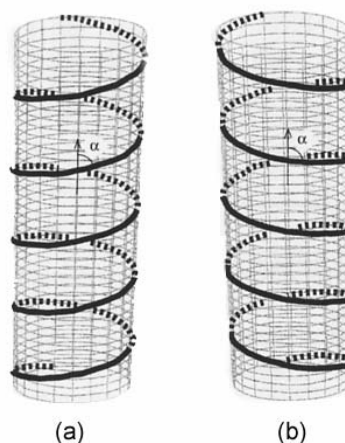
Figure 2-7 Schematic representation of (a) Z spiral microfibril orientation, (b) S spiral microfibrils orientation (Navi 2005)

Because the important role of MFA of S_2 layer, numerous comparative studies have been carried out by several researchers and by using different methods during the last decades to determine the comprehensive pattern of MFAs distribution in S_2 layer. Recent detailed studies of MFA in single wood cells have shown that MFA of S_2 layer could distribute non-uniformly along one wood fiber (Sedighi-Gilani, Sunderland et al. 2005; Sedighi-Gilani, Sunderland et al. 2006).

2.3.2 Microstructural difference between earlywood and latewood fibers

The wood fibers which grow up in summer and spring are called latewood and earlywood fibers respectively and have many microstructural differences.

Latewood fibers possess smaller diameter and thicker walls than earlywood fibers. The fibers are about 20-30 µm in diameter in the latewood and about 30-50 µm in the early-wood. In Figure 2-8, some of the morphological differences between the longitudinal views of two spruce latewood and earlywood such as differences in diameter or the formation of pits are visible.

Pits are the recesses in the cell wall that pemit liquid flow between adjacent fibers. They are called bordered pits when the arches out over the pits membrane. Average diameter of bordered pits is about 16.4 µm in earlywood and about 6.1µm in latewood (Brändström J. 2001). The bordered pits are mostly observed in earlywood fibers (see Figure 2-8-b) and in latewood fibers only the simple pits (see Figure 2-8-a) perform the role of transferring the fluid between the fibers and horizontal rays.

(a)   (b)
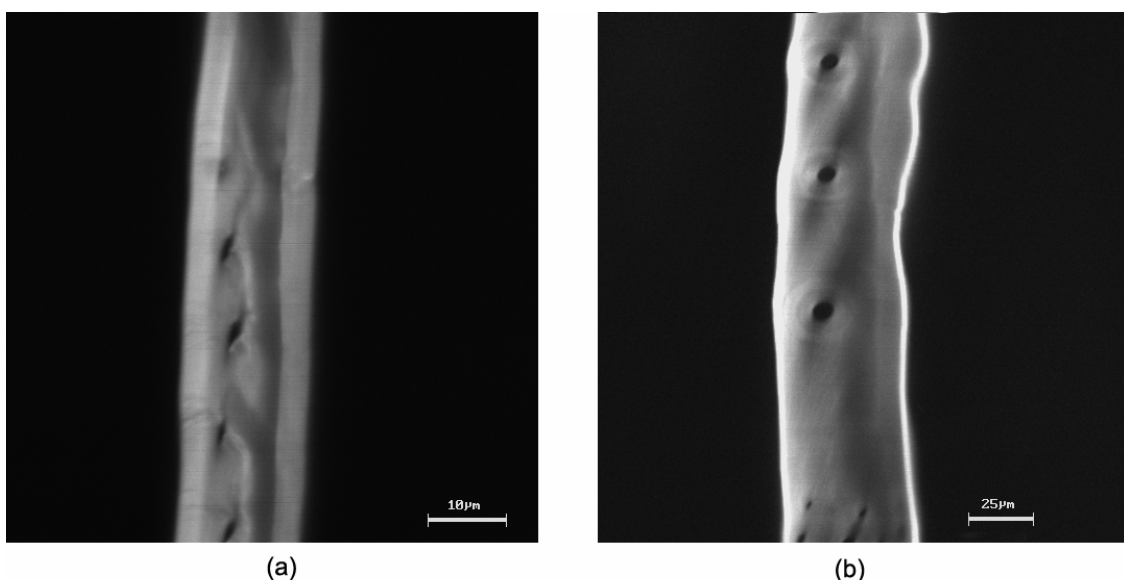
Figure 2-8 Morphology of latewood and earlywood fibers; (a) A latewood fiber with steep narrow simple pits, (b) An earlywood fiber with three bordered pits shown

In Figure 2-9, the differences between cross sectional views of latewood and earlywood fibers are shown. The wall thickness in latewood fibers is more than earlywood fibers.

(a)   (b)
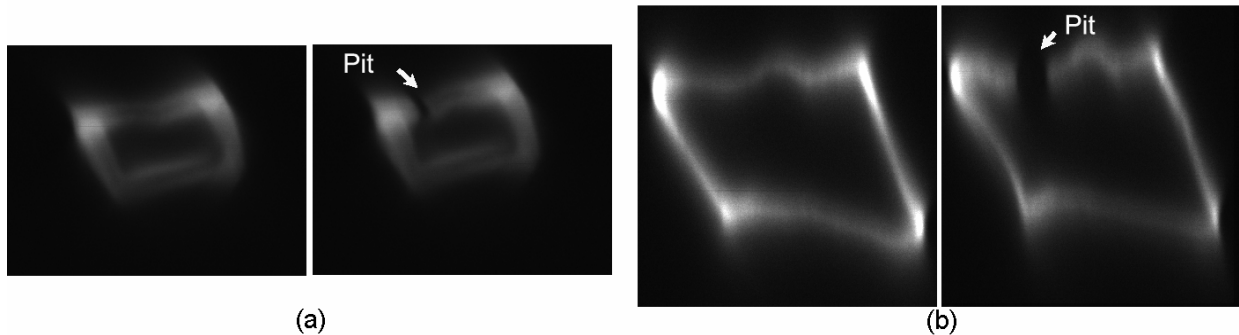
Figure 2-9 Observed earlywood and latewood cross section (RT plane) by confocal laser scanning microscopy; (a) cross sectional images of a latewood fiber, (b) cross sectional image of an earlywood fiber. Pits positions are shown by white arrows

Figure 2-10 shows how the bordered pits look in transversal planes.

As each pit in a cell wall is placed paralled to the other pit in the adjacent cell, liquid can flow from the lumen through the pit aperture of one cell, through the margo[2] portion of the membrane and out the pit aperture into the lumen of the adjacent cell. As this layer is so thin and each preparation for observation and experiment could remove it, it was not presented in Figure 2-10.
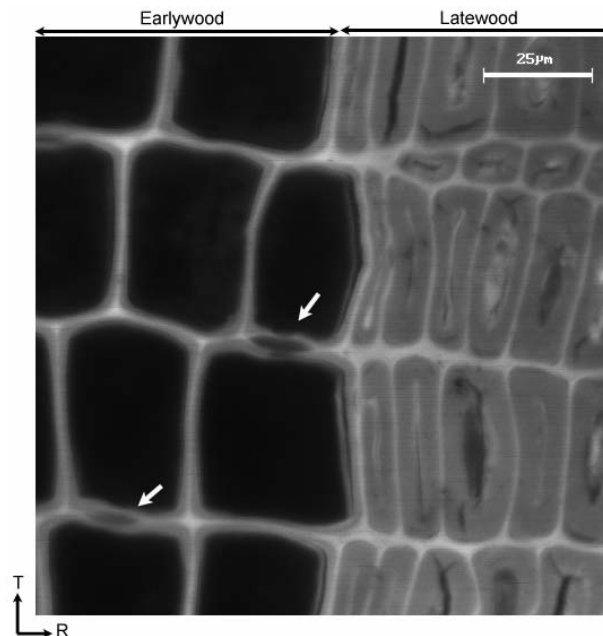
Figure 2-10 Transversal view of bordered pit in radial wall of earlywood fibers are shown by white arrows

---

[2] The thin perforated outer portion of a pit membrane lying between the torus and pit border in softwood bordered pits

2.3.3 Ray and cross-field zone

Wood rays consist of ribbon-like aggregation of food storing cells in all type of wood. They extend in the transverse direction from the bark to the tree center. The wall area between the radial wall of wood fibers and a ray cell is called *cross-field zone*. In this zone, the radial walls are covered with a number of steep narrow simple pits. The orientation of these simple pits has been considered as the mean MFA of whole fiber for a long time (Hiller 1964; Cockrell 1974), although this claim should be verified by using the new achievements in MFA measurement techniques.

In Figure 2-11 cross-field zone on the radial wall of earlywood and latewood fibers are shown. Figure 2-11-a shows some remained walls of a ray cell after cutting the wood chip in radial direction by microtomy. Also in Figure 2-11-b and c, the cross-field zones in an earlywood and latewood fibers are shown.
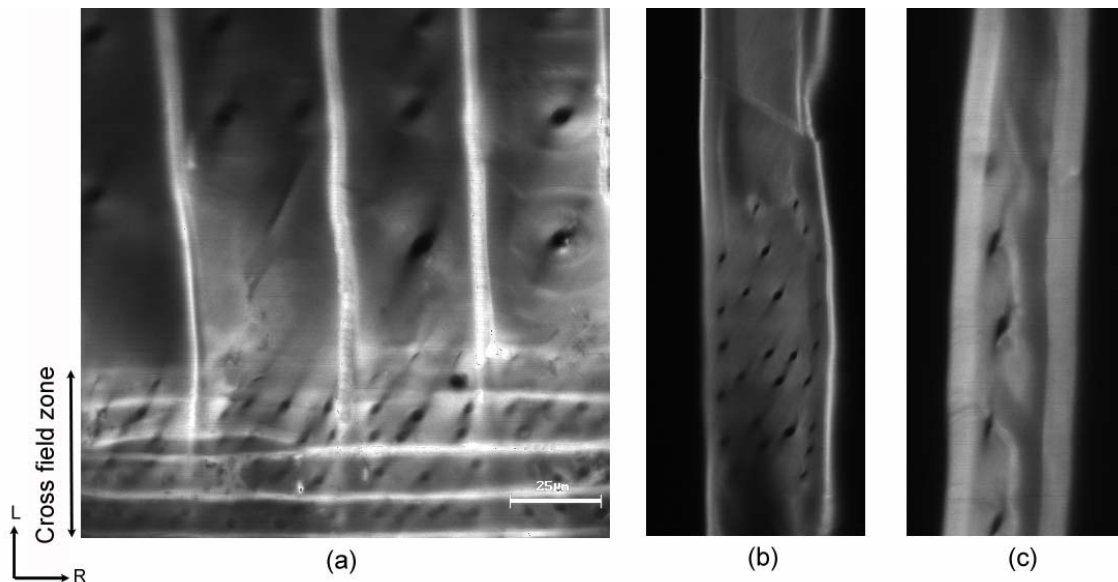
Figure 2-11 Cross-field zone; (a) some parts of the horizontal ray cells after microtomy were remained and the simple pits in the radial wall of earlywood fibers in this zone are visible, (b) simple pits in the crass field zone of an earlywood fiber, (c) simple pits in the crass-field zone of a latewood fiber

2.4 Compression wood

Compression wood is a part of the stem, which forms in the leeward side of leaning trunks. It can be found in many unpredictable positions of a tree trunk and recognized by the change of color in the stem (darker color) (see Figure 2-12).

Figure 2-12 Compression wood is recognized by the change of color in transversal cut of a spruce trunk

The interest to compression wood studies arises from its important effect on wood mechanical properties. High lignin contents (Côte and Day 1965), helical cavities in the cell wall (Timell 1978; Timell 1983; Yoshizawa and Ideia 1987), large microfibril angle (Färber, Lichtenegger et al. 2001; Bergander, Bränström et al. 2002) and low mechanical properties, especially in wet condition (Burgert, Fruhmann et al. 2004; Sedighi-Gilani and Navi 2004) are the main specifications of compression wood fibers.

Figure 2-13 show the helical cavities in radial wall of spruce compression wood fibers. Most of the times, these cavities are wider and easier to observe in latewood fibers (see Figure 2-13-b) than in earlywood fibers (see Figure 2-13-a).
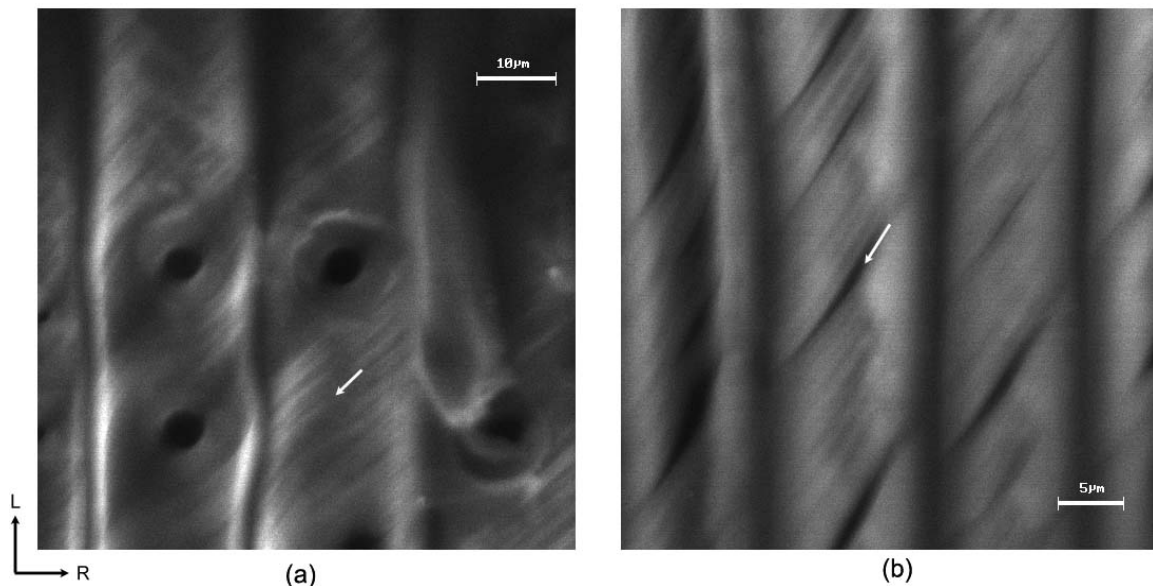
Figure 2-13 Helical cavities in spruce compression wood are parallel to the shown direction by white arrows; (a) earlywood, (b) latewood

2.5 Natural defects

Single wood fibers may contain different kinds of microstructural defects such as slip planes, dislocation, microcompression, nodes and misaligned zones, which can be seen using light microscopy. These defects which are considered as the wood fibers' weak points might break at mechanical treatments or make the fibers more sensitive to the chemical attacks (Nyholm, Ander et al. 2001).

Microstructural defects appear when there is a distortion in microfibrils orientation (Ander and Nyholm 2000). They are not only the change in microfibrils orientation, but also contain microcracks which ease the penetration of chemical solutions and enzymes into the cell wall.

Chapter 3   Microfibril angle non-uniformities

3.1 *Introduction*

The cellulose microfibrils, which are embedded helically in the hemicellulose and lignin matrix, have a reinforcing role in the wood fiber structure. Because of this role, the angle between their orientation and the fiber longitudinal axis which is called microfibril angle (MFA) is important in studying the mechanical properties of wood fiber. Any variation of MFA in a single wood fiber changes the local mechanical properties and consequently affects the overall mechanical properties of whole wood fiber.

In the last decades, numerous researchers studied the mean MFA of different wood fibers, especially in the S_2 layer, which is the thickest wall layer of the fiber. Different methods with different concepts were used while each had its own advantages and disadvantages; X-ray diffraction and small-angle X-ray diffraction (Reiterer, Jakob et al. 1998; Evans 1999; Lichtenegger, Reiterer et al. 1999; Barnett and Bonham 2004), orientation of pit apertures (Dadswell and Nicholls 1960; Hiller 1964; Cockrell 1974), soft-rot cavities (Khalili 1999; Anagnost, Mark et al. 2000; Brändström, Daniel et al. 2002; Anagnost, Mark et al. 2005), polarized light microscopy (Page 1969; El-Hosseiny and Page 1973), direction of crystals of iodine (Bailey and Vestal 1937; Senft and Bendtsen 1985) and confocal laser scanning microscopy (CLSM) (Batchelor, Conn et al. 1997; Jang 1998; Bergander, Bränström et al. 2002).

Depending on what one expects from the analysis, different methods should be used. Measuring the orientation of pit apertures gives only an overall estimation of MFA. X-ray diffraction technique when the beam size at the sample position is more than the width of one fiber, measure the mean MFA over some adjacent fibers. In contrast to these methods, polarized light microscopy shows the mean MFA of one wood fiber and the soft-rot cavities, direction of crystals of iodine and CLSM could be used in measuring the local MFA of the special areas on a wood fiber, although these methods are more time-consuming.

Sometimes, the measured MFAs with different methods which might have completely different principles are so different (Reiterer, Jakob et al. 1998). For example, the obtained mean

MFA for Picea abies latewood fibers by small-angle X-ray method, SAXS was reported as 20° (Jakob, Fratzl et al. 1994) while for the same wood and fiber type, the reported mean MFA by X-ray diffraction was 9° (Sahlberg, Salmen et al. 1997). It shows the importance of validation of different methods and also choosing the appropriate method based on the goals of the study.

Validation and improvement of MFA measurement methods could be achieved by comparing the obtained results from different techniques, (Jang 1998; Anagnost, Mark et al. 2000; Bergander, Bränström et al. 2002; Lichtenegger, Müller et al. 2003; Peter, Benton et al. 2003 ; Peura, Muller et al. 2005). Comparative studies have also shown that MFAs are different and decrease with increase of the growth rings (Lindstrom, Evans et al. 1998 ; Khalili, Nilsson et al. 2001) and the tree height (Donaldson 1992). However between the MFA and morphological features such as fiber width or thickness no correlation has been found (Anagnost, Mark et al. 2002; Bergander, Bränström et al. 2002).

Despite the number of studies that have attempted to give a comprehensive distribution of MFA in wood fibers, the definitive form of microfibril distribution within a single wood fiber is not yet completely understood. For a long time, the microfibril distribution in one wood fiber was considered uniform. Only recently methods like soft-rot cavity, X-ray micro-diffraction method, and improved iodine method have been utilized to measure the *local* MFAs within one single wood fiber (Khalili, Nilsson et al. 2001; Wang, Drummond et al. 2001; Anagnost, Mark et al. 2002; Lichtenegger, Müller et al. 2003; Andersson, Serimaa et al. 2005). Anagnost et al. (2002) showed the variability of MFA on radial wall with bordered pits and Khalili et al. (2001) non-uniformity even in non-pitted areas of earlywood fibers. Wang et al. (2001) determined the multiple lamellae nature of the S_2 layer and some changes in MFA within its different depths.

In this chapter the results of studying the MFA in S_2 layer of single spruce fibers by using the CLSM method is presented and the possibility of variation of MFA in one wood fiber is discussed. Earlywood and latewood fibers and fibers from different growth rings were tested and MFA in not-yet-investigated zones like around the bordered pits or inside the cross-field zones were measured. The results were compared in different parts of earlywood and late-wood fibers to understand the pattern and extend of variation of MFAs in different zones.

Another goal of the study was studying the MFA in compression wood fibers. In the wood literature, compression wood fibers are known for possessing large MFAs (Färber, Lichtenegger et al. 2001; Bergander, Bränström et al. 2002) and helical cavities in the fiber wall (explained in chapter 2). However the pattern of variation of MFA and the role of helical cavities in the fiber microstructure are not properly understood. In this chapter the results

of a comparative study about the local MFA of different points in compression earlywood and latewood fibers in relation to the orientation of natural helical cavities is presented.

3.2 CLSM method to measure the local MFA

Polarization confocal microscopy method is based on fluorescence dichroism of the wood fiber wall and analyzing the changes of the emitted light intensity over rotating the direction of the linear polarized laser beam by confocal laser scanning microscope (Jang 1998). First the wood fibers are dyed in Congo red. Because of the size and dipole character of Congo red molecules, they tend to be absorbed parallel to the cellulose chains. As a result the dyed fibers emit the strongest fluorescence when the excitation light is polarized parallel to the cellulose fibrils. Optical sectioning with *confocal* microscope let the fluorescent intensity is observed from a given layer (with minimum interference from other layers). This is one the main advantages of this method, as in the other measurements techniques the interference from the other layers of the fiber walls (S_1 & S_3) could affect the accuracy of the measurements when measurements in S_2 layer is aimed.

3.2.1 Fiber isolation by chemical method and sample preparation

To prepare the spruce fibers for MFA measurements, first the single fibers should be isolated. This could be done by using different methods. In chapter 4 the details about two different isolation techniques, which were used in this research, namely chemical isolation and mechanical isolation, are given. However there are two main reasons to study the MFA variation in chemically isolated fibers;

1. Isolating the fibers by chemical maceration is much easier.

2. Soft maceration has no negative influence on the orientation of cellulose microfibrils, even if it might degrade the lignin and hemicellulose components of the fiber wall (Burgert, Gierlinger et al. 2005).

To isolate the spruce fibers by chemical method, a modified Franklin procedure (acidic based maceration) was used. First a small cubic piece of spruce was saturated in deionized water to facilitate cutting thin layers (about 100 µm) with a microtome. The obtained thin wood tissues were macerated 48 hours in a solution of five parts acetic acid, one part hydrogen peroxide and four parts distilled water at 70°. This maceration procedure degrades the middle lamella and facilitates the isolation of single fibers.

After softly rinsing and filtering the obtained solution, a mass of white pulp fibers is obtained and single fibers could be easily isolated using a thin tweezers (see Figure 3-1).

Figure 3-1 Macerated spruce fibers in an acidic based solution

For more accuracy of measurements with CLSM, the macerated fibers should be stained with a fluorochrome solution. With the predefined set up for MFA measurement with CLSM, Congo red is the most convenient fluorochrome (Jang 1998) as comparing to other fluoro-chromes like Acridin orange it gives a higher difluorescence. So the macerated fibers were rinsed and stained with 0.05% Congo red solution for 30 minutes at 70°. Then after rinsing, the dyed single wood fibers were peeled out one by one by a teen tweezers and placed on a microscope slide.

3.2.2 MFA measurement

The method developed by Jang (1998) for measuring the mean MFA of single wood fibers by CLSM was used to study the variation of MFAs in one single wood fiber. A Carl Zeiss LSM 310 confocal laser scanning microscope, equipped with an argon laser (excitation at 488 nm) and a rotating half-wave plate turning the plane of polarization of the laser beam, was used for measurements. Argon laser was chosen as the absorbance spectera of Congo red for 488 nm wavelength is the highest.

Observations were performed with an X60 oil-immersion objective having a numerical aperture of 1.4. To prevent the movement of the immersed fibers in oil, they were fixed by sticking their ends to the covered microscope slide with double side scotch. Also to avoid errors due to the convexity of the fibers, they were softly pressed with a glass cover slip to flatten their top surface.

For each measurement, a small area of the fiber wall (less than 50 μm^2) was chosen and scanned at each 10° over the plane of 180°. The changes of the fluorescent intensity in each

step I, were plotted against the angle of polarization. The sinusoidal changes of fluorescent intensity fit to the equation:

$$I = A\cos^2(P - \theta) + I_{min}$$ 3-1

where A is the amplitude of the curve, I is the difluorescence intensity, I_{min} is the minimum difluorescence intensity, θ is the mean MFA of the chosen area, and P is the angle of excitation polarization. MFA of the chosen area is obtained by fitting the measured data (fluorescent intensities) to equation (3-1), shown in Figure 3-2-a.
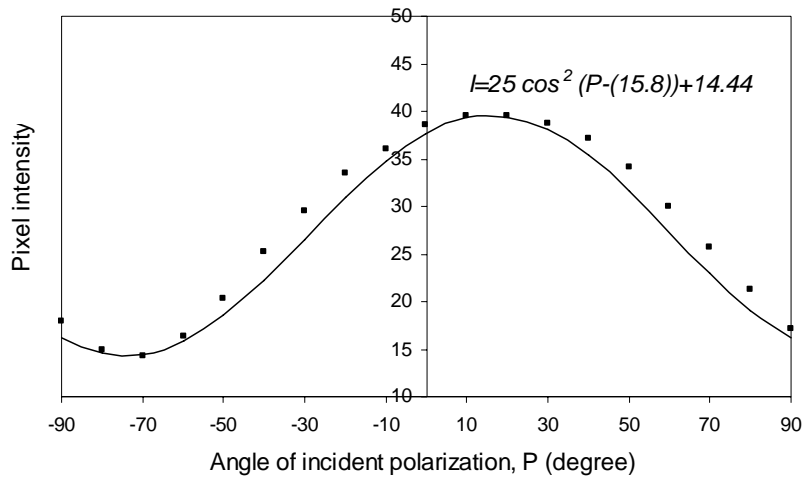
(a)
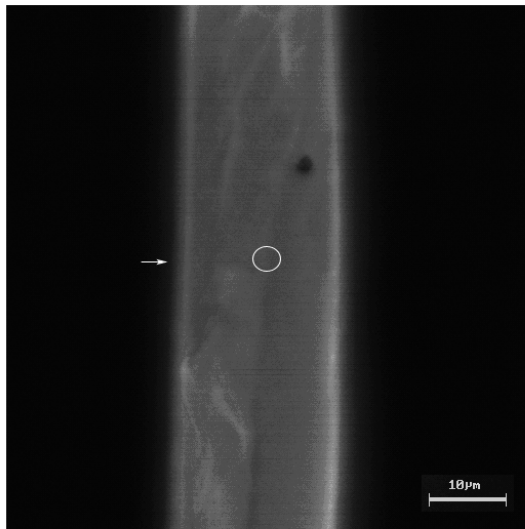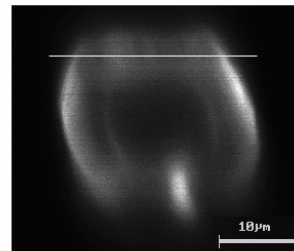
(b)   (c)

Figure 3-2 (a) Fluorescent intensity curve for the marked area in (b); θ =15.8° gives the best fit to equation (3-1), (b) focused area for microscopic scanning, (c) cross-sectional image of the latewood fiber indicating the focused area is located in S₂ layer

The CLSM method could guarantee that the obtained MFA belongs to the S_2 layer, with minimum interference from the other layers of the fiber walls (S_1 & S_3). To ensure this, in each measurement the cross-sectional image of the fiber close to the chosen area should be scanned using the blue excitation (488 nm) and then the confocal focalization position is refocused on the middle of the upper wall thickness (see Figure 3-2-b & c). As the S_2 layer is the thickest layer of the fiber wall, making up about 70-80% of the wall thickness (Fengel and Stoll 1973), we could be sure that the measurements in the middle of the fiber wall are in the S_2 layer. This process was repeated for each local measurement of MFA along one wood fiber.

3.3 MFA in normal spruce fibers

To determine the pattern and extend of variation of MFA in one wood fiber, numerous local MFAs along each of more than hundred fibers were measured. For this purpose, fibers from different parts of the softwood specimens were isolated and studied. MFA in different zones in earlywood and latewood fibers, taken from both juvenile and mature wood and also compression wood were measured. The measured MFAs in compression wood were compared to the orientation of helical cavities.

3.3.1 Earlywood fibers, radial and tangential walls

Measurements of MFA on the radial walls of earlywood fibers show that MFA is highly variable especially in the vicinity of the bordered pits. Measured MFAs between the bordered pits of earlywood fibers were usually smaller than the mean MFA in non-pitted zones (see Figure 3-3). Even the small negative values (relative to longitudinal axis) were often observed in the areas between two close-bordered pits. Reduction of MFAs was limited to the central band of the radial wall (zones A) and out of this band the microfibrils followed the mean angle of the fiber in non-pitted zones. Local reduction of MFA between bordered pits was confirmed by all detailed studies on spruce earlywood fibers. More detailed measurements result could be found in appendix A.

In the description of method in section 3.2.2, it was explained that the fibers should be first fixed on the microscope slide to avoid movements in the oil. Consequently, it is difficult to turn the fiber, after measuring the angle on one of its walls, and continue the measurements on the other walls. Hence we found some fibers that were occasionally placed corner-wise on the slide. After the soft pressing the upper surface by a glass cover slip, two adjacent tangential and radial walls were flattened and the appropriate surface for measurements on both walls was obtained. In Figure 3-4 the measured MFAs in radial and tangential walls of an earlywood fiber are shown. These data show that the high variation of

MFAs is limited to the radial walls and the microfibril orientation in the tangential walls is less variable.
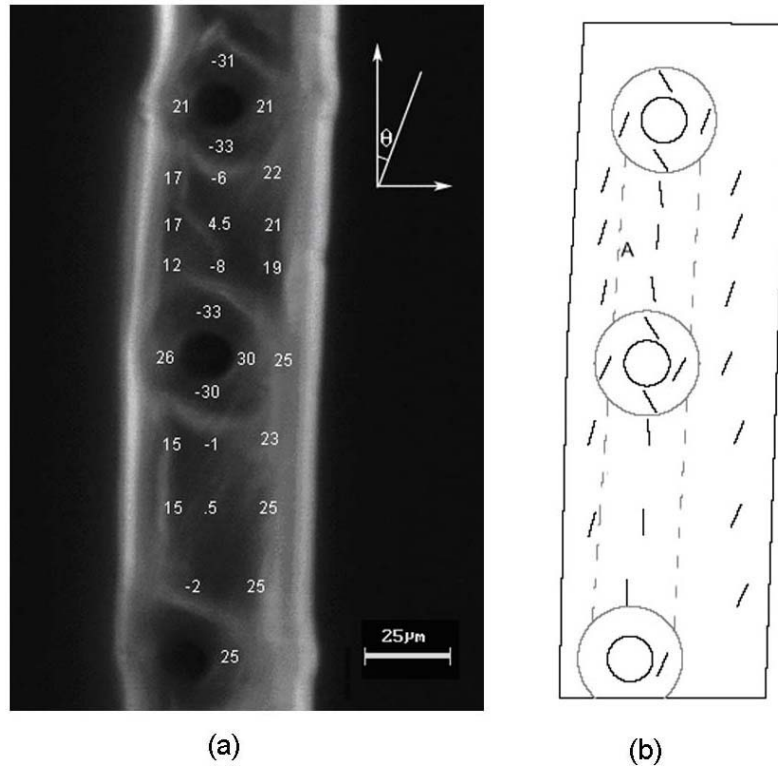
Figure 3-3 Variation of MFA in the radial wall of an earlywood fiber: (a) Measured MFAs and their locations; (b) plotted MFAs as measured in (a); lower MFAs are observed in the central band between bordered pits, marked as area A
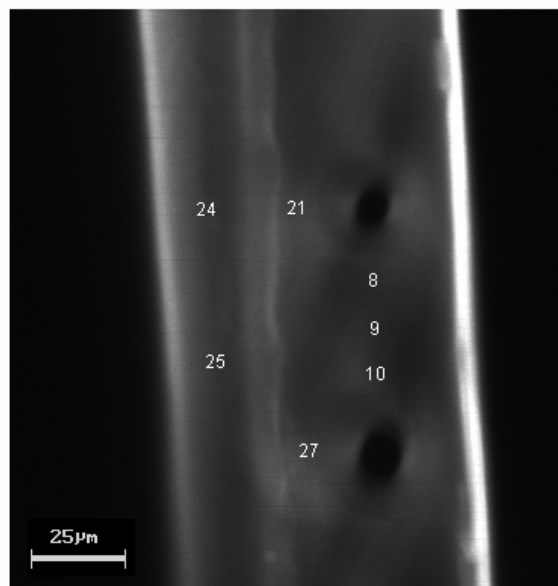
Figure 3-4 Measured MFAs in tangential wall, radial wall, and between two bordered pits; large reduction of MFA which occurs between the bordered pits, doesn't extend to tangential wall

23

3.3.2 Bordered pits in earlywood fibers:

Figure 3-5 shows the detailed measured MFAs of two examples of studied bordered pits in earlywood fibers. Representation of more measurements around bordered pits could be found in appendix A.
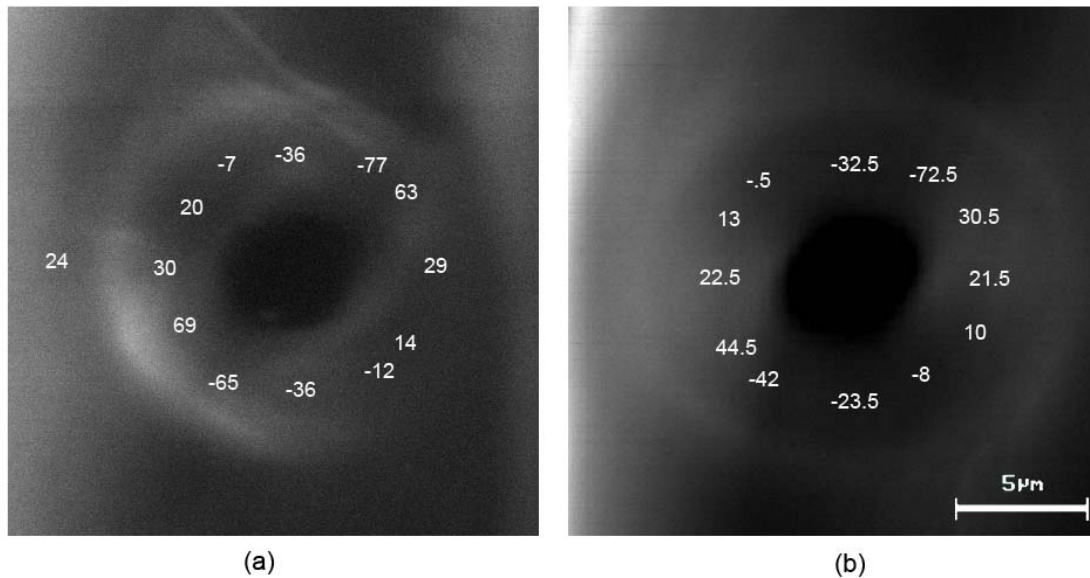
Figure 3-5 Measured data show the pattern of variation of MFA inside the border of a bordered pit

The schematic representation of microfibril paths through the measured local MFAs inside the border of the pits were plotted in Figure 3-6.
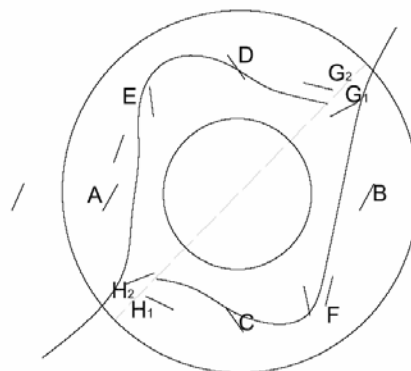
Figure 3-6 Schematic sketch shows the pattern of variation of MFA inside a border of a bordered pit

MFAs in zones A and B of this sketch had the same direction as of fiber MFA. In zones C and D, MFAs were negative relative to the fiber longitudinal axis (the S helical form) and in the zones E and F the measured MFAs had smaller values than the mean MFA of the fiber. In zones G and H when the local angle of smaller areas like, G_1, G_2, H_1 and H_2 were meas-

ured, large MFAs were obtained which were negative in zones H_1 and G_2 (in Figure 3-5-a are -65 ° and -77 ° and in Figure 3-5-b are -42° and -72.5°) and positive in zones G_1 and H_2 (in Figure 3-5-a are 63° and 69° and in Figure 3-5-b are 30.5° and 44.5°).

The sketch shows that microfibrils have a *deformed circular* pattern of distribution around the pits and inside the borders. The *circular orientation* of microfibrils inside the border had been earlier reported by other methods (Harada H. 1965; Khalili, Nilsson et al. 2001).

3.3.3 Crossed microfibrils:

In earlywood radial walls, the local measured MFAs in central band (zone A in Figure 3-3) were less than the mean MFA of the fiber. Even the small negative values (relative to longitudinal axis) were common in this region. There are two possibilities to explain this phenomenon; unidirectional arrangement of microfibrils (see Figure 3-7-a) and existence of crossed microfibril clusters in this region (see Figure 3-7-b).
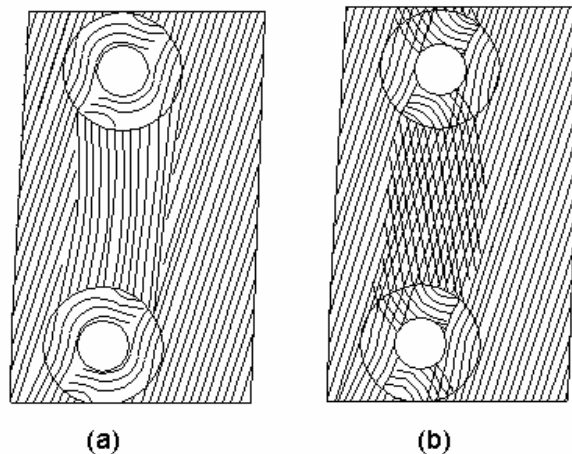
Figure 3-7 Two proposed patterns of microfibrils in the vicinity of two bordered pits based on the measured data: (a) unidirectional microfibril assumption; (b) crossed microfibril assumption

If it is assumed that on the radial wall between the bordered pits two clusters of microfibrils with different direction intertwine each other, the fluorescent intensity curve for each direction without the interference of the other direction is as Figure 3-8-a, for Z-helical form and Figure 3-8-b, for S-helical form. However the measurement results by CLSM would show the *resultant* of the two directions (see Figure 3-8-c). In this case the fluorescent intensity in each step of measurement (rotating the half-wave plate and measuring the light intensity) is the summation of fluorescent intensities in case (a) and (b) that their changes fit to equations I_1, and I_2.

$$I_1 = A\cos^2(P - \theta) + I_{min}$$

$$I_2 = A\cos^2(P+\theta) + I_{min} \qquad\qquad 3\text{-}2$$

Consequently the measured data are fitted to the resultant equation which is shown by I_{total}.

$$I_{total} = (2A\cos 2\theta)\cos^2(P) + 2(I_{min} + A\sin^2\theta) \qquad\qquad 3\text{-}3$$

(a)

(b)

(c)
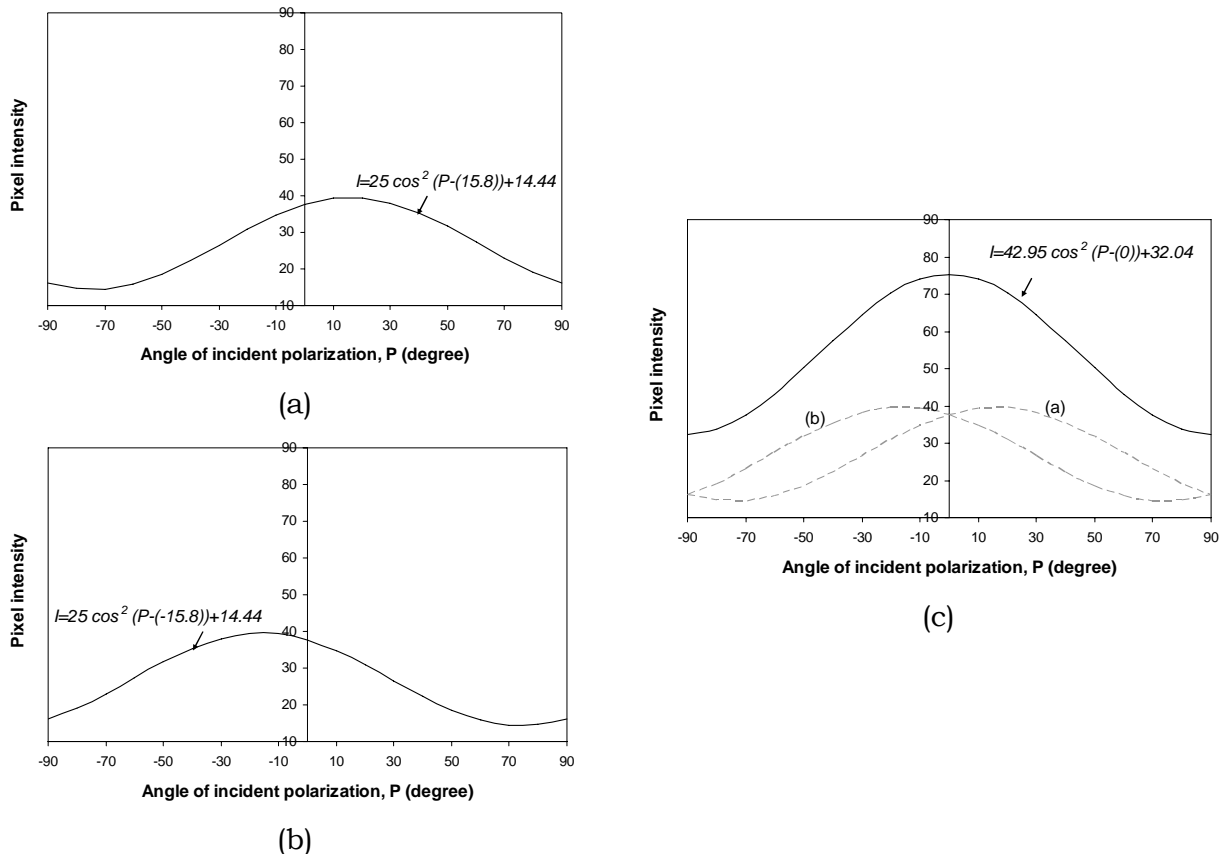
Figure 3-8 MFA of an area with two crossed planes of microfibrils; (a) fluorescent intensity curve for group of microfibrils with Z-helical form of arrangement, MFA =15.8°, (b) fluorescent intensity curve for group of microfibrils with S-helical form of arrangement, MFA =-15.8°, (c) obtained fluorescent intensity curve for the crossed microfibrils zone is the resultant of the two directions (MFA =0°)

Unfortunately, direct observation of cellulose microfibrils with CLSM is not possible and so the non-crossed unidirectional pattern of microfibrils cannot be rejected by this method. However frequently existence of the crossed microfibrils in the soft-rot fungi results (Khalili, Nilsson et al. 2001), led us to propose that microfibrils may have crossed pattern between border pits.

The origin of the crossed microfibrils between the bordered pits could be explained by analyzing the variation of MFAs inside the border of bordered pits (see Figure 3-5 and Figure 3-6). In most of the earlywood fibers the measured MFAs in the top and bottom regions of

the bordered pits had large negative values, S-helical form. It is possible that these microfibrils of inside the borders continue over the pit borders into the areas between two pits, intertwine with the Z-helical microfibrils in this region and make the crossed form.

3.3.4 MFA in cross-field zone:

Measuring the local MFA of the small areas between the simple pits of the cross-field zone in earlywood fibers usually showed uniform microfibril distributions (see Figure 3-9-a, b & c).
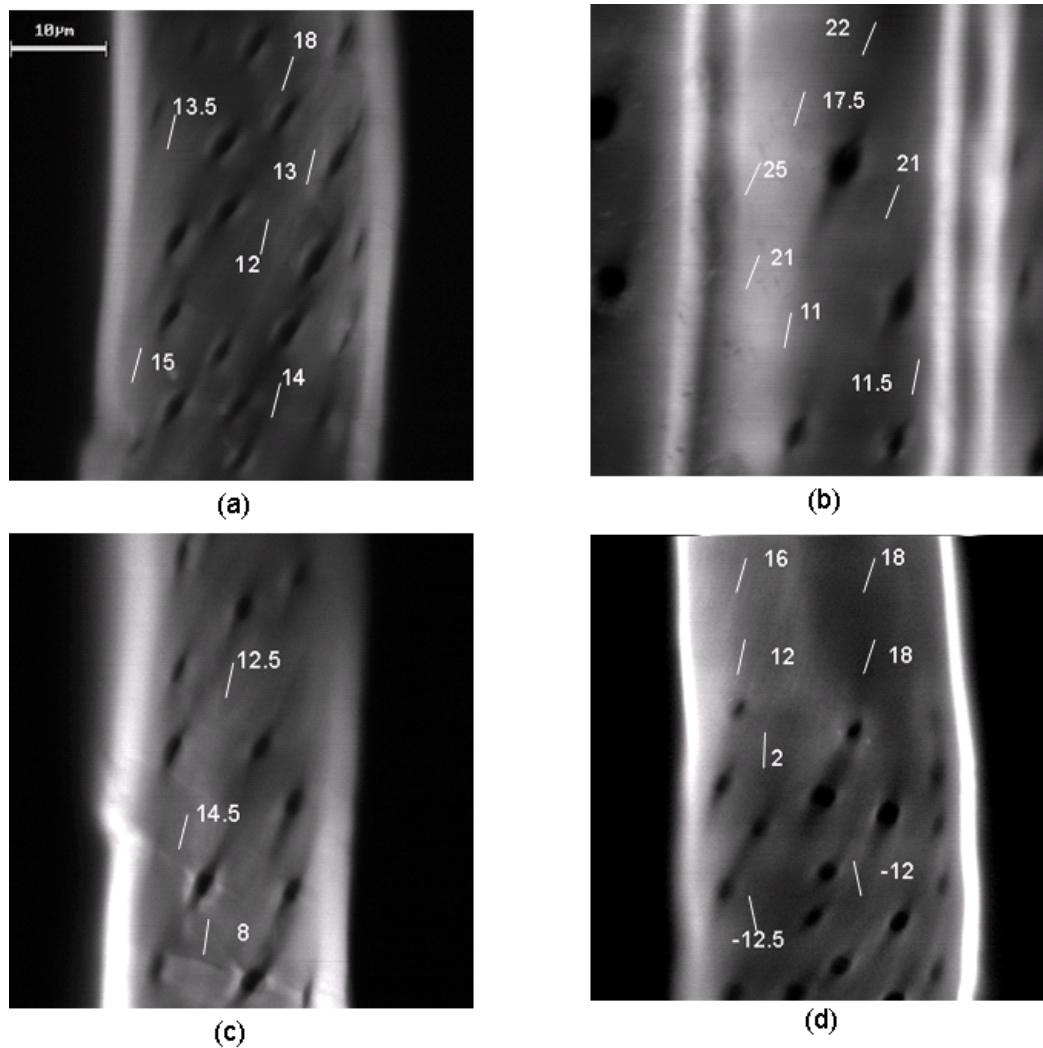
Figure 3-9 MFA in cross-field regions of earlywood fibers: (a, b & c) local MFAs were not very different; (d) MFAs were variable within the areas between the pits

Also the measured local MFAs were approximately parallel to the average orientation of pit apertures in this zone. However, in some of the fibers the measured MFAs between the pits were variable and even turned to very small or negative values (see Figure 3-9-d).

3.3.5 Latewood fibers:

Variation of MFAs within the latewood fibers is much smaller than the earlywood fibers. Even close to the steep narrow pits of the latewood fibers (which have been usually observed adjacent to the ray cells) the parallel helical arrangement of microfibrils is approximately uniform. In Figure 3-10 the measured MFAs in the different locations and the plotted MFAs as measured are shown. Also in appendix A, detailed MFAs in more latewood fibers are presented.
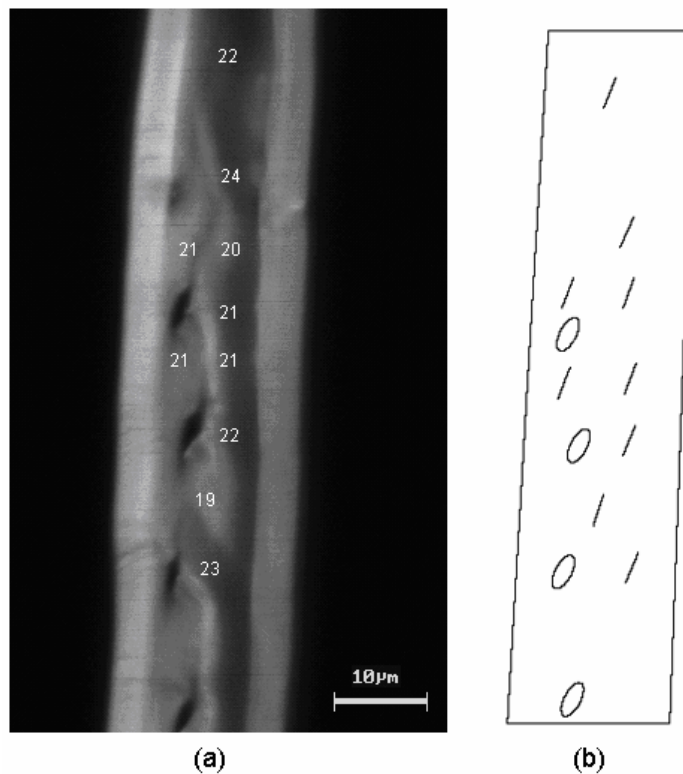
Figure 3-10 MFA uniformity in latewood fibers: (a) Measured MFAs and their locations; (b) plotted MFAs as measured in (a)

3.4 Comparative study in juvenile and mature wood fibers

A comparative study in different growth rings was carried out. In Figure 3-11, the variation of MFA in the wood fibers taken form rings 1 to 5 and 9 to 13 (juvenile wood), 24 to 32, 45 to 63 and 63 to 76 (mature wood) of a spruce sample are presented. Measured MFAs between bordered pits (which are always less than mean MFA in non-pitted areas) were ignored.

MFA decreases from pith to bark. This decrease of MFA in tree cross section, from pith to bark, has been reported by other methods like soft-rot fungi (Khalili, Nilsson et al. 2001).
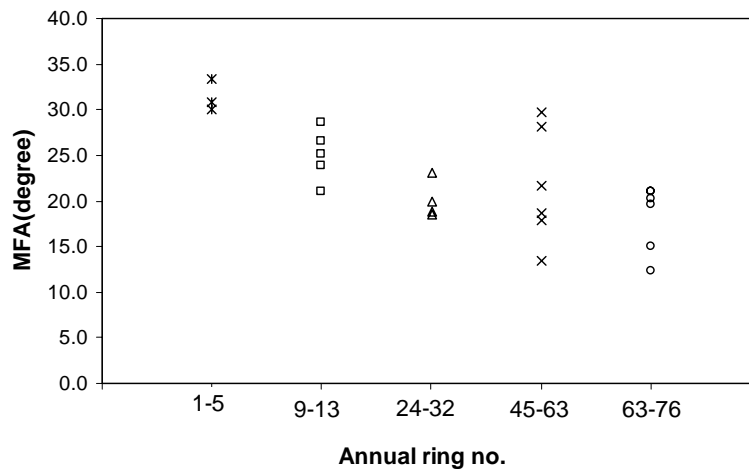
Figure 3-11 MFA as a function of annual growth rings, measured in rings 1 to 5, 9 to 13, 24 to 32, 45 to 63 and 63 to 76

3.5 MFA in compression wood

Figure 3-12 shows the variation of MFA close to the bordered pits of compression earlywood fibers (spruce and larch). MFAs between two close-bordered pits are less than local MFAs of the other parts of fiber. Usually the helical cavities (explained in chapter 2) of compression earlywood fibers are not as clearly visible as the latewood fibers. However in the regions where the orientation of helical cavities was visible, these orientations were comparable with the measured local MFAs by CLSM.
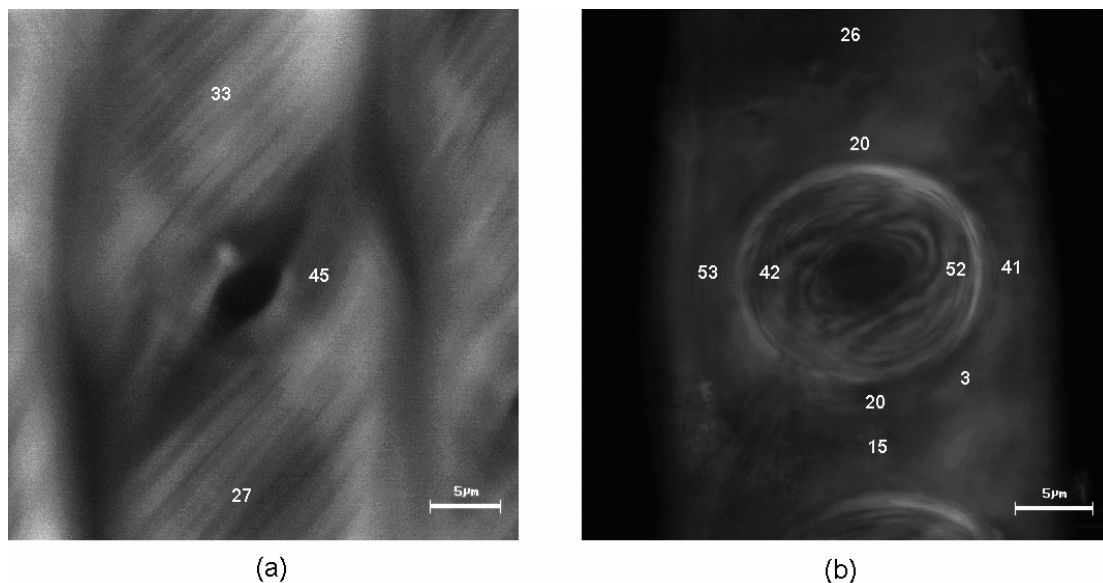
Figure 3-12 MFA close to the bordered pits of compression earlywood fibers; (a) spruce earlywood (b) larch earlywood

29

In Figure 3-13 two compression latewood fibers with their measured MFAs are shown. Natural helical cavities are apparently visible on the fiber surfaces and the local measured MFAs by CLSM have a good agreement with the orientation of these cavities.

(a)   (b)
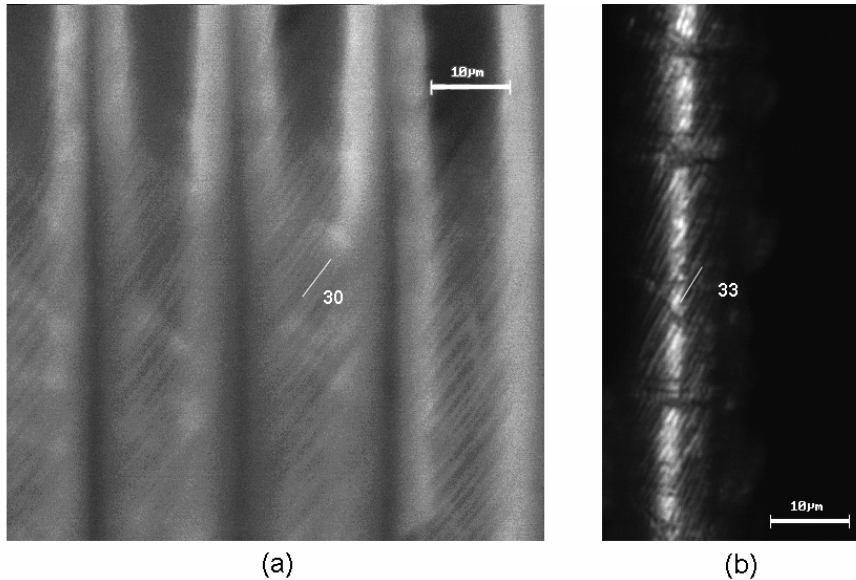
Figure 3-13 Measured MFA in compression latewood fibers, helical cavities of compression wood fibers are visible; (a) spruce latewood (b) larch latewood

To understand if there is a relation between the measured local MFA by CLSM and the orientation of natural cavities, these characteristics were compared in 12 spruce and larch latewood fibers. Figure 3-14 shows there is a relatively good agreement between both series of data, orientation of cavities and orientation of cellulose microfibrils in S_2 layer.
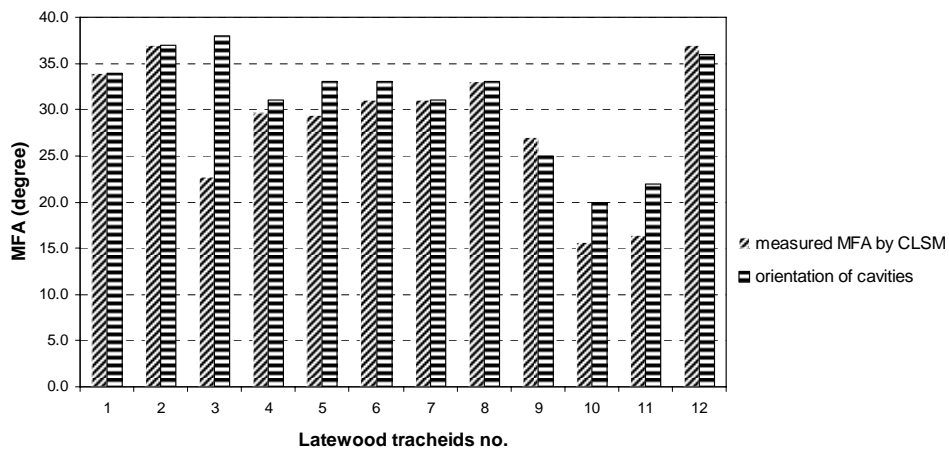
Figure 3-14 Relative agreement between measured MFA of 12 spruce and larch compression latewood fibers and the orientation of their helical cavities

3.5.1 Comparing the measured angle with CLSM and X-ray diffraction methods

MFA of larch fibers in different growth rings were measured by X-ray diffraction technique (Fioravanti and Sodini 2005) and compared to the measured values by confocal laser scanning method, Table 3-1. The rings numbered 5, 6 and 7 contained the compression wood fibers and ring 4 was normal wood. In this table, CLSM columns present the measured local MFAs in some points along different fibers of each ring. The measured values between bordered pits of earlywood fibers were considerably less than MFA in other parts of the fibers and confirmed the results of the former part, section 3.3.1.

Ring no.	Latewood		Earlywood	
	CLSM*	X-ray	CLSM*	X-ray
4	30, 33°	22°	13, 36, 33° Between bordered pits: 18, 5, 10.5°	26°
5	34, 37, 23, 30°	32°	45, 44, 49° Between bordered pits: 32, 26, 24°	37°
6	23, 30, 31°	31°	26° Between bordered pits: 21, 21, 18°	42°
7	37°	28°	56,61,54,47° Between bordered pits: 13, 12, 11, 52°	39°

*MFAs were measured in some different points along different fibers of each ring

Table 3-1 Measured MFA by X-ray method in different growth rings and by CLSM in single fibers of the same rings

Comparing the results of measurements by X-ray diffraction technique and confocal laser scanning method shows some discrepancies. These discrepancies rises from the fact that in the X-ray method the measured MFA corresponds to the mean value of some adjacent wood fibers, while in confocal laser scanning method a *local* MFA in one chosen area of the fiber wall and in the S_2 layer (with minimum interferences of the other layers) is measured. Even in the new X-ray micro-diffraction technique which is used for measuring the MFA of one wood fiber, it cannot be guaranteed that the measured MFA belongs to S_2 layer, without the interference of other wall layers.

3.6 Concluding remarks

Using CLSM to measure the mean MFA of wood fibers is not a new technique. However, in this study we used it for the first time to investigate the *variation* of MFA within the individual wood fibers.

Local MFAs were measured in different parts of earlywood and latewood fibers of compression wood and normal wood. By focusing on arbitrary chosen small areas along the wood fibers, special zones like inside the border of the pits or cross-field zones were investigated.

MFA was highly variable within the radial wall of earlywood fibers, especially in the vicinity of the bordered pits and less variable in the latewood fibers and tangential wall of earlywood fibers. However, a considerable amount of the radial wall surfaces is between the bordered pits and variation of MFA in these regions could have an important influence on the fiber

mechanical behavior. Measurements of MFA in different growth rings from pith to bark showed that MFA in juvenile wood is generally larger than in mature wood. In compression wood, MFA of earlywood and latewood fiber were compared to the orientation of natural helical cavities in the fiber walls. In many cases, the measured MFA in compression wood had a good agreement with these natural helical cavities.

After treating the fibers in soft-rot cavity and direction of crystals of iodine methods, continuous paths of cellulose microfibrils are apparent in some occasional locations of the fiber wall. Contrary to these methods, with CLSM methods the continuous paths of cellulose microfibrils along the fiber can't be observed. Nevertheless the microfibrils' paths could be estimated by measuring MFAs in numerous points along the fiber. In spite of this disadvantage, CLSM method has the advantage to give the MFA of each area of the fiber which is the subject of the study. It could measure the MFA of S_2 layer, without the interference of other wall layers. These characteristics, despite of the laboriousness of the method, make CLSM a reliable method to study the microstructure of wood fibers.

Chapter 4   Uniaxial tensile tests of single wood fibers

4.1 Introduction

The effective mechanical properties of single wood fibers are related to their mean MFA. The experiments have shown that the wood fibers with small mean MFA have high elastic moduli that decrease with an increase in the mean MFA (Page, EL-Hosseiny et al. 1977).

Tensile behavior of single wood fibers in relation to their mean MFA is complex (Page and El-Hosseiny 1983). Wood fibers with small mean MFAs indicate a brittle failure mode while the fibers with large mean MFAs show a ductile behavior, with high strain rates (Burgert, Keckes et al. 2002). There are also some experimental evidences of dependency of the fibers behavior to their location in the tree stem; growth rings or tree height (Groom, Shaler et al. 2002; Mott, Groom et al. 2002). The longitudinal Young's modulus of the fibers from the juvenile core of the tree is less than that from the fibers from mature part. Also the shape of the stress-strain curves of the fibers is dependent on their maturity or juvenility. The behavior of the fibers from mature part is linear until failure, whereas the fibers from juvenile part show non-linear behavior.

Other features of wood microstructure that affect the mechanical behavior of wood fibers are within fiber defects and heterogeneities such as pits, cross-field zones, dislocations and microcompressions. Mott et al. (1995) showed that defects are highly influential in controlling the mechanical properties of wood fibers.

Non-uniformity of MFA within a wood fiber, which was shown in chapter 3, is one of the main heterogeneities in the fiber structure that affects the *effective* mechanical properties of wood fiber by changing the *local* mechanical properties. However the experimental verification of this effect on the tensile behavior of wood fibers is not yet available.

Studying the dependency of wood fiber properties on its previous loading history, by cyclic tensile tests, reveals more details about their complex behavior in tension. Navi et al. studied the behavior of thin wood tissues under controlled cyclic tensile loading (Navi, Rastogi et al. 1995). The tensile behavior of the wood thin tissue from macroscopic point of view was analogous to an elasto-plastic material with positive hardening. They showed that the load-

elongation curves of thin spruce tissues consisted of three distinct segments. The first segment, before the decrease of the curve slope at point 1, was almost a straight line. After this point which was the first yield point of the specimen, material the underwent large permanent deformations (second segment). However, the unchanged slope of the unloading-loading cycles showed that the stiffness of the specimen after the yield point did not decrease. After this state in the third segment, the slope of the curve increased significantly with no yielding in the specimen.
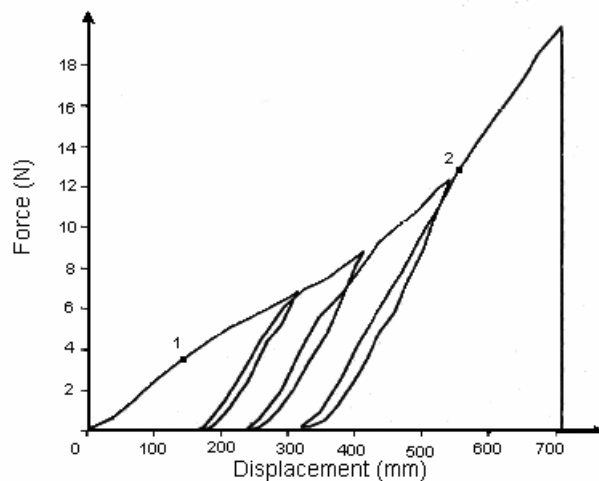
Figure 4-1 Cyclic tensile testing of a thin wood tissue (30 x 3 x 0.014 mm), (Navi, Rastogi et al. 1995)

Cyclic tensile tests on single pulp fibers, were first carried out to get the durability parameters of pulp fibers at high temperature and humidity (Wild, Provan et al. 1999). These experiments indicated the fibers' cyclic elastic behavior before yielding. Other existing experimental work in studying the cyclic tensile behavior of compression wood fibers as well as thin tissues is the recent work of (Keckes, Burgert et al. 2003). Their results, which were obtained by experiments in the wet condition, confirmed that the stiffness of material does not decrease after the yield point.

The complex tensile behavior of wood fibers cannot be explained without considering their microstructural heterogeneities and the influences of these heterogeneities on the mechanical properties of fibers (sedighi-Gilani and Navi 2004; Sedighi-Gilani and Navi in press). The major goal in this chapter is to investigate the relation between the tensile and cyclic tensile behavior of different single wood fibers and their microstructure. For this purpose, the isolated fibers from normal and compression spruce samples were tested and the effect of different parameters such as MFA non-uniformities, existence of pits and cross-field zones, different isolation techniques and humidity variation was discussed. The small size of the

developed mini-press gives us the opportunity to place it on the microscope stage and perform in-situ observation during tensile tests.

4.2 Tensile testing mini-press

To carry out the tensile tests and cyclic tensile tests on single wood fibers, a tensile testing mini-press was developed. This machine records the forces corresponding to the manually applied displacements. Because of the portability and small size of the machine which makes it mountable on the microscope stage, the in-situ observation during experiments is possible. Figure 4-2 shows the testing machine under the microscope.
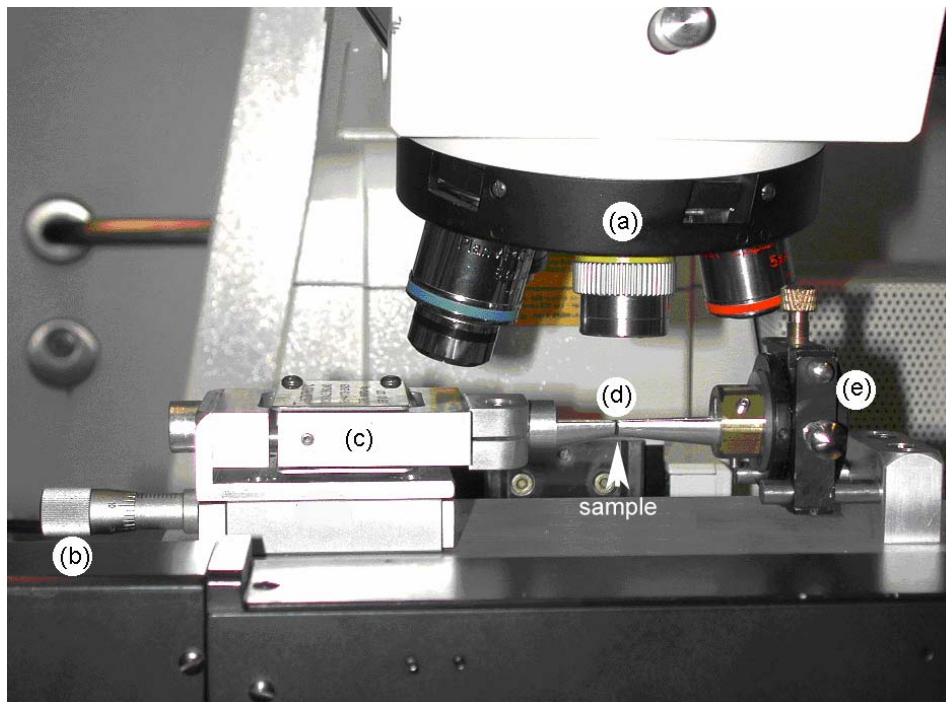
Figure 4-2 Tensile testing set up; (a) microscope, (b) displacement screw of mini-press, (c) force transducer, (d) the gripping position where sample is placed, (e) micro-band

The metallic screw, marked (b), is the displacement screw which is used for manually applying displacements of 10 μm in each step and enables us to perform displacement controlled tensile tests. The metallic box, marked (c), is the force transducer which measures the applied forces to the fiber. The maximum possible load measured by the force transducer is 20 N, which is much higher than that necessary for a single wood fiber (< 0.5 N). However testing and calibrating of the transducer for small forces demonstrated the precision of the transducer, even for small forces. To grip the wood fiber between the displacement beams, marked (d), two semi-circular steel pieces with conical slots were mounted at the ends of displacement beams to grip the sample. The prepared sample with two spherical shape epoxy droplets at its ends (is explained in 4.3.4) are put in these holes

and are gripped between them in tension. In Figure 4-3-a one of these semi-circular steel pieces is shown.

(a)   (b)
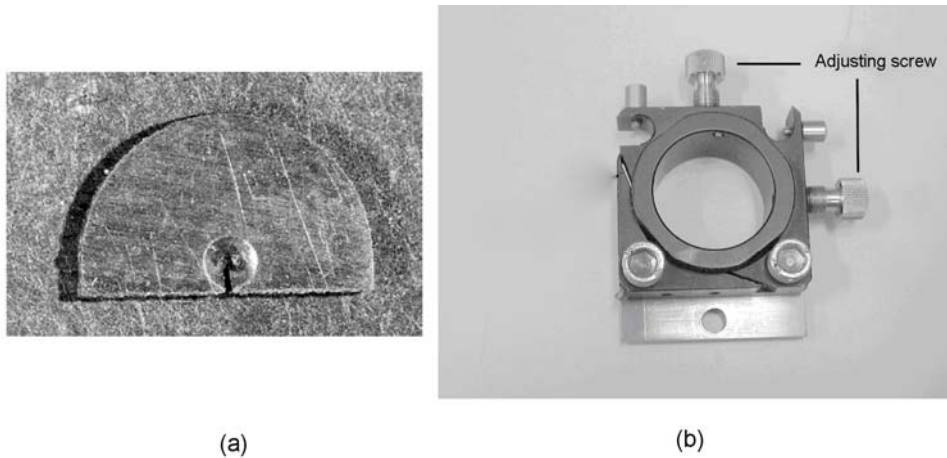
Figure 4-3 Tensile testing mini-press elements; (a) semi-circular steel piece with conical holes working as the clamps, (b) micro-band with two screws for adjusting the fiber alignment

Because of the small size of the specimens, placing a fiber specimen between the clamps of machine, with its longitudinal axis properly aligned with the force direction, is difficult. To ease the placing of specimen between the machine clamps, in a correct alignment, a device which could align the longitudinal axis of the tracheid with the force axis was developed and installed on the mini-press, marked (e) in Figure 4-2. Figure 4-3-b shows the structure of the micro-band which has two vertical and horizontal adjusting screws and can vertically and horizontally move one end of the tracheid to align its longitudinal axis with the force direction.

4.3 Preparation of fibers for tensile tests

To prepare the wood fibers for tensile tests first single wood fibers should be isolated. Single spruce fibers were isolated by using mechanical and chemical isolation methods. Comparing with chemically isolated fibers, mechanically isolated fibers are intact and could show the mechanical properties and behavior of the intact wood fibers. In chemical isolation technique, the degree of degradation of hemicellulose and lignin is unknown. However, testing the isolated fibers with chemical maceration methods because of the importance of mechanical properties of pulp fibers in the paper manufacturing is important. Also comparing the mechanical properties and behavior of chemically and mechanically isolated fibers might reveal more about the mechanisms underlying the fibers tensile behavior.

For both isolation methods, first the small cubic pieces (1 x 1 x 1 cm^3) of normal and compression wood were sawed from a spruce stem and saturated in deionized water to facilitate their cutting. Using microtome, thin layers with 100 µm thickness were cut and kept in

deionized water. Detail of the methods to isolate the single fibers from the prepared wood chips is discussed in following section.

4.3.1 Mechanical isolation methods

The mechanical isolation method for wood fibers is based on the much lower stiffness of bounding medium between fibers than the stiffness of main fibers. The thin layers were cut in the radial direction of spruce cub. In radial direction, as is shown in Figure 4-4, alternation of earlywood and latewood rings is visible which enables to isolate both earlywood and latewood fibers.
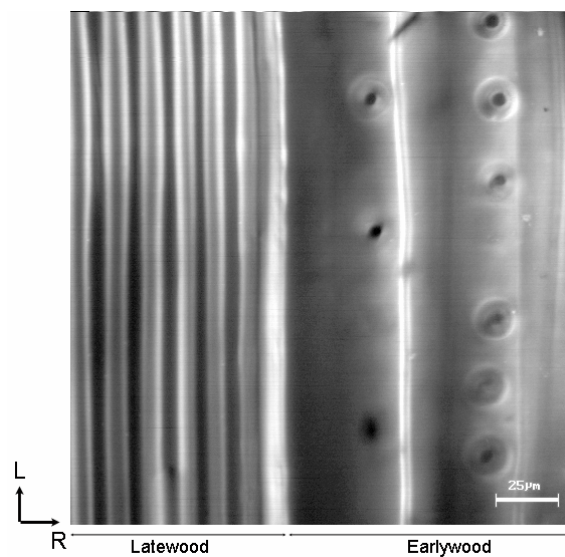
Figure 4-4 Alternation of earlywood and latewood fibers are visible in spruce cut in radial direction

One thin wet wood chip is placed on a microscope slide on the microscope stage and under microscopic observation the earlywood and latewood fibers are directly peeled out using very fine tweezers. Isolated fibers are kept in a small box for future treatments.

Fibers isolation with this method is difficult and needs some expertise. In earlywood growth rings, because of the thinner fiber walls and abundance of bordered pits that makes numerous weak points along the fiber length, fiber isolation is more difficult.

4.3.2 Chemical isolation methods

Single softwood fibers could be isolated after macerating in different types of chemical solutions with acidic or alkali bases. Based on solution constituents, different names are referred to these methods, such as 45% yield kraft method, Holocellulose method, Jeffrey or Chromium acid method and Franklin method. For this study two types of wood maceration methods, based on the acidic and alkali solutions were tried.

The procedure to get the chemically isolated fibers by macerating in an *acidic solution* was explained in section 3.2.1. To get the isolated wood fibers by maceration in an *alkaline solution*, the wood chips are periodically treated in:

(1) NAOH 4% at 80^0 for 2 hours.

(2) Acidic tampon of 75 ml sodium chlorite 1.7 %, 27 gr sodium acetate in 200 ml water, and 75 ml acetic acid 96% in 800 ml water at 70°C for 1 hour.

This treatment is repeated as long as the obtained mass after rinsing and filtering becomes white. In our spruce samples, 6 to 7 times of treating and rinsing of the chips were enough to get the white mass of pulp fibers.

4.3.3 Twisting of single wood fibers

A major difficulty in manipulating the single wood fibers is their tendency to twist after isolation and drying. The results of tensile tests on twisted fibers, because of stress concentration in the twisted zones are different from those of them which are non-twisted and their obtained stress-strain curves do not show the overall behavior of the intact wood fibers. So before any treatment on the isolated fibers, they were microscopically observed and the twisted fibers were removed.

It was found that the chemically isolated wood fibers are more sensitive to humidity changes. Most of the peeled fibers through the wet mass of macerated fibers twisted as soon as they came out of water. The tendency to twist was significantly higher in alkali macerated fibers comparing to the isolated fibers by acid maceration. However a few percent of the chemically isolated fibers remain non-twisted after drying. In Figure 4-5-a an isolated spruce fiber after maceration in the alkaline solution is shown when it is still in water and Figure 4-5-b shows this fiber twists after drying on the microscope slide. The fiber untwisted again when put back in the water. Figure 4-5-c shows an isolated fiber by maceration in the acidic solution. This fiber remained non-twisted after drying (see Figure 4-5-d).

Though still present, the twisting tendency of mechanically isolated fibers was much smaller that that of chemically macerated fibers. These observations led us to conclude that a relation exists between the twisting phenomenon and degree of degradation in the fiber structure during the isolation process. Figure 4-6 shows three isolated spruce fibers with different isolation techniques, observed by scanning electron microscopy (SEM). The images show that the wall material in the mechanically isolated fiber was approximately intact while in chemically macerated fibers was partially damaged.
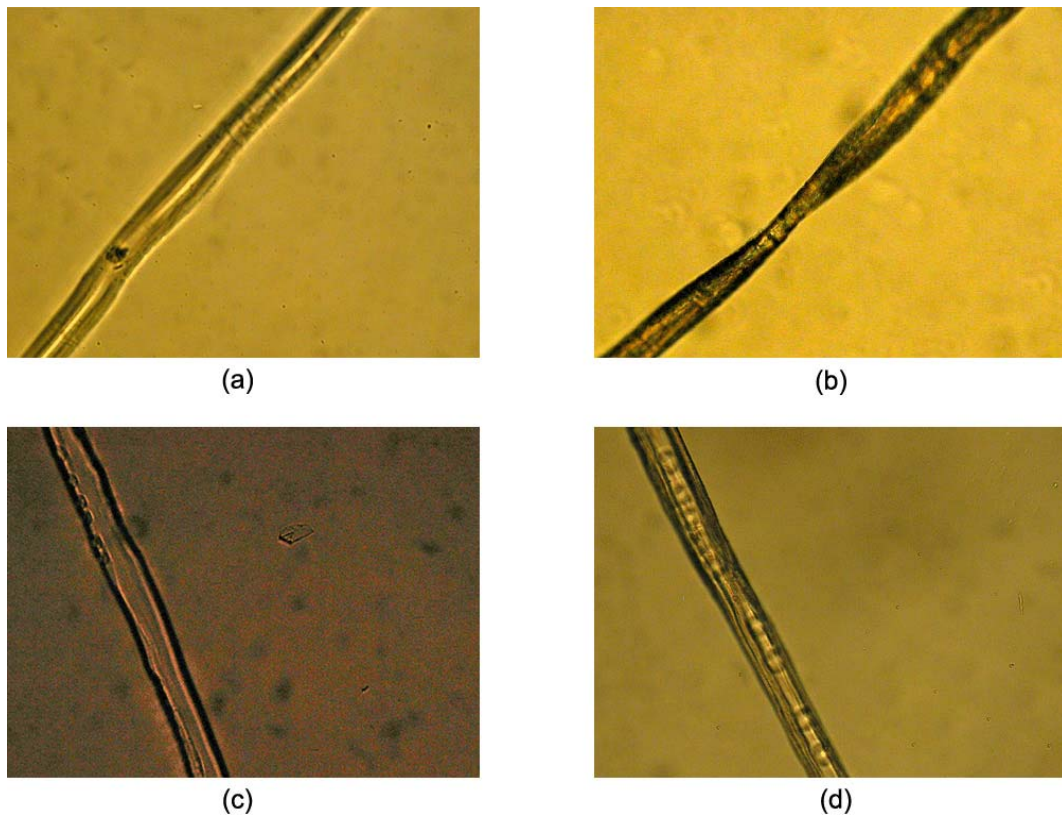
Figure 4-5 Chemically isolated spruce fibers under light microscopy; (a) an isolated fiber after maceration in the alkali based solution, inside water, (b) the same fiber dried on microscope slide, (c) an isolated fiber after maceration in the acid based solution, inside water, (d) the same fiber dried on microscope slide
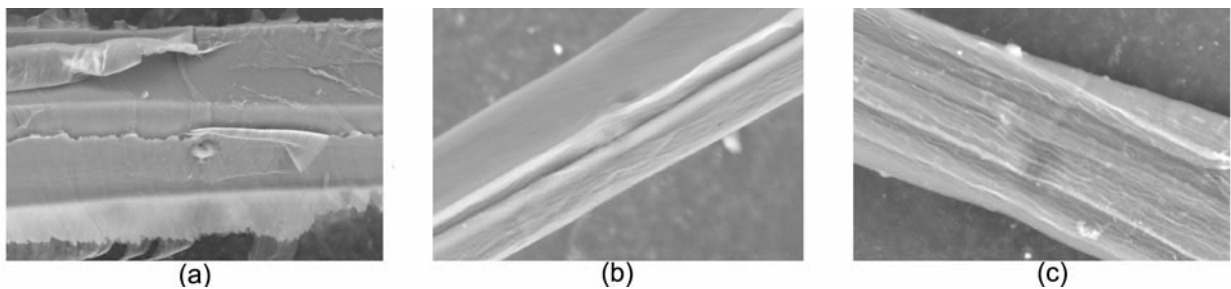
Figure 4-6 Isolated fibers with different methods observed by SEM; (a) mechanical isolation, (b) isolated by maceration in an acidic solution, (c) isolated by maceration in an alkali solution

Recently a detailed microscopic study between the chemical and mechanically isolated fibers has shown that the chemical treatment leads to degradation of lignin and hemicelluloses matrix. On the other hand in the mechanical isolation, delamination takes place at the interface between the S_2 wall layer and the compound middle lamella (Burgert, Fruhmann et al. 2005). It could be confirmed by studying the percentage of chemical constituents of the fibers after maceration in different chemical solutions. For example, in this study the Klason

method was used for measuring the lignin percentage in the pulp fibers (Tappi 1998). Measurements were performed twice for each maceration type. The results which are presented in Table 4-1 showed that the remaining lignin in the fiber walls after acidic maceration is 2.42 times higher than after alkali maceration. Also they are both less than the lignin percentage in intact fibers which is about 23% in S_2 layer (Fengel 1969).

Macerating solution kind	Remained lignin in the cell wall %
Alkali based	3.8
Acidic based	9.2

Lignin proportions were measured by Klason method

Table 4-1 lignin percentage in the fiber walls after chemical maceration

There are some discussions in literature about the accuracy of the results of different lignin measurement methods and possibility of overestimation in Klason method (Jung, Varel et al. 1999; Hatfielda and Fukushimab 2005). However as here only a comparison between different isolation techniques was aimed at, a constant overestimation in all results would not change the conclusion that the wall constituents are degraded in chemical maceration.

4.3.4 Fixing the fiber in machine

To make fiber anchor points to fix them in tensile testing mini-press, two droplets of epoxy resin are put at the ends of each single fiber (Kersavage 1973). A simple system was used to place the epoxy resin droplets at the ends of the fiber (Perez, Pittet et al. 2000). This system is mainly a Teflon frame with two sheets of brass which are fixed inside the ditches over the Teflon frame. The wood fiber is placed over these sheets and fixed on the top of the Teflon frame by double faces scotch. Water between the brass sheets holds the fiber by capillarity. The droplets of epoxy resin could be put on the free heads of the fiber using a thin tweezers in the free distances between the brass and the Teflon (about 1 mm). In Figure 4-7 a schematic representation of a wood fiber with two droplets of epoxy resin at its end is shown. Sample preparation is performed at the room temperature and humidity, under microscopic observation. Figure 4-8 shows a prepared spruce fiber with this method.
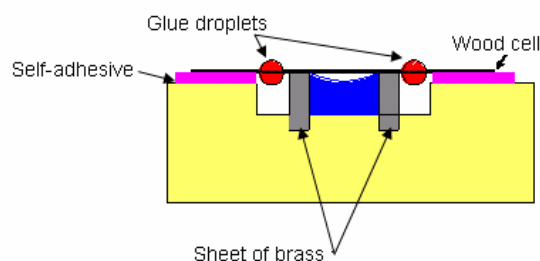
Figure 4-7 Schematic representation of the method to place the epoxy resin droplets at the ends of the single wood fiber
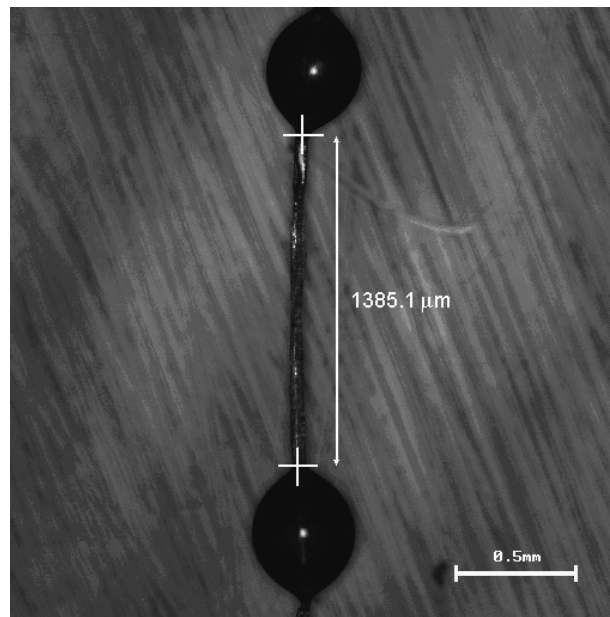
Figure 4-8 A spruce fiber with two droplets of epoxy resin at its ends as the anchoring points, effective length of the fiber is 1385.1 μm

4.4 *Fiber tensile behavior*

To understand different phenomena that might occur in tensile behavior of single wood fibers, two series of experiments, simple tensile tests and cyclic tensile tests were carried out on single fibers from different parts of the tree. Before each test, the fiber specifications and type (earlywood or latewood), existence of bordered pits, cross-field zones and other natural defects were microscopically investigated.

4.4.1 Stress-strain curve under tension

For each applied displacement, the mini-press allows us to measure the corresponding force. The force transducer records the amount of generated forces and its relaxation (or antirelaxation in unloading). A part of registered force-time curve by transducer for 20 μm, 40 μm and 30 μm applied displacements is shown in Figure 4-9.

A force-displacement curve is plotted by knowing the applied displacement at different steps and recording their corresponding forces when the fiber becomes totally relaxed. The obtained force-displacement curve is converted to stress-strain curve by considering the effective length and net cross-sectional area of the fiber before test. The effective length is the length of the fiber that is between the epoxy spheres and measured by microscopy before test, shown in Figure 4-8. Also the cross sectional area of the fiber is measured by CLSM and scanning through the depth of fiber by argon laser of 488 nm wavelength.
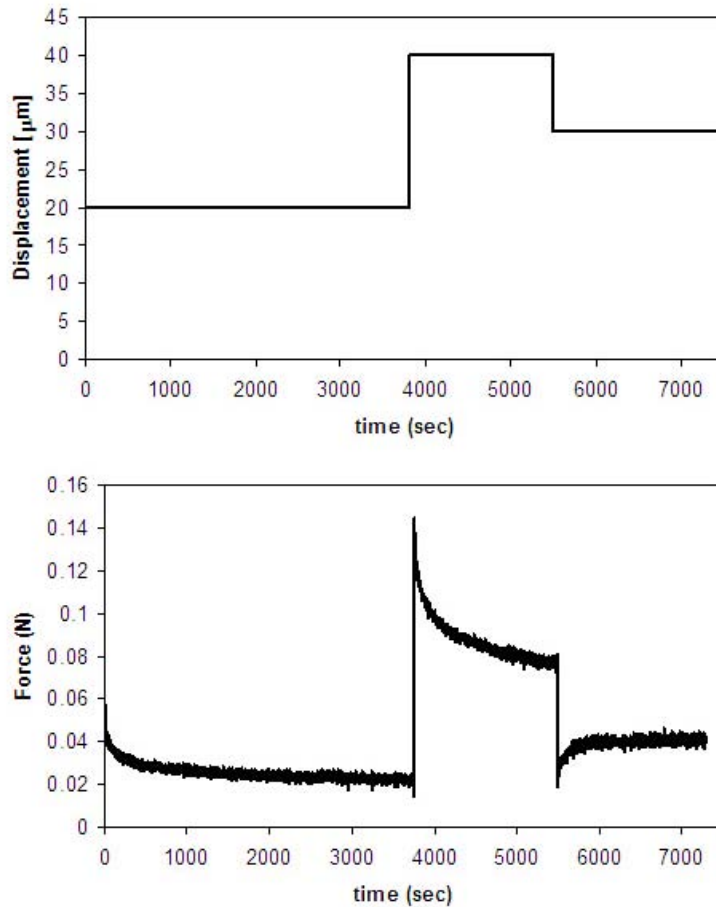
Figure 4-9 A part of step-wise force-time curve for a single wood fiber and relaxation (antirelaxation in third step) of force after 20 μm, 40 μm and 30 μm applied displacements

4.4.2 Tensile tests on single fibers in relation to MFA

Like any other fiber reinforced composite, mechanical properties of wood fibers are related to the orientation of the reinforcing microfibrils. Theoretical calculation of the longitudinal Young's modulus of the single wood fibers as the function of mean MFA has been of interest over the last three decades (Cave 1968; Cave 1969; Salmén and de-Ruvo 1985; Salmén, Kolseth et al. 1986; Koponen, Toratti et al. 1989; Koponen, Toratti et al. 1991; Navi 1998; Gassan, Chate et al. 2001). Obtaining different effective Young's moduli from tensile tests that increase upon reduction of MFA confirms this dependence (Page, EL-Hosseiny et al. 1977).

The complex aspects of wood fibers tensile behavior usually appear after yielding. The results of two series of experiments, (a) tensile tests on single pulp fibers (Page and El-Hosseiny 1983) and (b) tensile tests on mechanically isolated wood fibers (Burgert, Keckes et al. 2002), show their non-linear behavior, especially when they have large mean MFAs.

(a) The experimentally obtained stress-strain curves for different pulp fibers show that fibers with different MFAs have completely different behavior beyond yield point (Page and El-Hosseiny 1983). In Figure 4-10 the schematic representation of some of these tested pulp fibers with different MFAs are shown. As this figure shows, the stress-strain curves of single fibers are totally different for different MFAs. The fibers with large MFA show ductile behavior, having the potential for large strains while fibers with small MFA show brittle failure and high elastic modulus.
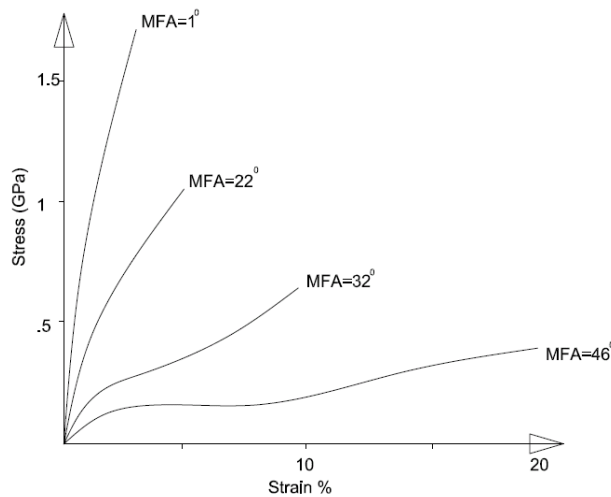
Figure 4-10 Presented stress-strain curves of single pulp fibers with different mean MFAs by Page and El-Hosseiny (1983)

(b) Later, performing the tensile tests on the mechanically isolated wood fibers from different parts of the tree confirmed the dependence between the fiber tensile behavior and its mean MFA (Burgert, Keckes et al. 2002). Fibers with bigger MFAs had higher strains and lower stiffness than fibers with small MFAs.

At the time when these experiments were carried out, it was thought that MFA is uniform along one wood fiber. Also the applied methods for measuring the MFAs were polarized light microscopy in case-(a) and X-ray diffraction method in case-(b). In polarized light microscopy method, the measured angle is a mean value over the fiber length and X-ray diffraction method gives the average MFA of a few adjacent fibers. Consequently the obtained tensile behaviors by these two series of experiments have been categorized based on mean MFAs of the fibers.

However the recent studies have shown the non-uniformity of MFA within a wood fiber (Sedighi-Gilani, Sunderland et al. 2005). Also, other kinds of defects, such as slip planes, dislocations and microcompressions which are prevalent in the structure of wood fibers are the origin of distortion in microfibrils orientation (Ander and Nyholm 2000). This local

variation of MFA changes the local mechanical properties of the wood fibers and conse-
quently affects their overall mechanical behavior. So in the tensile tests of single fibers as
well as in the modeling of their tensile behavior in relation to microstructure (chapter 5),
special attention should be paid to MFA variation.

Mechanical behavior of single wood fibers in relation to MFA heteroge-neities:

In this section the results of tensile test on mechanically isolated wood fibers when local
MFAs in different points along each of them were measured are presented. To measure MFA
by confocal laser scanning microscopy, as it was explained in section 3.2.1, samples should
be dyed by Congo red. For this purpose, the prepared samples were placed in a small paper
bag, made of filter papers, and stained in 0.05 % Congo red solution at 70°C for 30 minutes
before test. After rinsing the dyed samples, MFA measurements process was followed as was
explained before (in section 3.2.2).

Figure 4-11-a and b illustrate the response of some individual spruce fibers under axial
tension. The local MFAs in different non-pitted zones along each fiber were measured prior
to experiments. The results are summarized in Table 4-2. As MFA measurement with the
CLSM technique needs many manipulations may harm the fibers before test, measurements
were not tried in more than 3 or 4 points along each fiber. Consequently there is not much
information about the exact morphology of cellulose microfibrils in the other parts. However
the obtained stress-strain curves and measured MFAs indicate that the tensile behavior of a
wood fiber is not a simple function of mean MFA as was proposed by Page and El-Hosseiny
(1983).

Fiber no.	MFA (Deg)	Average (Deg)
(a)	32, 30, 30.5, 29	30
(b)	28, 24.5, 36	30
(c)	18, 20, 25	21
(d)	35, 20.5, 21	26
(e)	25	25
(f)	23, 24.5, 25	24
(g)	24, 26	25
(h)	22, 22.5, 22, 25	23
(i)	19, 14, 24, 20	19
(j)	60.5, 59.5, 60	60

**Table 4-2 Measured local MFAs in non-pitted zones of tested fibers and their averages in each
fiber**
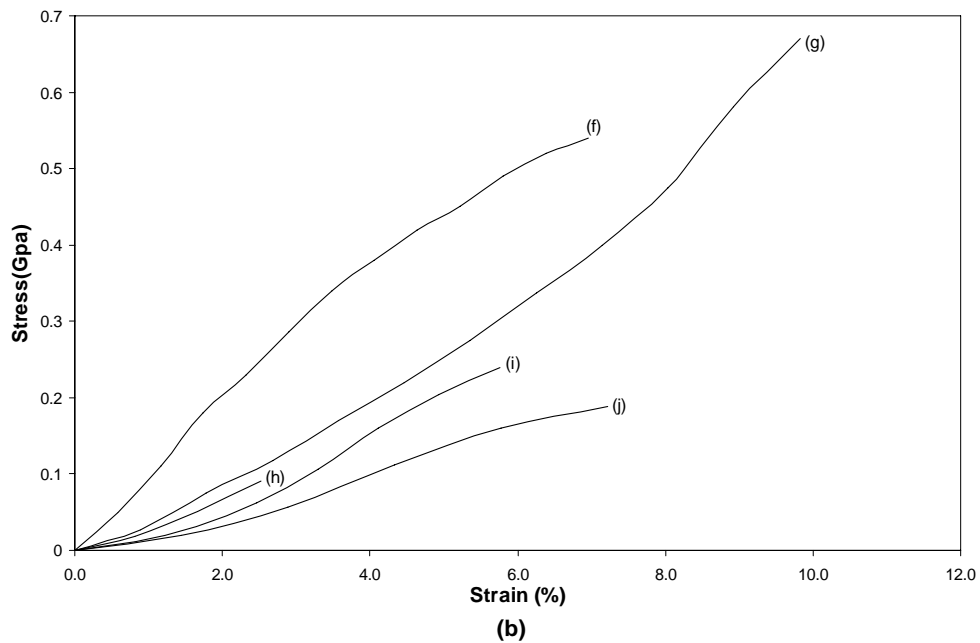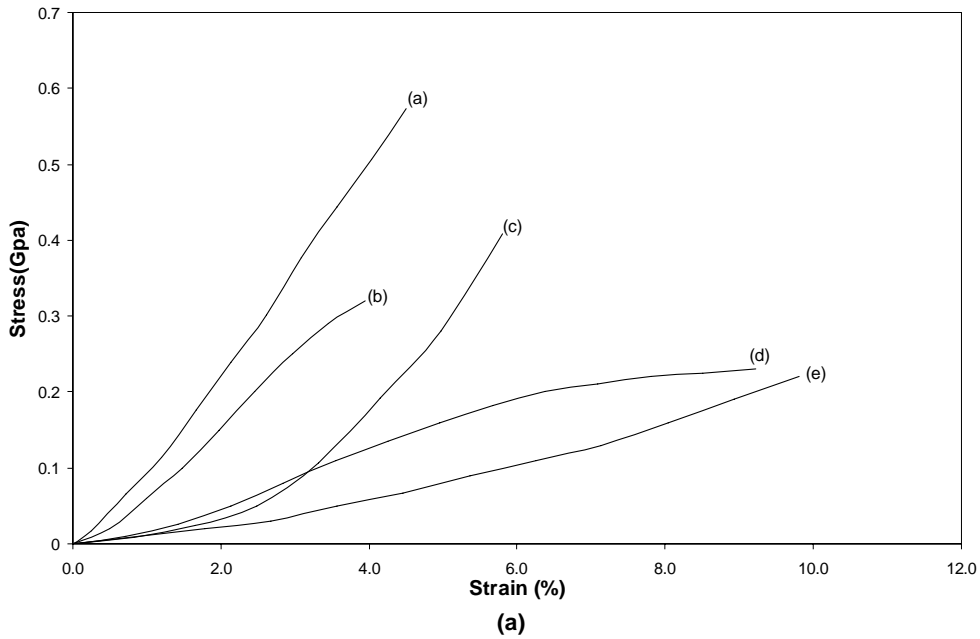
Figure 4-11 Stress-strain curves of dry wood fibers under tensile test, measured local MFAs at some points along the fibers have been mentioned in Table 4-2

The shape and slope of the stress-strain curves for fibers with similar mean MFAs (average between the few measured data) could be different. For example the stress-strain responses of fibers (a) and (b), with similar mean MFAs, though in fiber (b) the measured MFAs were

more non-uniform, were different. Other examples are different behavior of fibers (d), (e), (f) and (g) and also fibers (c), (h) and (i) with approximately similar averages between their measured MFAs.

Defects and especially existence of a *cross-field zone*, reduces the strength of the fibers. For example in fiber (h) of Figure 4-11-b, which is an earlywood fiber covered by two cross-field zones and numerous bordered pits, an early failure is observed. Another fiber with low mechanical properties is fiber (j) which was an earlywood fiber with large measured MFAs, 60.5°, 59.5° and 60°.

In this study, the information that exists about the microstructure of fibers is only the measured MFAs at 3 or 4 points along each fiber and microscopic observation to control the existence of cross-field zones and bordered pits. With this little amount of data, explaining what really happens in a wood fiber microstructure under tensile test is not easy. This is why developing a model that makes a connection between the macroscopic tensile behavior of wood fibers and their microstructure is necessary.

Conclusions which could be based on the results in this section are:

- Tensile behavior of a wood fiber is not a simple function of mean MFA as was believed before.

- Three significant tensile behaviors were recognized; linear stress-strain curves, e.g. fiber (a), concave stress-strain curve, e.g. fiber (c) and segmented stress-strain curve, e.g. fiber (d).

- Defects, cross-field zones and pits reduce the strength of the fibers.

4.4.3 Tensile tests on single fibers, isolated with different isolation techniques

Although the main aim of this chapter is analyzing the tensile behavior of intact mechanical isolated wood fibers, comparing the tensile behavior of chemically and mechanically isolated wood fibers could be useful in understanding the role of matrix constituents that might be degraded by chemical maceration.

As the tendency to twist in the chemically isolated fibers is stronger and their twisting is more probable, it is important to check the samples before the test and choose only the proper and non-twisted fibers.

In Figure 4-12 the stress-strain curves of some isolated fibers with mechanical and chemical maceration (in acidic solution) methods are presented. The measured local MFAs in non-pitted zones of the fibers are as Table 4-3. For fiber (b) MFA was not measured.

Fiber no.	MFA (Deg)	Average (Deg)
(a)[*]	12	12
(c)[*]	28, 39, 35, 34	34
(d)[*]	28, 20.5, 43	31
(e)[*]	30, 29, 19	26
(f)	32, 30, 30.5, 29	30
(g)	23, 24.5, 25	24
(h)	28, 24.5, 36	30
(i)	19, 14, 24, 20	19
(j)	35, 20.5, 21	26
(k)	25	25

*Chemically isolated fibers

Table 4-3 Measured local MFAs in non-pitted zones of tested fibers and their averages in each fiber
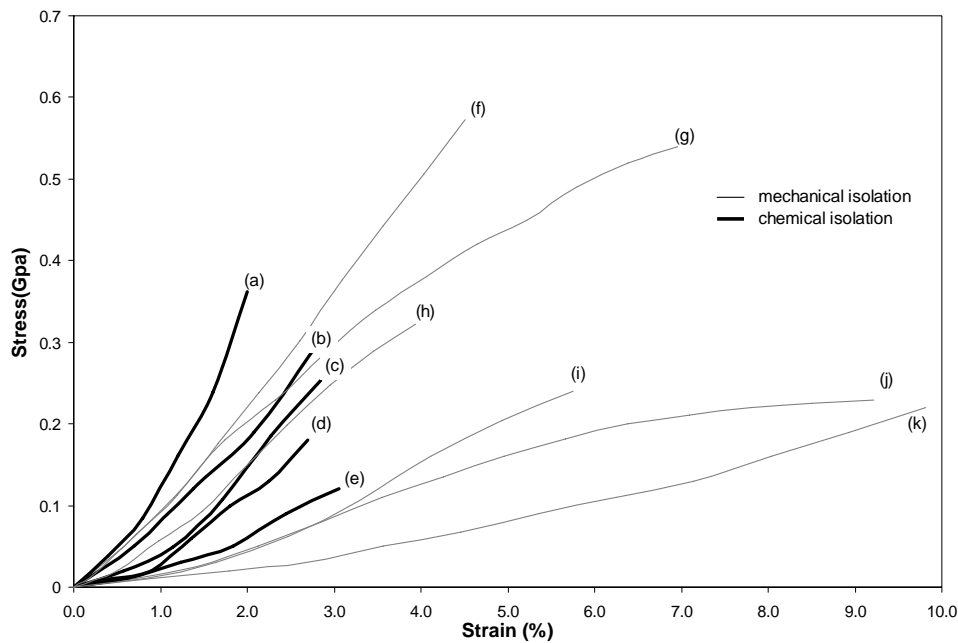
Figure 4-12 Stress strain curve of some isolated spruce fibers with different methods; thick-lines correspond to chemically isolated fibers and thin-lines correspond to mechanically isolated fibers

As Figure 4-12 shows, the strengths of the chemically macerated fibers (thick lines) were apparently lower than that of the mechanically isolated fibers. However the general shape of stress strain curves for isolated fiber with both isolation techniques was similar and the uneven behavior which has been reported by Burgert et al. (2002) for chemically isolated

fibers was not observed. Those unpredictable behaviors could be attributed to the experimental difficulties and probably using the twisted fiber in experiments.

Lower strength of the chemically isolated fibers while the general shape of the stress-strain curves for both isolation methods is similar reveals the important role of the hemicellulose and lignin matrix especially at high strains.

4.4.4 Tensile test on single compression wood fibers in wet and dry conditions

Compression wood fibers in comparison to normal fibers, have higher lignin content (Côte and Day 1965), larger MFAs (Färber, Lichtenegger et al. 2001; Bergander, Bränström et al. 2002) and lower stiffness (Burgert, Keckes et al. 2002).

In this section, the results of tensile tests on some isolated spruce fibers from the compression part of a spruce stem are presented. To compare the tensile behavior of compression wood fibers in wet and dry conditon, two series of experiments were performed; one group of fibers were tested at the room temperature and humidity and the other in wet condition. To perform the tensile tests in wet condition, the sample should be kept soaked in distilled water during the experiment. Figure 4-13 shows the stress-strain curves of the compression fibers tested in wet and dry conditions.
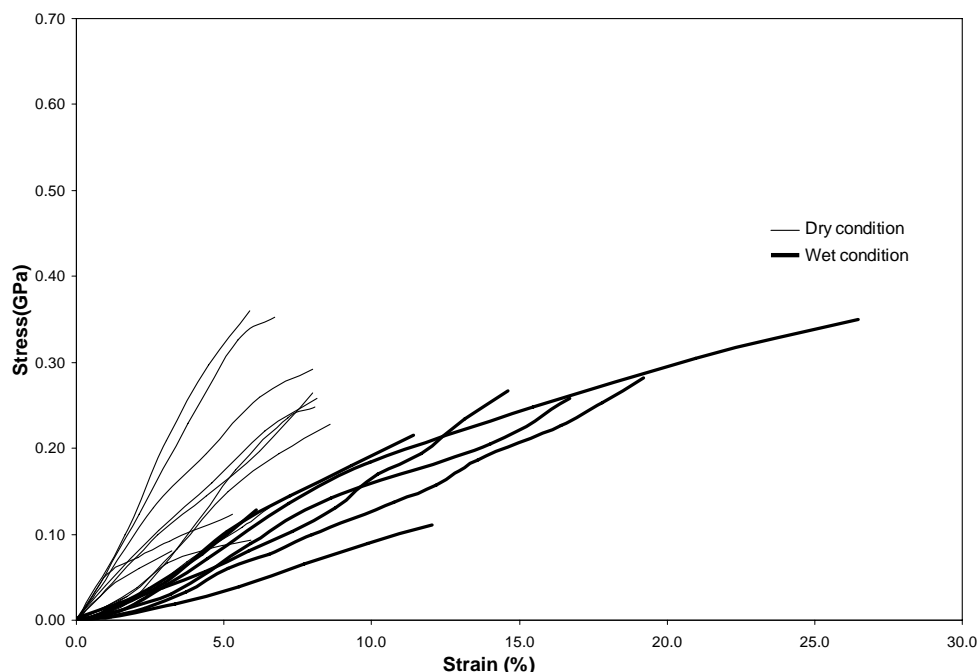
Figure 4-13 Compression wood fibers tested in dry and wet condition; tested fibers in dry condition show apparently lower strain potential and higher stiffness than tested fibers in wet condition

Fibers tested in the wet condition show higher strain rates and lower stiffness than tested fibers in dry condition. This phenomenon is attributed to the hygroscopic nature of wood polymers, lignin, hemicellulose and cellulose and the fact that the moisture has a softening effect on them (Salmén, Kolseth et al. 1986).

4.4.5 Cyclic tensile test results

Cyclic tensile tests provide us more information about the behavior of wood fibers in tension. In Figure 4-14 the behavior of two compression and one normal spruce fibers under cyclic tensile test are shown.

The stress-strain curve of wood fibers in cyclic tensile tests and tensile tests might have three distinct segments. In the first segment, which is the elastic state, the slope of the stress-strain curve is proportional to the effective Young's modulus of the intact fiber. However at some states of loading the slope of the curve shows a tendency to decrease which is probably the first yield point of the fiber. Beyond this point, the fibers undergo a large mainly irreversible deformation and the slope of the stress-strain curve decreases but still remains positive (second segment). Positive slope of the stress-strain curve after the yield point means that no strain localization occurs. Also the stiffness of the fiber and its elastic limit increase, (increasing slope of the loading-unloading cycles which are shown by dashed lines in Figure 4-14). After this state, a third segment is recognized by a high constant slope.

These phenomena have been attributed to the damage and microfibrils evolution in the fiber wall which will be discussed in chapter 5.

The important observations in cyclic tensile test could be summarized as:

1. Force-history dependent behavior of fibers in tension.

2. Positive slope of the stress-strain curve after the yield point.

3. Increase of the Young's modulus (and elastic limit).

4. Residual strains after each cycle.

5. High strain rates up to 20% in wet compression wood fibers.
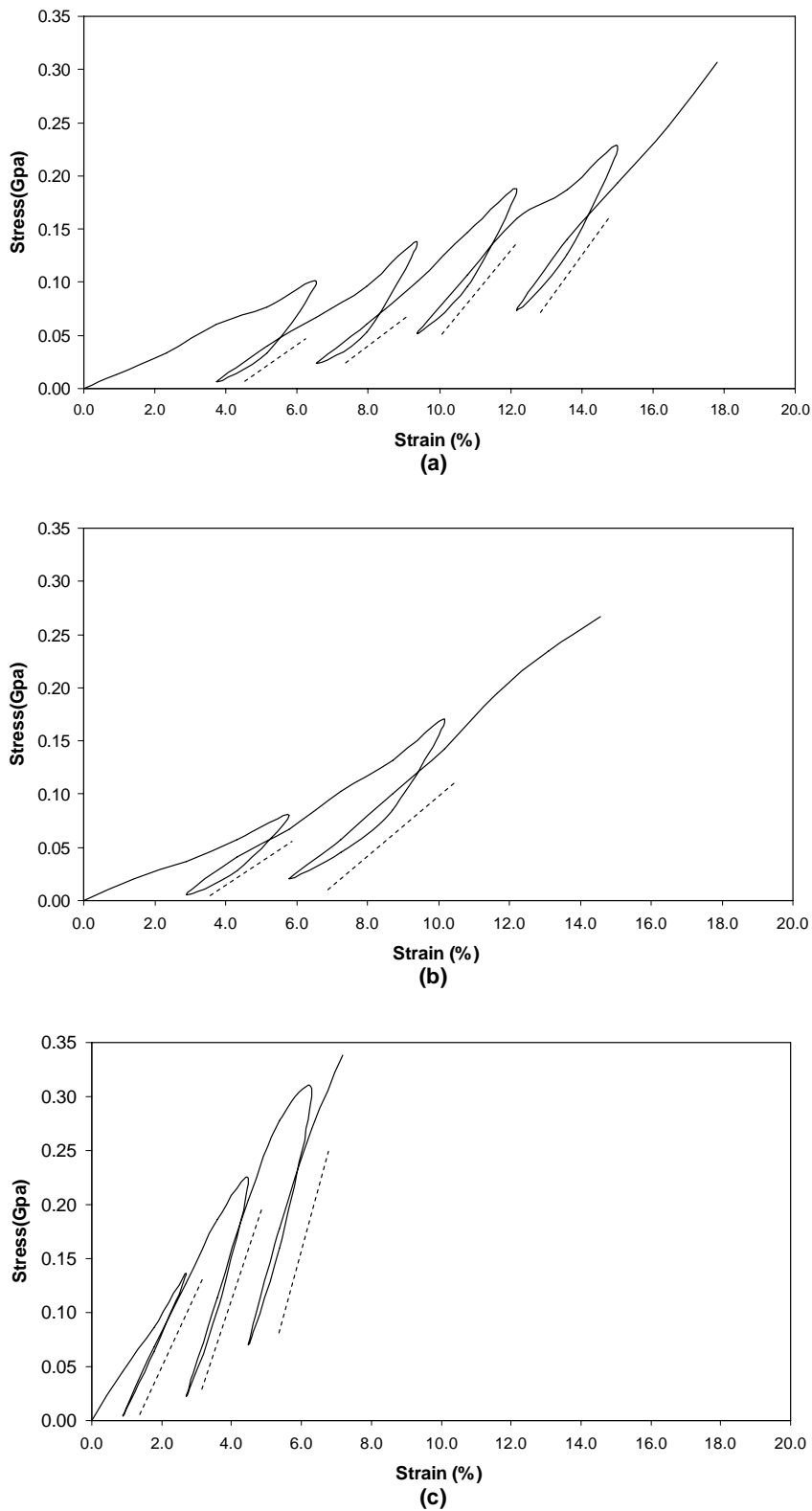
Figure 4-14 Stress-strain curve of single fibers under cyclic tensile test; (a) wet compression spruce fiber, MFA=37°, (b) wet compression spruce fiber, MFA=32°, (a) dry normal spruce fiber, MFA= 25° (MFA was measured in one point of each fiber)

4.5 In-situ observation of tensile test

With the experimental set-up which was shown in Figure 4-2, the tensile behavior of the single wood fibers could be observed in-situ by microscopy. This observation let us see how the visible defects act in tension and where the fiber finally fails.

In-situ observation of tensile tests showed that defects have important effects on the tensile behavior and stress-strain curves of single wood fibers. Existence of cross-field zones in a wood fiber can considerably decrease its strength in tensile test and causes its early failure. Also, in fibers having defects like cross-field and bordered pits zone, fiber failure often occurs close to these areas Figure 4-15. This phenomenon is a confirmation to earlier observations using environmental scanning electron microscopy (Mott, Shaler et al. 1995). By in-situ observation of the pulp fibers tensile test, it was shown that the pit fields are the most influential defects that control the position of failure in wood fibers.
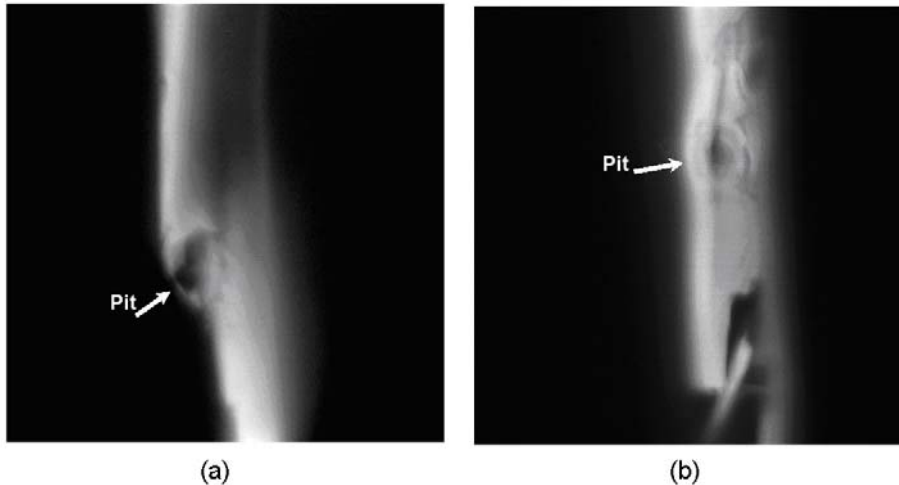
Figure 4-15 Earlywood fiber after failure; (a) failure adjacent to a bordered pit, (b) failure between two bordered pits

However the fiber failure might occur in the other non-pitted zones as well as the pitted zones. In Figure 4-16, the broken end of a latewood fiber in a non-pitted zone is shown.

Figure 4-16 Failure point in a latewood fiber

51

4.5.1 In-situ observation of non-localized multi-damage process

In Figure 4-17-a a single spruce fiber is shown which has been loaded in tension and an early crack has already been initiated at point A. The initiated crack grew upon increasing the applied displacement (see Figures 4-17-b to e). However, the final fiber failure occurred at point B (see Figure 4-17-f) where it was not expected.

(a)

(b)

(c)

(d)

(e)

(f)
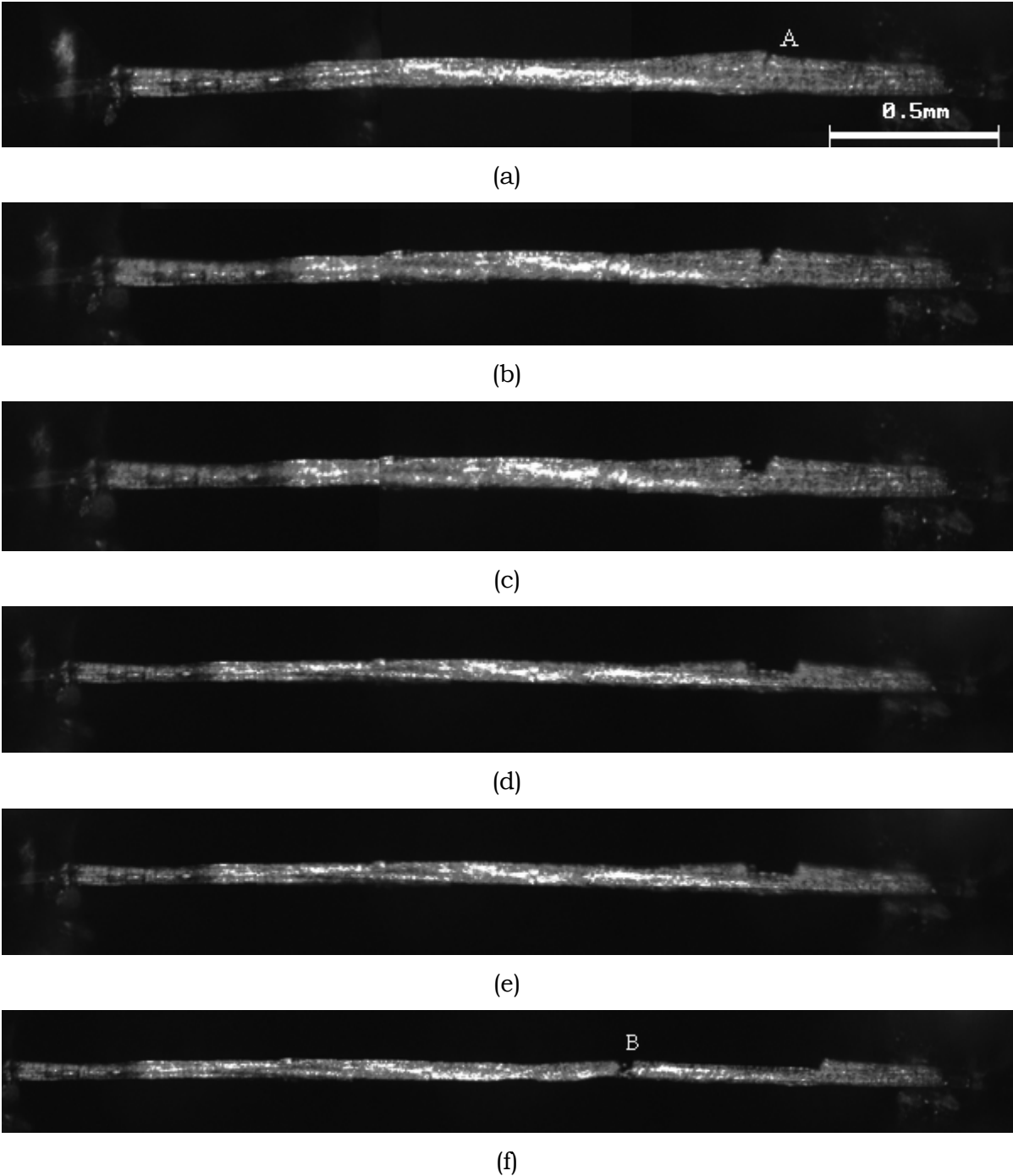
Figure 4-17 Non-localized damage in fiber tensile test; (a) local failure has been initiated at point A, (b to e) failure progresses, (f) final fiber failure at point B

These images of in-situ observations show the non-localized damage of single fiber under tensile test. This phenomenon is one of the assumptions of the presented model in chapter 5 to explain the microstructural evolution of fiber during the tensile test.

4.6 Concluding remarks

The behavior of single wood fibers under tensile test and cyclic tensile test was studied. Earlywood and latewood fibers, isolated with different isolation methods, were used in experiments and the behavior of isolated fibers from normal wood or compression wood in different wet and dry testing conditions was investigated. The effect of microstructural heterogeneities, defects, MFA and its non-uniformities on the non-linearity of behavior was examined.

Tensile behavior of wood fibers is complex and the non-linearity of the stress-strain curve is influenced by a range of MFA non-uniformities and natural defects. Three different types of behaviors were observed in the experiments; linear, concave and segmented stress-strain curves.

Cyclic tensile tests showed that the behavior of the single wood fibers is force-history dependent. After a special loading state, the fiber shows irreversible strains and the elastic limit and stiffness of the fiber increase in tensile loading.

In-situ observation of the fiber tensile tests showed that the position of early opened crack and the final failure might be different and the non-localized multi-damage might occur.

Multi-damage phenomenon and the complex behavior of a single fiber in tensile test led us to develop a model which could explain the macroscopic behavior of fibers from a microme-chanical point of view.

Chapter 5   Modeling the tensile behavior of single wood fibers

5.1 Introduction

As the observation of the evolution of wood fiber ultra-structure under tension has not been achieved yet, understanding the mechanism of their behavior by mechanical tests is still difficult. Consequently the analytical or numerical tools should be applied to model the tensile behavior of single fibers. Model should have a micromechanical approach and link the non-linear macroscopic behavior of the wood fibers to their morphology and the mechanical properties of their chemical constituents.

Mark was one of the first researchers who calculated the mechanical properties of wood fibers considering microstructural aspects (Mark 1967). Following this work, many researchers tried to develop two and three dimensional models based on the micromechanical approach and predicted the longitudinal Young's modulus of a single fiber as a function of MFA. Cave calculated the variation of the longitudinal Young's modulus with different mean MFAs and showed that it falls steeply as the mean MFA in the fiber walls increases (Cave 1968; Cave 1969). Later the laminated fiber wall model was developed considering the multilayer structure of wood fibers wall and different orientation of microfibrils in different layers (Salmén and de-Ruvo 1985; Salmén, Kolseth et al. 1986). Bergander and Salmén showed the contribution of different wood polymers in the longitudinal and transversal properties of the fiber wall (Bergander and Salmén 2002). To calculate the three-dimensional properties of the fiber wall with different layers, some researchers used the laminate plate model and thick laminate tube model (Koponen, Toratti et al. 1989; Koponen, Toratti et al. 1991; Gassan, Chate et al. 2001). Some others used homogenization with numerical and finite element tools and calculated these three-dimensional continuum properties (Navi and Huet 1989; Harrington, Booker et al. 1998; Persson 2000).

Despite progress in calculating the elastic properties of the fiber walls and wood fibers, these models could only predict the behavior of wood fibers in the *elastic zone*. The related studies to the complex tensile behavior of wood fibers after the yield point are still rare.

Navi et al. (1995), by presenting the non-linear force-elongation curves of thin spruce samples, mentioned the differences between the tensile ehavior of bulk wood and a very thin wood specimen. In contrast to tensile behavior of bulk wood (shown in Figure 5-1-b), thin wood specimens showed a segmented stress-strain curve with three different slopes (see Figure 5-1-a). The first segment was almost a straight line. At some level of loading, the slope of the force-extension curve decreased and a yield point was observed. Beyond this point, in the second segment, the slope of the curve was still positive and the specimen showed residual strains in unloading (cyclic tensile tests on thin wood specimen, see Figure 4-1). From a macroscopic point of view the specimen behaved as an elasto-plastic material with positive hardening. After this state a third segment was observed with a constant higher slope and no yield occurrence in the specimen until final failure.
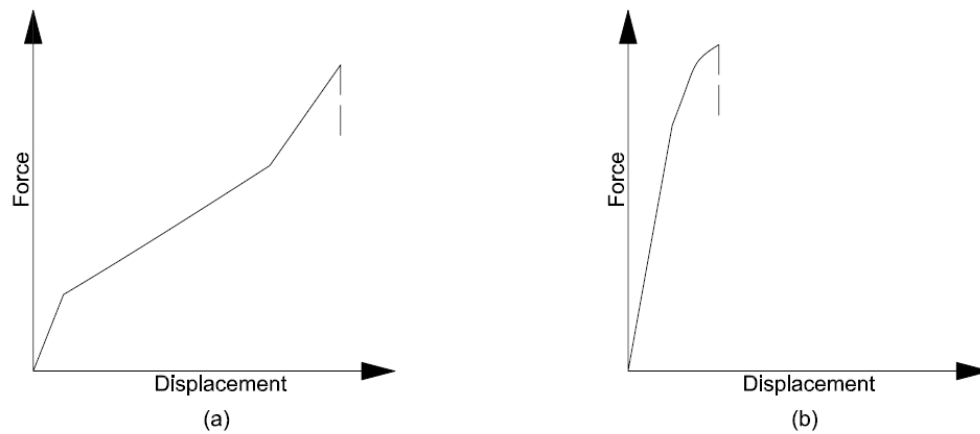
Figure 5-1 Typical force-extension curve in thin wood sample and bulk wood are different (Navi, Rastogi et al. 1995); (a) sample dimensions 2.74 x 0.19x 28 mm³, (b) sample dimensions 20 x 4 x 160 mm³

To explain these observations, they assumed that the MFA is non-uniform in each wood fiber and after the yield point matrix could locally degrade where MFA is higher. They considered that local MFAs reduce in the damaged zones and this reduction results in the residual strains in the specimen and also recovery of the reduced stiffness.

Their model was based on two main assumptions which were confirmed by later studies: MFA non-uniformities and local degradation of matrix after the yield point. On one hand, improvement of the experimental facilities and continuing the detailed studies on MFA, revealed more about the distribution of microfibrils in a wood fiber. Investigating the varia-tion of local MFAs in single wood fibers using different techniques such as soft-rot cavity (Khalili, Nilsson et al. 2001; Anagnost, Mark et al. 2002), improved iodine method (Wang, Drummond et al. 2001) and confocal laser scanning microscopy (Sedighi-Gilani, Sunderland et al. 2005; Sedighi-Gilani, Sunderland et al. 2006) proved that microfibrils orientation in

one wood fiber is non-uniform. On the other hand, the plausibility of local degradation of the matrix was shown by molecular dynamic model (Navi, Pittet et al. 2002). In this model it was shown that the induced shear strain by applying a shear stress parallel to a small assembly of parallel molecules of crystalline and amorphous cellulose (hemicellulose), is significant in the amorphous region while in the crystalline cellulose, it is not considerable.

In chapter 4, it was indicated that the behavior of different single wood fibers in tension are different. The complex tensile behavior of fibers was divided to three different types; linear stress-strain curve, concave stress-strain curve and segmented stress-strain curve. Figure 5-2 shows the experimentally obtained stress-strain curves corresponding to these three typical behaviors of fibers. The stress-strain curve for fibers (A) and (B), which were two normal mechanically isolated spruces fibers, were the approximately linear and the concave responses, respectively. But the stress-strain curve of fiber (C), which was a compression spruce fiber, was a segmented one with three distinct segments.
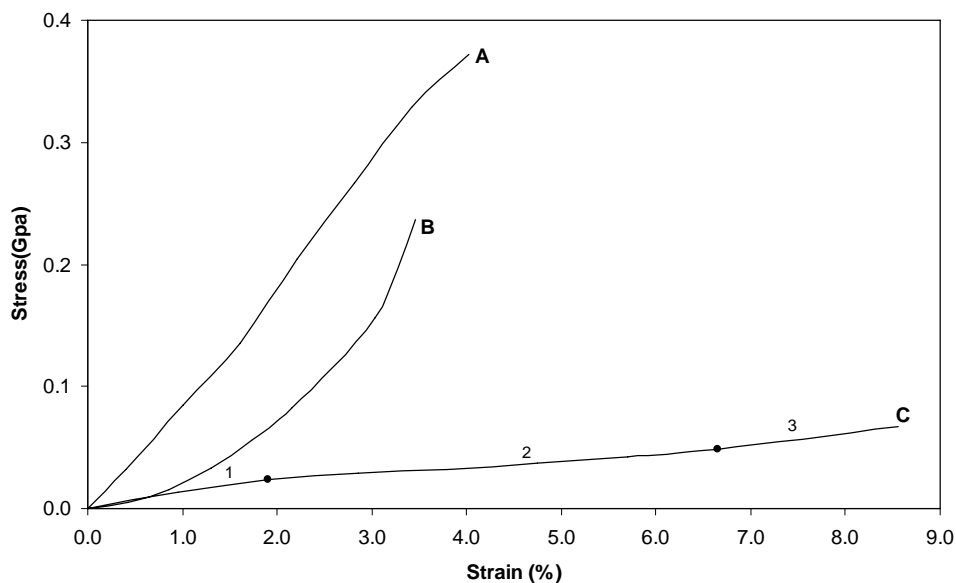
Figure 5-2 Tensile behavior of different wood fibers; fibers (A) and (B) were isolated from normal part of the spruce stem and fiber (C) was from compression part

Similarities between the experimental results of tensile tests on single compression wood fiber and thin wood specimen, indicated that a similar mechanism might govern the material behavior (Sedighi-Gilani, Pittet et al. 2003; Navi and Sedighi-Gilani 2004).

In this chapter, to explain the underlying mechanism in tensile behavior of single wood fibers, a micromechanical-based model is developed. It is assumed that damage process in

the matrix which initiates in the weakest location in the fiber (as fiber has a heterogeneous structure), is accompanied by microfibrils evolution. Microfibrils in the damaged zone tend to straighten up and reduce their angle with the longitudinal axis of fiber. Local reduction of MFA recovers the reduction of stiffness in the damaged zone and let damage initiate in (or move to) the second-weakest zone of the fibers and later in the other zones until the final failure of the fiber. By using this successive non-localized damage assumption (the experimental evidence of non-localized damage was shown in chapter 4, see Figure 4-17) and accompaniment of local MFAs reduction, mechanism of the complex behavior of single wood fibers under axial tension is discussed.

5.2 Local properties of the fiber wall

In this part, method to calculate the local Young's modulus of the intact fiber wall for a given MFA is explained.

5.2.1 Geometrical assumptions

To calculate the elastic properties of the fiber wall material, some geometrical assumptions were made. The first assumption was considering the wood fiber as a long hollow cylinder of length L. It is known that the fiber wall contains three secondary layers S_1, S_2 and S_3 and each layer of the wall is composed of lignin and hemicellulose matrix reinforced by helically wound microfibrils. However, for simplicity it was assumed that the wall is made of only S_2 layer. As this layer is the thickest layer of the fiber wall, making about 70-80% of the wall thickness (Fengel and Stoll 1973), its mechanical properties are the most influential parameters in the mechanical properties of whole wood fiber.

5.2.2 Laminate formulation

Several formulations exist to relate the effective elasticity matrix of a heterogeneous laminate to the properties of its layers and constituents. One of these methods is the developed three-dimensional laminate formulation by Cho et al. (1972). The effective moduli of the equivalent homogeneous laminate could be calculated by:

$$C_{ij} = \sum_{k=1}^{n} V^k \left[C_{ij}^k - \frac{C_{i3}^k C_{3j}^k}{C_{33}^k} + \frac{C_{i3}^k \sum_{l=1}^{n} \frac{V^l C_{3j}^l}{C_{33}^l}}{C_{33}^k \sum_{l=1}^{n} \frac{V^l}{C_{33}^l}} \right] , \; (i,j=1,\,2,\,3,\,6) \qquad \text{5-1}$$

$$C_{ij} = C_{ji} = 0 \; (i=1,2,3,6; \; j=4,\,5) \qquad \text{5-2}$$

$$C_{ij} = \frac{\displaystyle\sum_{k=1}^{n} \frac{V^k}{\Delta'_k} C_{ij}^k}{\displaystyle\sum_{k=1}^{n}\sum_{l=1}^{n} \frac{V^k V^l}{\Delta'_k \Delta'_l} (C_{44}^k C_{55}^l - C_{45}^k C_{54}^l)} \quad (i,j=4,\,5)$$

5-3

$$\Delta'_k = \begin{vmatrix} C_{44}^k & C_{45}^k \\ C_{54}^k & C_{55}^k \end{vmatrix}$$

5-4

In these equations, $[C_{ij}]$ (for i, j = 1, ... 6) is the effective elasticity matrix of the fiber wall (S_2 layer) and is calculated by using the volume fractions and the stiffness properties of three constituents: cellulose, hemicellulose and lignin. C_{ij}^k is considered as the stiffness of cellulose, hemicellulose and lignin (for k = 1, 2 & 3 respectively) and V^k are their volume fractions. Figure 5-3 shows the schematic structure of the fiber wall which was assumed as a laminate of the three constituents.
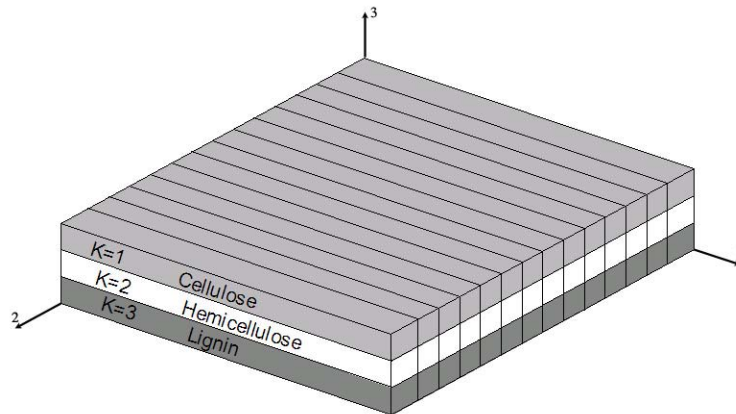
Figure 5-3 Fiber wall is assumed to be made of three layers of cellulose, hemicellulose and lignin. Direction 1 is the principal axis of the microfibril chains

5.2.3 Properties of chemical constituents

Many researchers have attempted to determine the properties of wood chemical constituents by different approaches: measurements, calculation from molecular models and estimation on the basis of the behavior of the similar materials. The data concerning the properties of wood constituents could be collected through the existing literature of the field, (Sakurada, Nukushina et al. 1962; Mark 1967; Cave 1978; Cousins 1978; Tashiro and Kobayashi 1991; Nishino, Takano et al. 1995). To calculate the equivalent properties of the fiber walls by numerically homogenization, Persson (2000) reviewed different reports and summarize the mechanical properties of wood constituents. As the reported values for stiffness coefficients of each constituent, cellulose, hemicellulose and lignin were various, to consider the differ-

ent reported values in the model, he introduced a range of variation for each stiffness coefficient.

Native cellulose (cellulose of form I) is a highly crystalline material whose mechanical properties, in contrast to hemicellulose and lignin, are not dependent to moisture changes. Cellulose is assumed as a transversely isotropic material (isotropic in the perpendicular plane to the microfibrils direction) and is characterized by five independent stiffness coefficients. Table 5-1 shows the chosen range of stiffness coefficient in Persson's model for cellulose. The indices 1, 2, 3 in this table denote the three principal directions while 1 is in the principal direction of microfibril chains.

Coefficient	Low	High
E_1(GPa)	130.0	170.0
E_2(GPa)	15.0	20.0
G_{12}(GPa)	3.0	6.0
ν_{21}	0.01	0.01
ν_{32}	0.50	0.5

Table 5-1 Range of variation in stiffness coefficients for cellulose

Hemicellulose, as its molecules tend to be aligned with the cellulose chains, is assumed as a transversely isotropic material and lignin is an amorphous material with isotropic stiffness properties. The stiffness of an isotropic material is defined by two coefficients. To validate and compare our computational result with other numerical results, moisture content was chosen similar to Persson's model, 12%. In this condition the chosen range of variation of stiffness coefficient for hemicellulose and lignin are as Table 5-2 and Table 5-3, respectively.

Coefficient	Low	High
E_1 (GPa)	14.0	18.0
E_2 (GPa)	3.0	4.0
G_{12} (GPa)	1.0	2.0
ν_{21}	0.10	0.10
ν_{32}	0.40	0.4

Table 5-2 Range of variation in stiffness coefficient for hemicellulose

Coefficient	Low	High
E (GPa)	2.0	3.5
ν	0.33	0.33

Table 5-3 Range of variation in stiffness coefficient for lignin

5.2.4 Calculation of wall stiffness coefficients

The averages of the highest and lowest stiffness coefficients of each constituent (from Table 5-1, 5-2 and 5-3), which are presented in Table 5-4, were considered for calculation of the stiffness coefficients of the fiber wall.

Constituents	Coefficient	Value
Cellulose	E_1(GPa)	150.0
	E_2(GPa)	17.5
	G_{12}(GPa)	4.5
	ν_{21}	0.01
	ν_{32}	0.50
Hemicellulose	E_1(GPa)	16.0
	E_2(GPa)	3.5
	G_{12}(GPa)	1.5
	ν_{21}	0.1
	ν_{32}	0.4
lignin	E(GPa)	2.75
	ν	0.33

Table 5-4 chosen mechanical properties of wood constituents for model

Similar to Persson's model, the volume fraction of constituents with 12% moisture contents was assumed to be 44.5 % for cellulose, 31.6% for hemicellulose and 23.9% for lignin.

C_{ij}^k, the elasticity matrix of the cellulose, hemicellulose and lignin (for k = 1, 2 & 3) are calculated as:

$$C_{ij}^1 = \begin{bmatrix} 150.516 & 3.0103 & 3.0103 & 0 & 0 & 0 \\ 3.0103 & 23.393 & 11.727 & 0 & 0 & 0 \\ 3.0103 & 11.727 & 23.393 & 0 & 0 & 0 \\ 0 & 0 & 0 & 4.5 & 0 & 0 \\ 0 & 0 & 0 & 0 & 4.5 & 0 \\ 0 & 0 & 0 & 0 & 0 & 5.833 \end{bmatrix}$$

5-5

$$C_{ij}^2 = \begin{bmatrix} 18.876 & 3.146 & 3.146 & 0 & 0 & 0 \\ 3.146 & 4.691 & 2.191 & 0 & 0 & 0 \\ 3.146 & 2.191 & 4.691 & 0 & 0 & 0 \\ 0 & 0 & 0 & 1.5 & 0 & 0 \\ 0 & 0 & 0 & 0 & 1.5 & 0 \\ 0 & 0 & 0 & 0 & 0 & 1.25 \end{bmatrix}$$

5-6

$$C_{ij}^3 = \begin{bmatrix} 4.074 & 2.006 & 2.006 & 0 & 0 & 0 \\ 2.006 & 4.074 & 2.006 & 0 & 0 & 0 \\ 2.006 & 2.006 & 4.074 & 0 & 0 & 0 \\ 0 & 0 & 0 & 2.696 & 0 & 0 \\ 0 & 0 & 0 & 0 & 2.696 & 0 \\ 0 & 0 & 0 & 0 & 0 & 2.696 \end{bmatrix}$$

5-7

These data and the laminate formulation (Cho, Carleone et al. 1972) were used to calculate the elasticity matrix of the fiber wall in a MATLAB program (Appendix B). The calculated matrix is the elasticity matrix of the fiber wall in the principal axes of the microfibrils:

$$[C_{ij}] = \begin{bmatrix} 73.874 & 2.744 & 2.667 & 0 & 0 & 0 \\ 2.744 & 11.335 & 3.367 & 0 & 0 & 0 \\ 2.667 & 3.367 & 6.894 & 0 & 0 & 0 \\ 0 & 0 & 0 & 2.511 & 0 & 0 \\ 0 & 0 & 0 & 0 & 2.511 & 0 \\ 0 & 0 & 0 & 0 & 0 & 3.635 \end{bmatrix}$$

5-8

Elastic properties of the wall material are calculated by using the effective compliance matrix, $[S_{ij}]$ which should be equal to the inversion of elasticity matrix:

$$[S_{ij}] = \begin{bmatrix} 1/E_1 & -\upsilon_{21}/E_2 & -\upsilon_{31}/E_3 & 0 & 0 & 0 \\ -\upsilon_{12}/E_1 & 1/E_2 & -\upsilon_{32}/E_3 & 0 & 0 & 0 \\ -\upsilon_{13}/E_1 & -\upsilon_{23}/E_2 & 1/E_3 & 0 & 0 & 0 \\ 0 & 0 & 0 & 1/G_{12} & 0 & 0 \\ 0 & 0 & 0 & 0 & 1/G_{13} & 0 \\ 0 & 0 & 0 & 0 & 0 & 1/G_{23} \end{bmatrix}$$

5-9

The calculated elastic properties by matrices calculations are presented in Table 5-5 and compared to the obtained elastic properties in other works for the S_2 layer (Harrington, Booker et al. 1998) and both S_1 and S_2 layers (Persson 2000). These results were obtained by homogenization and finite element analysis.

Coefficient	Matrices calculation	Numerical results[1] (Persson 2000)	Numerical results[2] (Harrington, Booker et al. 1998)
E_1(GPa)	72.63	72.6	63.96
E_2(GPa)	9.66	7.48	9.16
E_3(GPa)	5.84	6.13	9.85
G_{21} (GPa)	2.51	3.13	3.02
G_{31} (GPa)	2.51	2.97	3.38
G_{23}(GPa)	3.63	1.75	2.96
v_{21}	0.02	0.0234	0.33
v_{31}	0.025	0.0208	0.33
v_{32}	0.29	0.438	0.39

1: in S_2 and S_3 layers
2: in S_2 layer

Table 5-5 Calculated elastic properties of wall material by matrix calculation and finite element analyses

This table shows that the calculated elastic properties for the fiber wall material by three-dimensional laminate formulation agreed with the obtained results by homogenization and finite element technique.

These elastic properties characterize the wall material in the direction of principal axes of microfibrils (see Figure 5-4-a) and to get the elastic properties in the principal direction of the fiber (see Figure 5-4-b), the matrix of elastic properties should be transformed.
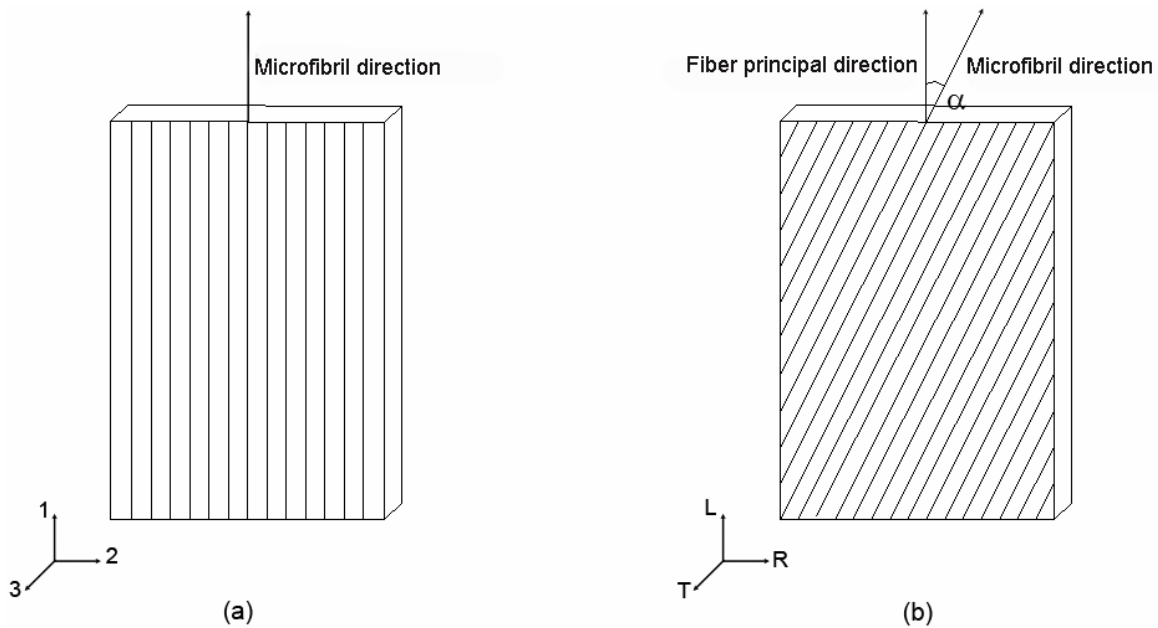
Figure 5-4 Obtained properties in principal axes of the microfibrils, (a) should be transformed to fiber principal direction, (b)

Transformation of elasticity matrix from the local coordinate (1,2, 3) to the global (L, R, T) is done by using the following transformation:

$$\left[C_{ij}^{\alpha} \right] = \left[G^{T} \right]\left[C_{ij} \right]\left[G \right]$$
5-10

where α is the angle between the direction of microfibrils and the fiber longitudinal axis (MFA), $\left[C_{ij}^{\alpha} \right]$ is the elastic properties in the fiber principal direction and $\left[G \right]$ is the transformation matrix between the local and global coordinate system.

$$[G] = \begin{bmatrix} a_L^x a_L^x & a_L^y a_L^y & a_L^z a_L^z & a_L^x a_L^y & a_L^z a_L^x & a_L^y a_L^z \\ a_R^x a_R^x & a_R^y a_R^y & a_R^z a_R^z & a_R^x a_R^y & a_{RL}^z a_R^x & a_R^y a_R^z \\ a_T^x a_T^x & a_T^y a_T^y & a_T^z a_T^z & a_T^x a_T^y & a_T^z a_T^x & a_T^y a_T^z \\ 2a_L^x a_R^x & 2a_L^y a_R^y & 2a_L^z a_R^z & a_L^x a_R^y + a_L^y a_R^x & a_L^z a_R^x + a_L^x a_R^z & a_L^y a_L^z + a_L^z a_L^y \\ 2a_T^x a_L^x & a_T^y a_L^y & 2a_T^z a_L^z & a_T^x a_L^y + a_T^y a_L^x & a_T^z a_L^x + a_T^x a_L^z & a_T^y a_L^z + a_T^z a_L^y \\ 2a_R^x a_T^x & a_R^y a_T^y & 2a_R^z a_T^z & a_R^x a_T^y + a_R^y a_T^x & a_T^z a_L^x + a_T^x a_L^z & a_R^y a_T^z + a_R^z a_T^y \end{bmatrix}$$ 5-11

a_{local}^{global} is the direction cosines between the local and global directions respectively.

The longitudinal Young's modulus of the fiber wall for a given MFA is calculated from the transformed elasticity matrix and then the Young's modulus of the fiber is calculated by multiplying a porosity ratio (to consider the fiber lumen) in the Young's modulus of the fiber wall. Assuming the porosity ratio of the fiber lumen as 0.3, the calculated Young's modulus of wood fiber with MFAs varying from 0° to 50° is as Figure 5-5.
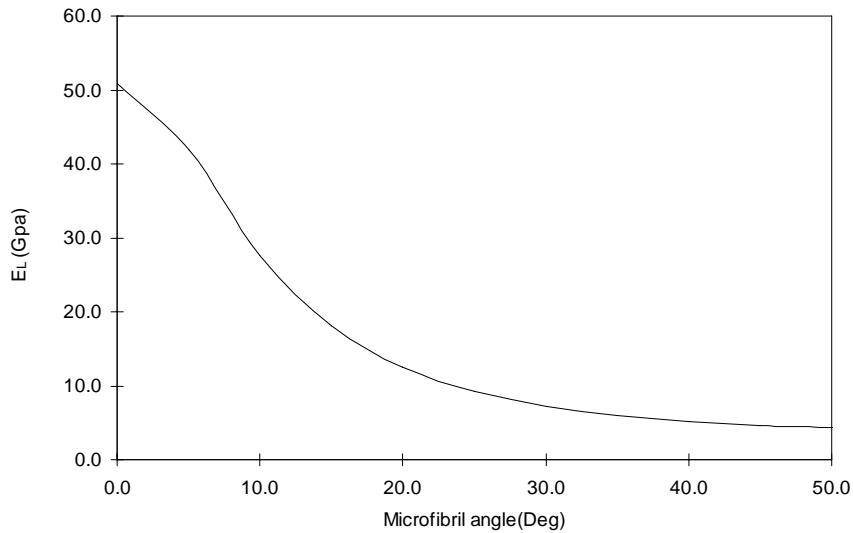
Figure 5-5 Calculated Young's modulus of wood fiber as a function of MFA

5.3 Model assumptions

As was shown in Figure 5-5, Young's modulus of a single wood fiber for a given MFA was calculated. These Young's modulus could explain the behavior of fibers with linear stress-strain curves, but not the complex behavior of other fibers and their underlying mechanism.

To explain the complex aspects of the tensile behavior of the wood fibers, a micromechanical model was developed, based on the following assumptions:

1. MFA non-uniformities (heterogeneities in the fiber microstructure).

2. Possibility of matrix degradation after a certain loading state.

3. Increase of the Young's modulus and positive hardening after yielding.

4. Occurrence of multi-damage in tensile test.

The experimental evidences of increase of the Young's modulus and positive slope of stress-strain curve after yielding and also multi-damage phenomenon were shown by tensile and cyclic tensile tests on single wood fibers and in-situ observations in chapter 4. The other assumptions are explained in the following sections.

5.3.1 Effective properties of the wood fiber

The structure of wood fibers is highly heterogeneous with different kind of defects. For model simplification, it is assumed that all kind of defects which could cause the variation of local Young's modulus along the fiber are replaced by MFA non-uniformities. This assumption is not far from reality as variation of MFA within one wood fiber has been shown (Sedighi-Gilani, Sunderland et al. 2005) and also most of the defects in wood fibers like dislocations, micro compressions, and slip planes are known as distortion in microfibrils orientation (Ander and Nyholm 2000).

From this discussion it could be considered that the hollow mono-layer cylinder of length L (in geometrical assumptions in section 5.2.1) is divided into numerous segments while MFA and longitudinal Young's modulus are constant in each segment and changes from segment to segment. The longitudinal Young's modulus and MFA which belong to one specific segment are called the *local longitudinal Young's modulus* and the *local MFA*. In Figure 5-6 a part of an earlywood fiber and its corresponding schematic geometry which is used in the model are shown.
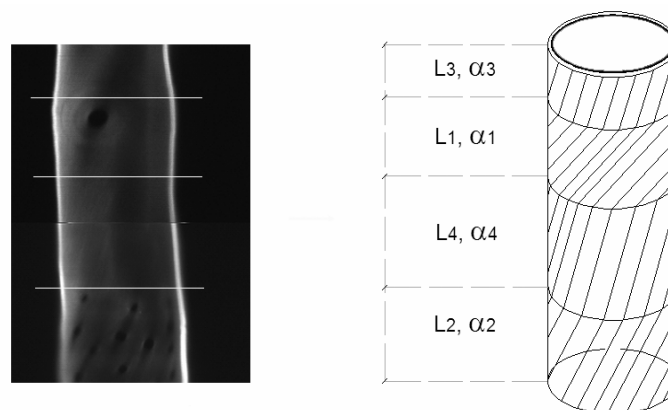
Figure 5-6 A part of an earlywood fiber and the schematic sketch of the model geometry; heterogeneities are replaced by MFA non-uniformities

Local MFAs in different segments along the fiber are different and assumed to be a set $(\alpha_1, \alpha_2, \ldots \alpha_n)$ such that:

$$\alpha_1 > \alpha_2 > \ldots > \alpha_n \qquad\qquad 5\text{-}12$$

Each α_i is assumed to be constant along the segment length, L_i belonging to the set $(L_1, L_2 \ldots L_n)$ such that:

$$L_1 + L_2 + \ldots L_n = L \qquad\qquad 5\text{-}13$$

The local Young's modulus E_i (for $i = 1,\ldots n$), as Figure 5-5 shows, is a decreasing function of the MFA, α_i:

$$E_1 < E_2 < \ldots < E_n \qquad\qquad 5\text{-}14$$

So the effective modulus of the whole intact fiber can be computed from:

$$\frac{1}{E_{eff}} = \frac{1}{L}\left(\frac{L_1}{E_1} + \frac{L_2}{E_2} + \ldots + \frac{L_n}{E_n}\right) \qquad\qquad 5\text{-}15$$

E_{eff} corresponds to the fiber effective modulus before any degradation.

5.3.2 Damage in the fiber wall

Experimental results show that the tensile strength of the fiber reinforced composites is a function of fiber direction and as Figure 5-7 shows the material tensile strength reduces with increase of the fibers angle (Tsai 1992).
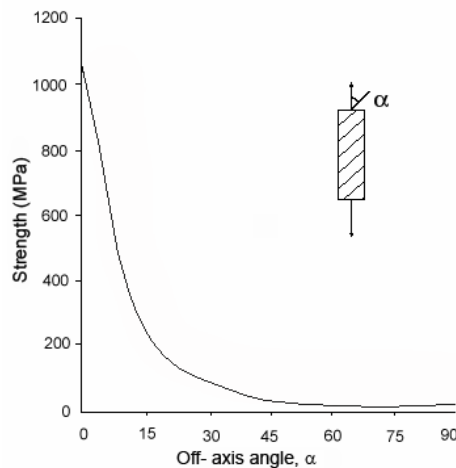
Figure 5-7 Uniaxial tensile strength of E-glass/epoxy unidirectional ply, from Tsai (1992)

Consequently in the tensile behavior of a wood fiber, the lowest tensile strength corresponds to the region with the highest MFA.

In fiber composite materials, when the fibers rigidity is much higher than the matrix rigidity, shear deformation of the matrix under tension becomes dominant and leads to the *matrix damage* (Plummer, Pittet et al. 2002). With a similar explanation, it could be assumed that the wood fiber degradation occurs mainly in the matrix of hemicellulose and lignin, not in the cellulose microfibrils.

Putting these together one can make the hypothesis that beyond the yielding point of the wood fiber material, the initiation of matrix degradation is expected in the weakest segment of the fiber, where the local MFA has the highest value.

Toward simplifying the calculation of the effect of matrix degradation on the local Young's modulus, it was assumed that matrix damage at the microstructural level is isotropic and can be defined by the following equation:

$$\sigma = (1 - \omega)E\varepsilon \qquad\qquad\qquad 5\text{-}16$$

where ω is damage parameter and $\omega=0$ indicates the intact matrix state. The damage parameter grows at various stages of the degradation and reaches to $\omega = 1$ in final failure. In this model, reduction of the matrix elastic parameters does not affect the Poisson's ratio, obeying the Kachanov isotropic damage theory (Kachanov 1986).

5.3.3 Local Young's modulus in the damaged zone

To demonstrate the influence of local damage of the matrix (while microfibrils are assumed intact) on the local longitudinal Young's modulus of the damaged segment, the stiffness coefficients of the fiber segments are recalculated after reducing the mechanical properties of matrix. Reduction of the mechanical properties of hemicellulose and lignin is a function of damage parameter, 1-ω, for ω varying from 0 to 1. Table 5-6 shows the reduced properties of the hemicellulose and lignin after 90% reduction ($\omega=0.9$). As was explained before, this reduction does not affect the Poisson's ratio.

Constituent	Coefficient	Properties after 90% damage
Hemicellulose	E_1 (GPa)	1.6
	E_2 (GPa)	0.35
	G_{12} (GPa)	0.15
	ν_{21}	0.1
	ν_{32}	0.4
Lignin	E (GPa)	0.275
	ν	0.33

Table 5-6 Reduced mechanical properties of the matrix constituents for $\omega=0.9$

In Figure 5-8 the influences of 50%, 70% and 90% reduction of the mechanical properties of matrix on the local longitudinal Young's modulus of a damaged segment are shown. $E_{L50\%}$, $E_{L70\%}$ and $E_{L90\%}$, correspond to local Young's modulus of a damaged segment for 0.5, 0.7 and 0.9 damage parameters, respectively.
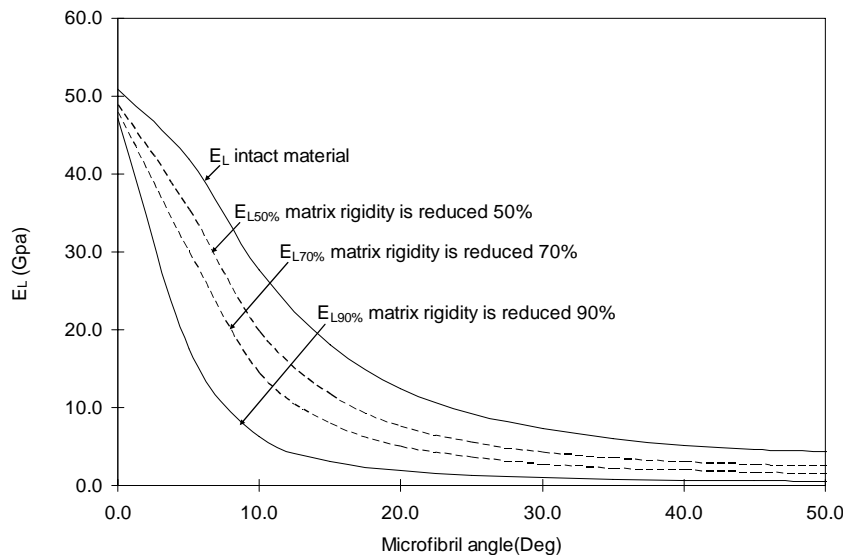
Figure 5-8 Local longitudinal Young's modulus in terms of MFAs, for intact fiber (E_L) and after reduction of the mechanical properties of matrix ($E_{L50\%}$, $E_{L70\%}$, $E_{L90\%}$)

5.4 Model of the fiber tensile behavior

It was assumed that beyond the yield point, matrix damage initiates in the weakest segment of the fiber, corresponding to the highest local MFA. To explain the occurred phenomena during damage process in the fiber microstructure, different mechanisms were suggested and the macroscopic behaviors of the fiber based on these underlying mechanisms were derived. In the first proposed scenario, it was assumed that the local MFA of the damaged zone remains unchanged and in the others, it was considered as a decreasing function of damage parameter. The main idea was illustrating the influences of local damage and reduction of local MFA on the overall behavior of the single wood fiber in tension.

Variation of local MFA in the damaged zone has two main consequences:

a) Variations of the local Young's modulus become the function of both damage parameter and MFA variation (, which is discussed in this section).

b) Generation of irreversible strains in the damaged zones (, which is explained in section 5.4.1).

Scenario 1:

After damage initiation and during damage processes which mainly occurs in the matrix of the weakest segment of the wood fiber (corresponding to the highest MFA), the local MFA remains unchanged. In this mechanism, as Figure 5-9-a shows, the local Young's modulus of the damaged segment reduces corresponding to the lines AA_1, while point A indicates the Young's modulus and MFA of the weakest segment of the fiber. Occurrence of such a mechanism leads to linear behavior of the wood fiber (see Figure 5-9-b) and its brittle failure in the segment where damage had initiated. This phenomenon indicates localized damage with no residual deformation.

(a)

(b)
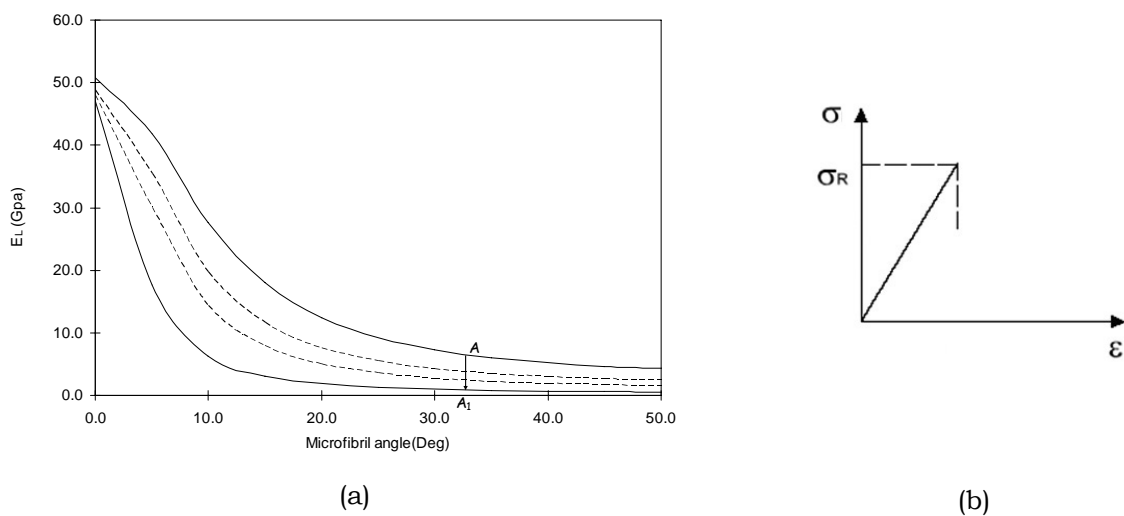
Figure 5-9 (a) Reduction of the local elastic modulus in the damaged segment of the fiber, while local MFA remains unchanged, (b) schematic representations of the linear behavior and brittle failure of the fiber

Scenario 2:

The local MFA of the weakest segment of the fiber reduces as it damages. Reduction of local MFA is such that the reduction of local Young's modulus due to matrix damage is fully recovered. Occurrence of this mechanism (reduction of local MFA in damaged zone while properties are unchanged) would be represented by the line AA_2 in Figure 5-10-a, while point A indicates the Young's modulus and MFA of the weakest segment of the fiber. In this case, the induced strains by MFA reduction are irreversible (explained in section 5.4.1) and the macroscopic behavior of whole wood fiber would be analogous to the response of a perfect plastic material with large plastic deformations and unchanged stiffness (see Figure 5-10-b).

(a)   (b)
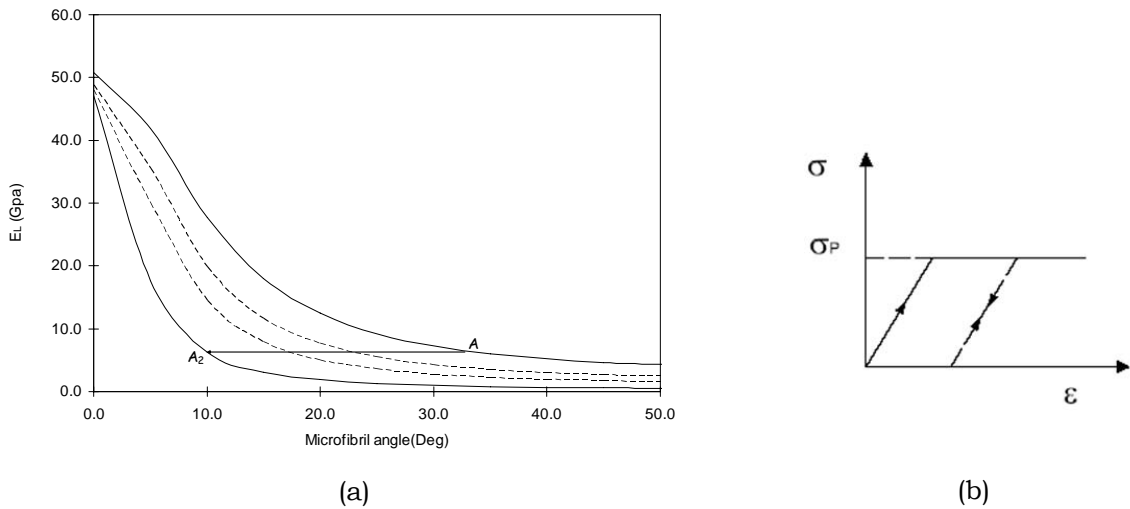
Figure 5-10 (a) Reduction of MFA in the damaged segment recovers the local reduced elastic modulus, (b) schematic representations of the fiber macroscopic behavior by elasto-perfect plasticity

Scenario 3:

After damage initiation in the weakest fiber segment, in different states of the progress of damage, local MFA and local longitudinal Young's modulus reduce simultaneously. Occurrence of this mechanism corresponds to the line AA_3 Figure 5-11-a, while point A indicates the Young's modulus and MFA of the weakest segment of the fiber. In this case, because of the irreversible strains (local MFA reduction) and reduction of local stiffness in the damaged segment, strain localization occurs and the stress-strain curve of the whole wood fiber obeys a negative hardening (strain softening) after the peak load. Schematic representation of the macroscopic behavior of the fiber, if such mechanism occurs, is as Figure 5-11-b.

(a)   (b)
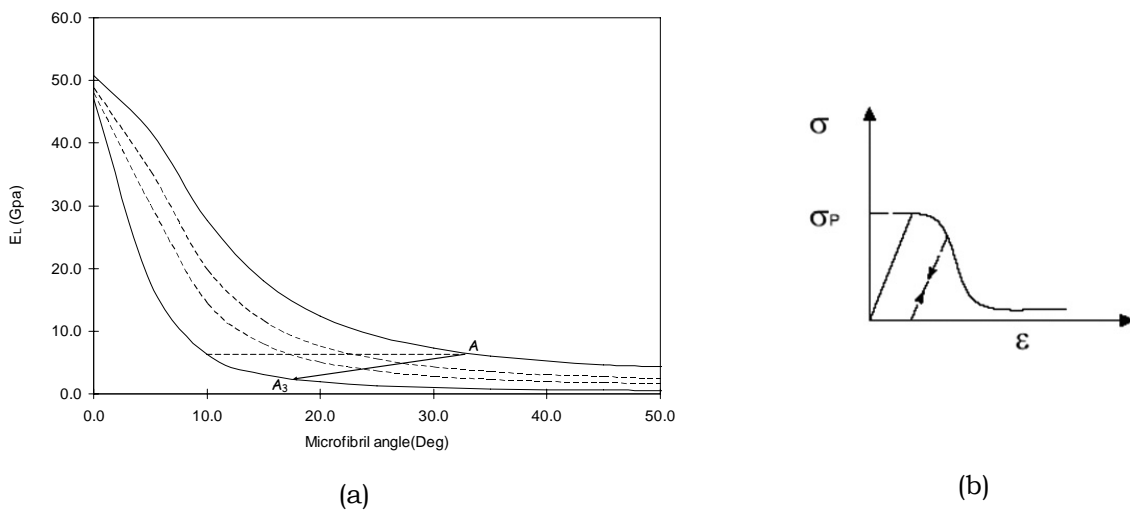
Figure 5-11 (a) Simultaneously reduction of the local elastic modulus and local MFA in damaged segment, (b) schematic representations of strain localization and softening

In all the cases above, the final failure of the wood fiber occurs in the segment where damage initiated, the weakest one and multi-damaging does not occur. Also it is important to note that the derived macroscopic behaviors of the fiber (in Figures 5-10-b and 5-11-b), based on the mentioned different mechanisms, are not similar to stress-strain curve results of tensile tests in chapter 4. These are the main shortcomings which should be overcome in the final scenario.

Scenario 4:

Increase of the effective Young's modulus and positive hardening after the yielding (assumptions of the model and experimental observations) could occur only if local Young's modulus of the damaged segment increases, which has to be because the local MFA is reduced. Occurrence of this mechanism corresponds to line AA_4 in Figure 5-12-a, while point A indicates the Young's modulus and MFA of the weakest segment of the fiber. In this scenario the initiation of incremental damage in the weakest segment of the fiber lets the microfibrils to straighten and this local reduction of MFA increases the local Young's modulus (to the Young's modulus at the point A_4). When the local Young's modulus in the weakest segment of the fiber (E_1 in equation (5-14)), increases to the modulus in the second-weakest segment of the fiber (E_2), damage can initiate in this zone too and later in the other zones until the final failure of the fiber.
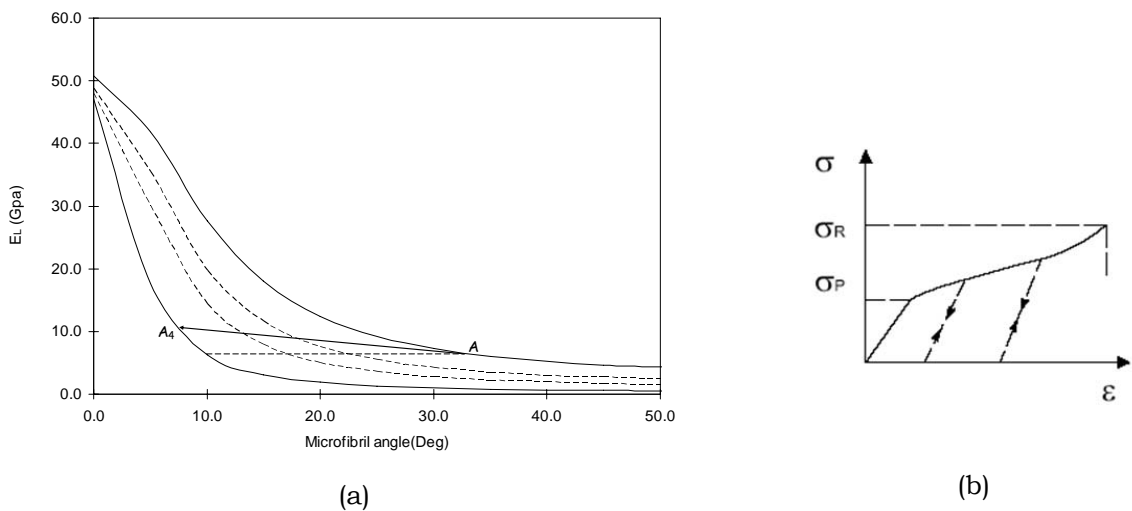
Figure 5-12 (a) Increase of the local elastic modulus and reduction of local MFA in damaged segment, (b) elasto-plasticity with positive hardening

The possibility of occurrence of successive damage in different zone of the fiber in this mechanism agrees with the in-situ observation in chapter 4, non-localized multi-damage of the wood fibers under tensile tests. Also it could explain the potential of large strains which was observed in tensile tests. The schematic macroscopic behavior of wood fibers in such

condition would be similar to Figure 5-12-b. After the yield point, the slope of the stress-strain curve remains positive and no strain softening occurs until final failure. Damage and microstructural evolution in each segment leads to increase of its local Young's modulus and effective properties. Experimental evidence of this phenomenon was shown in the results of cyclic tensile tests in chapter 4.

Simultaneous reduction of the local MFA and increase of the local Young's modulus may lead to another macroscopic behavior of fiber, a concave stress-strain curve as is illustrated in Figure 5-13-b. This behavior was observed in some of experimentally obtained stress-strain curves, especially in latewood wood tracheids, which usually possess smaller MFAs and less heterogeneity. This mechanism corresponds to variation of MFA and Young's modulus, presented with line AA_5 in Figure 5-13-a. In this case, damage in the matrix of the weakest segment permits the slipping between the microfibrils and matrix, causing in turn a reduction of local MFA. MFA reduction and sticking between the slipped elements after microfibril evolution (section 5.4.2) increase the local Young's modulus to the Young's modulus at the point A_5 (a larger value than point A_4 in Figure 5-12-a).

(a)   (b)
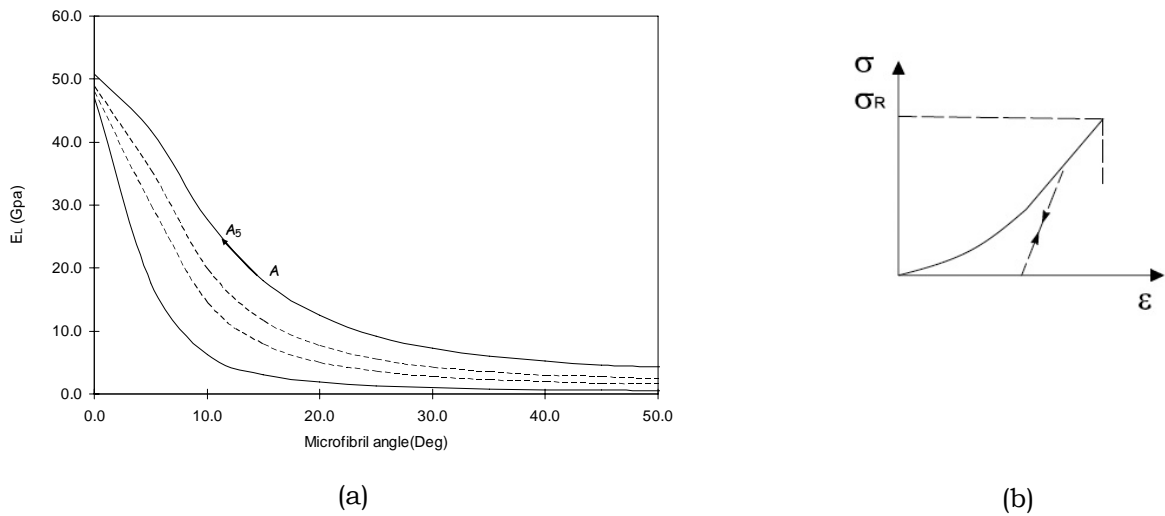
Figure 5-13 (a) Increase of the local elastic modulus and reduction of local MFA in damaged segment, (b) concave stress-strain curve

5.4.1 Irreversible strains

Cyclic tensile tests in chapter 4 showed that beyond the yield point, the fiber undergoes large and mainly irreversible deformation. The total strain of the fiber, after the yield point could be explained by:

$$\varepsilon_t = \varepsilon_e + \varepsilon_\alpha \qquad\qquad 5\text{-}17$$

where ε_e and ε_α are the elastic and irreversible strains respectively. Reduction of local MFAs in damaged zones leads to generation of irreversible strains in fiber. Figure 5-14 shows a segment of the modeled fiber before and after MFA reduction.
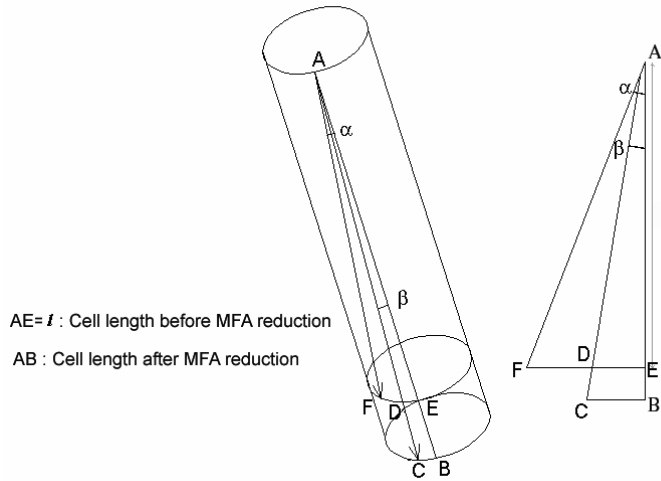
Figure 5-14 Schematic representation of MFA reduction and the induced elongation

In this figure $AE = l$ is the length of the intact segment and α is its local MFA. If the length of the fiber segment is elongated to AB, AF is moved to AC (AC=AF, the length of cellulose microfibril is constant) and MFA is reduced from α to β. Consequently the residual strain due to MFA reduction would be:

$$\varepsilon_\alpha = \frac{BE}{AE} \qquad\qquad\qquad 5\text{-}18$$

Replacing the *BE* and *AE* equivalents in Equation (5-18), the residual strain ε_α is calculated from the following equation:

$$\varepsilon_\alpha = (\frac{\cos\alpha}{\cos\beta} - 1) \qquad\qquad\qquad 5\text{-}19$$

Equation (5-19) shows the importance of the induced strains by MFA reduction, on the macroscopic tensile behavior of the whole wood fiber. The irreversible strain due to MFA reduction in a fiber segment with small MFA is smaller than in a fiber segment with high MFA. Figure 5-15 shows that reduction of local elastic modulus (due to damage) in a segment with small local MFA is recovered by a smaller angle reduction than in a segment with large MFA. For example, the MFA of a segment with local MFA of point B, is reduced to B' (MFA changes from 14° to 4°) while in a segment with local MFA of point A, is reduced to A' (MFA changed from 33˚ to 7.5˚). Based on Equation (5-19), the residual strain due to MFA

reduction in the fiber segment with MFA of point B, is 2.8% and in fiber segment with MFA of point A is 18.2%.
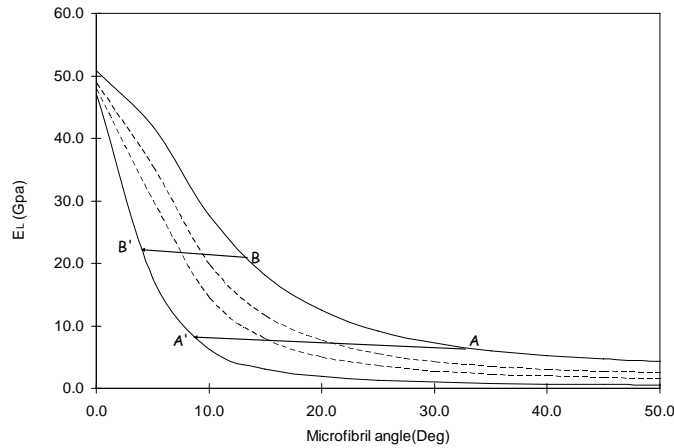
Figure 5-15 Reduction of local elastic modulus in a segment with small local MFA is recovered by a smaller angle reduction than in a segment with large MFA

5.4.2 Other mechanisms

The other model which has been developed to explain the elastic-perfect plastic macroscopic behavior of compression wood fibers under tensile loading is that of Keckes et al. (2003). As in their cyclic tensile tests, the stiffness of the fibers did not decrease, they assumed that the shear relaxation *does not damage* the matrix (Keckes, Burgert et al. 2003; Fratzl, Burgert et al. 2004) and consequently the MFA reduction does not occur. In this model, as neither damage nor MFA reduction are occurred, the material properties remain unchanged. The residual tensile strains of fibers were attributed to the permanent shear relaxation of the matrix and slipping-sticking between matrix and cellulose microfibrils. They assumed that at a certain shear stress level, bonds between the matrix and cellulose microfibrils disentangle, followed by a flow in the matrix material and entangle again when stress is released.

In fact in the fiber wall ultrastructure, a *limited* intracrystalline tensile deformation could take place by slipping-sticking between the cellulose microfibrils and the amorphous matrix (Navi, Pittet et al. 2002). Slipping-sticking mechanism without MFA reduction leads to an elastic-perfect plastic macroscopic behavior (see Figure 5-10-b), only for a limited strain rate and the potential of large strains (up to 20% in tensile tests in chapter 4) can not be explained by this model. Also it cannot explain the non-localized damage phenomenon which was in-situ observed in the tensile tests.

From this discussion one can conclude that the slipping-sticking without MFA reduction cannot be the main governing mechanism in the fiber tensile behavior although it could be

considered as a contributing phenomenon which helps the high strain rates of wood fibers. What might occur after the yielding of the wood fiber are both mechanisms: successive degradation of the matrix in the weak zones which allows the reduction of MFA and slipping-sticking.

5.5 Concluding remarks

In this chapter a model was developed to explain the mechanism involved in the tensile behavior of the wood fibers at micro level. The developed model was successful in explaining the three different types of behavior: linear, concave and segmented tensile stress-strain curves. Two important aspects of wood fiber microstructure were considered in model:

- Microstructural heterogeneities, which cause some segments of the fiber to be weaker in initiation and growth of local damage above a given force limit.

- Possessing the helically oriented microfibrils that allows the MFA to be reduced in the damaged zones.

The influence of successive (isotropic) degradation of the matrix on the longitudinal Young's modulus of the fiber wall was shown and different probable mechanisms, which might occur during damage, were discussed. These discussion coupling to the experimental evidences, led us to suggest that microfibrillar evolution and multi-damage are the main governing phenomena in tensile behavior of wood fibers. The linear stress-strain domain for a fiber with non-uniform MFA is governed by the lowest force level corresponding to the highest MFA. Beyond this level, damage initiates in the matrix of the weakest segment and in turn, leads to decrease of the MFA in the damaged zone. Depending on the local MFA size as well as the damage state, the generated irreversible strain could be significant or small. Furthermore, increase in the applied forces results in growth of the tensile damage in matrix and further MFA reductions, which is accompanied by recovery and increase of the stiffness in the damaged segment. This process leads to the possibility of damage initiation in the other weak segments and multi-damaging phenomenon. It was explained that the experimentally observed large strains and multi-damaging phenomenon cannot be explained by only the slipping-sticking model, although it could be considered as an involving mechanism in microstructural evolution of the fiber wall.

Successive damage with accompaniment of local MFAs reduction and local stiffness increase make the fiber more *homogeneous*. This might be the responsible of the high slope of the experimentally obtained stress-strain curve (third segment) before failure.

Chapter 6   Mixed lattice-continuum model to study the wood fracture at fiber level

6.1 Wood fracture mechanics, heterogeneities and microstructure

Wood has a heterogeneous structure at both micro and macro levels. Heterogeneities, such as within fiber defects and MFA variations, differences in geometry and arrangement of earlywood and latewood fibers, ray cells and knots affect the mechanical properties and fracture behavior of wood in different directions and in different samples. Consequently, to investigate the mechanism of wood fracture at the cellular level, the influences of morphological features and heterogeneities on fracture should be considered.

The orthotropic nature of wood gives it six main orientations of crack plane in three principal growth axes. These crack orientations are denoted by RL, LR, LT, TL, TR and RT and are presented in Figure 6-1. The first index in the notation of orientation specifies the direction perpendicular to the plane of the crack, and the second index specifies the direction of crack extension. Considering the three modes of fracture[3] for each crack orientation, 18 basic fracture situations are identified.

For a long time, different approaches such as microscopic observation of the fracture surface, experimental measurements of the fracture parameters and modeling have been implemented to study the mechanism of wood fracture in relation to its morphological features. The grain direction is one of the most influential structural features in wood fracture mechanics. It has been shown that the fracture toughness in LR and LT orientations is usually six or seven times higher than RL, TL, RT and TR fracture orientations (Schniewind and Barrett 1969). The other structural feature which has a dominant influence on wood fracture behavior is the cell size: the different diameters and thicknesses in earlywood and latewood fibers (Boatright and Garrett 1983).

---

[3] Mode I; the opening mode, Mode II; the in-plane shear mode and Mode III; the perpendicular-to-plane shear mode
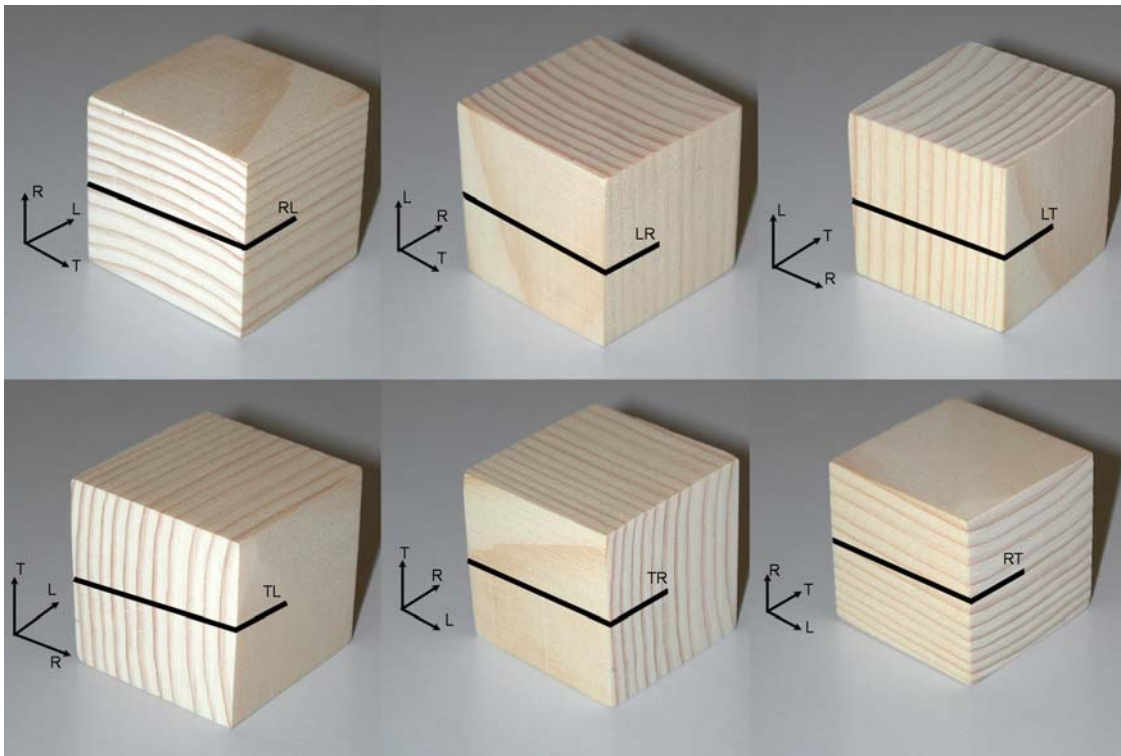
Figure 6-1 Different fracture orientations in wood, R, T and L indicate radial, tangential and longitudinal directions

Mode I, RL and TL orientations:

Differences between geometry and arrangement of earlywood and latewood fibers induce different fracture behavior to wood in TL and RL fracture orientations (Job L. Navi P. 1996; Navi and Sedighi-Gilani 2006). Microscopic observation of fracture surface, with CLSM showed that in Mode I fracture in RL orientation, the first crack is located along a line in earlywood while in fracture in TL orientation crack begins in the latewood (see Figure 6-2). Also these figures show that crack propagation in the RL orientation consists of intercellular separation of cells and intercellular break of the cell walls. In the TL orientation, the crack is propagated at the interfaces between S_1 and S_2 or in the middle lamellae. A schematic representation of intracellular and intercellular fracture model is shown in Figure 6-3.

Mode I, RT and TR orientations:

Further in-situ studies by CLSM showed two different fracture mechanisms that involve in the crack propagation in RT and TR directions (Dill-Langer, Lütye et al. 2002). These different fracture mechanisms are rupture of earlywood cell walls in the case of crack propagation in the tangential direction and rupture of the interface zone between adjacent fibers in the case of crack progression in the radial direction (see Figure 6-4).
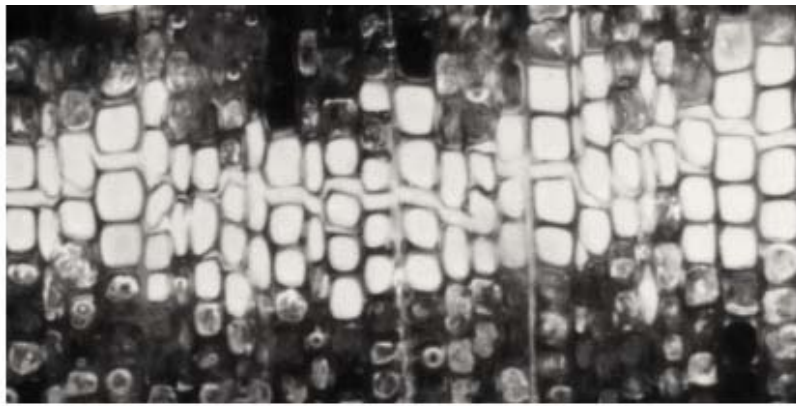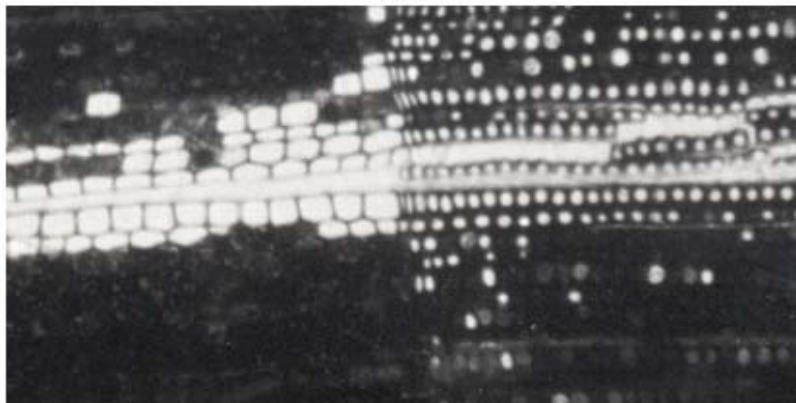
Figure 6-2 Crack pattern in Mode I fracture in the RL and TL orientations; (a) in the RL orientation crack propagation initiates in earlywood, (b) in the TL orientation cracking initiates in latewood (Job L. Navi P. 1996)
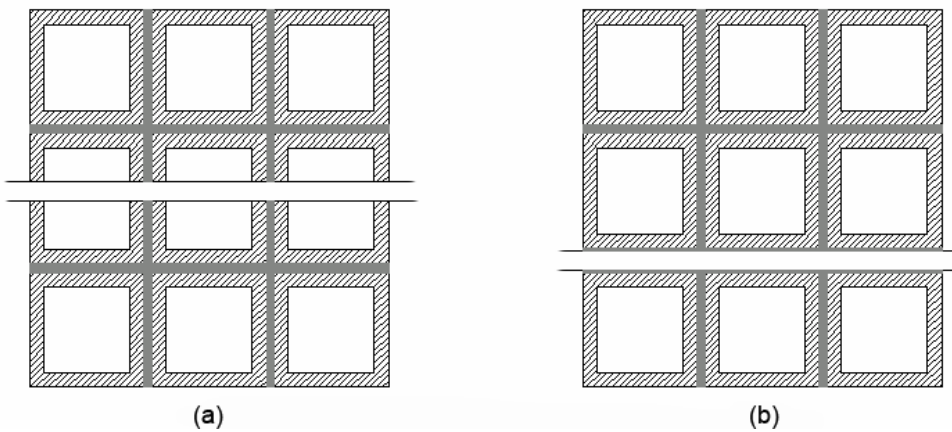
Figure 6-3 Intracellular (a) and intercellular (b) fracture
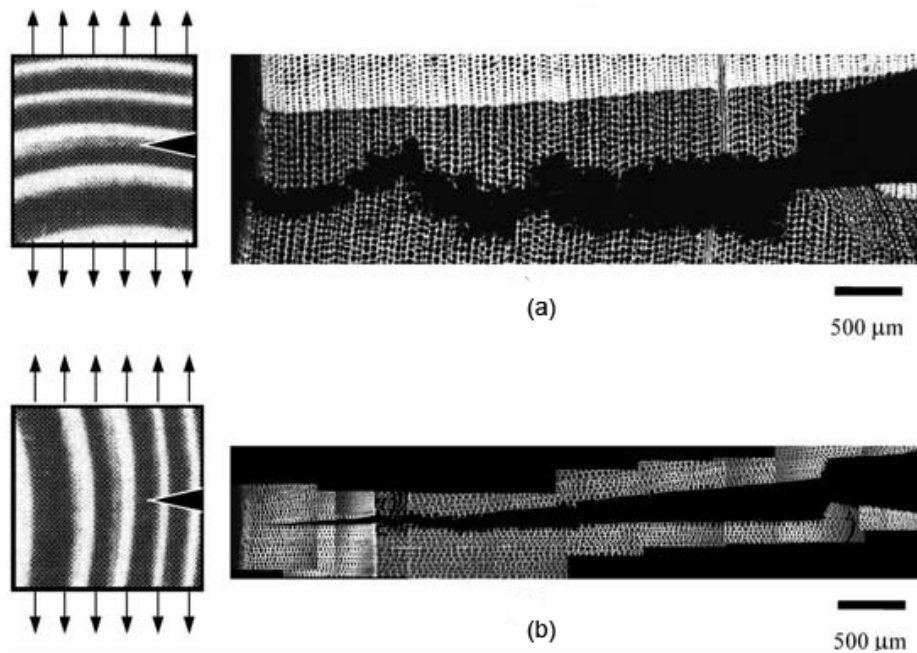
Figure 6-4 Crack pattern in Mode I fracture in RT and TR orientations, (a) in RT orientation crack propagates in earlywood cell walls, (b) in TR orientation crack propagates along the interface between adjacent fibers (Dill-Langer, Lütye et al. 2002)

Other in-situ observations of crack propagation and network of microcracks at wood micro-level (by using scanning electron microscopy) showed that bridging behind the crack tip is the main toughening mechanism in wood fracture which contributes to its non-linear behavior (Vasic S. Smith I. Landis E. 2002).

The *microscopic ob*servation of fracture surface has been a great help to understand the mechanisms of crack propagation in wood in relation to microstructural heterogeneities, although the application of *micromechanical approach* in *modeling* the wood fracture is in the preliminary steps. There are few attempts to consider the wood heterogeneities in the linear or non-linear continuum-based fracture models (Cramer and Goodman 1986; Cramer and Fohrell 1990; Holmberg, Persson et al. 1999). However, due to the difficulties of considering the wood heterogeneities in a continuum-based model, the introduced heterogeneities to these models were simplified and prevent the models from showing the major observed phenomena in microscopic observations and experiments. It indicated that the continuum framework is not the best choice to take into account the discrete and highly heterogeneous nature of wood.

6.1.1 Lattice approach to model the wood fracture

Compared to the continuum-based fracture models, the morphology based model, i.e. *lattice model* might be an appropriate approach to study the wood fracture at micro level. There is no doubt that the lattice fracture model differs from the theory of continuum fracture

mechanics and is far from its concepts. But the potential of a lattice model in considering the *porous* and *heterogeneous* structure of wood makes it an appropriate tool in studying the wood fracture behavior at the fiber level (, which is still difficult in continuum fracture modeling). Lattice fracture model is well adapted to map the ordered anisotropic microstructure of wood. The other advantage of lattice model is the simplicity of the physical interpretation of the fracture state in each step of the solution. These advantages make the lattice fracture model an interesting approach to study the mechanism of wood fracture at cellular level.

The main idea of lattice model is simulation of the material structure and mechanical properties by construction of a network of interconnected discreet line elements. The defined network can be two-dimensional or three-dimensional and has a random or regular structure.

This approach was first developed to study the theory of elasticity (Hrennikoff 1941). Later lattice model was used in modeling the fracture process by removing the elements reaching a strength criterion at different loading steps. Schlangen and VanMier were one among of the first who used the lattice fracture model in concrete, aiming to simulate the quasi-brittle material behavior (Schlangen E. Van Mier J.G.M. 1992). In their model, beam elements were chosen in such a way that they represented the different phases of heterogeneous materials (aggregates, matrix and interfaces). After that, the lattice fracture model was applied for several years in analyzing concrete and sandstone fracture. All these studies confirmed that lattice fracture model is successful in predicting the influence of material microstructure on the pre-peak and softening behavior of force-displacement curve and crack propagation paths (VanMier 1996; Schlangen and Garboczi 1997; VanVliet 2000; Prado and VanMier 2003).

Recently, the lattice model has been used in studying the Mode I fracture in different crack orientations in wood; RT and TR orientations (Wittel, Dill-Langer et al. 2005)and RL orientation (Landis, Vasic et al. 2002; Landis E. Davids W.G. Parrod P. Vasic S. 2003). These two-dimensional lattice fracture models showed the convenience of this model to simulate the force-displacement curves and crack patterns of wood samples. Lattice model can be used in analyzing the fracture at different level of structure, from micro to macro level. In the developed models by Landis et al. (2002), wood fracture was simulated at the growth ring level while each wood bundle was represented by a lattice element. Heterogeneities were introduced in the model by assigning different stiffness and strength to the lattice elements. Figure 6-5 shows that the results of their model agreed with the results of fracture tests in small softwood samples (Vasic S. 2000).
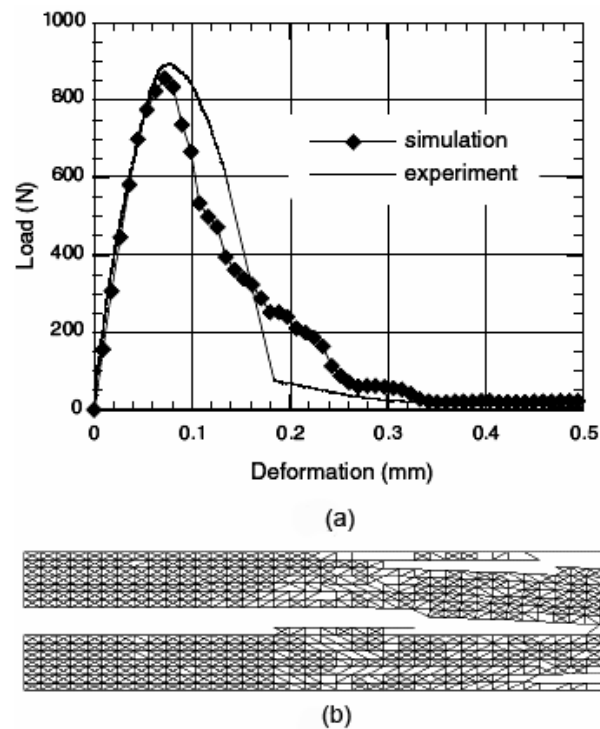
Figure 6-5 (a) Comparison of two-dimensional lattice simulation and experimental load-displacement curve for a 20 x 4 x 20 (length, width, thickness) spruce sample, (b) fracture pattern in lattice, (Landis *et al.* 2002)

Application of this approach to a model with a more detailed geometry (for example at the cellular level) can help investigate the mechanism of wood fracture at smaller scales. Another reason, which encourages the application of a more detailed geometry with a finer mesh, is improving the accuracy of results. Dependence of the peak load and post-peak behavior of the modeled material on the mesh fineness is one of the negative points of the lattice fracture model. Consequently, using a finer mesh and more detailed lattice leads to getting more accurate results.

In this chapter, a method for developing a three-dimensional lattice model for the study of the Mode I fracture in a small softwood sample in RL orientation is explained. Working on a three-dimensional geometry allows monitoring the crack propagation paths in all directions. To be able to study the fracture behavior at cellular level, the defined lattice elements should have the arrangement and size of the wood fibers, earlywood and latewood fibers and their bonding medium.

The number of elements needed to define the three-dimensional geometry of the lattice at the cellular level is quite large. To reduce the number of needed elements for such a fine mesh, a mixed technique based on coupling the lattice and continuum medium is used. For this purpose, the critical regions of the specimen where crack propagation is more probable

82

are modeled by introducing a fine lattice mesh while the other regions are considered as a continuum.

6.2 Lattice geometry

The lattice network, which represents the wood material, should have a prescribed arrangement similar to that of wood structure. Because of the computational limits, copying all the aspects of the real wood microstructure in the lattice geometry is still difficult. On the other hand, if the structure of material has essential differences with the replaced lattice geometry, the simulation results are affected by these differences. Consequently, the constructed lattice should contain different elements which can perform the role of the main elements of wood microstructure. It is assumed that the most critical parts of the wood microstructure in fracture of a small wood specimen in RL and TL orientation are the fibers, the bonding medium between the fibers (with lower mechanical properties than fibers) and the heterogeneities at the micro-level.

The wood fibers in a lattice are represented by a series of parallel beam elements whit the beams centers placed in the center of the cell lumens (see Figure 6-6). Also the bonding medium between the fibers is represented by ordered diagonal and vertical beam elements. In section 6.4 it is explained how the characteristics of these elements should be defined to make the overall lattice properties similar to those of a wood specimen.
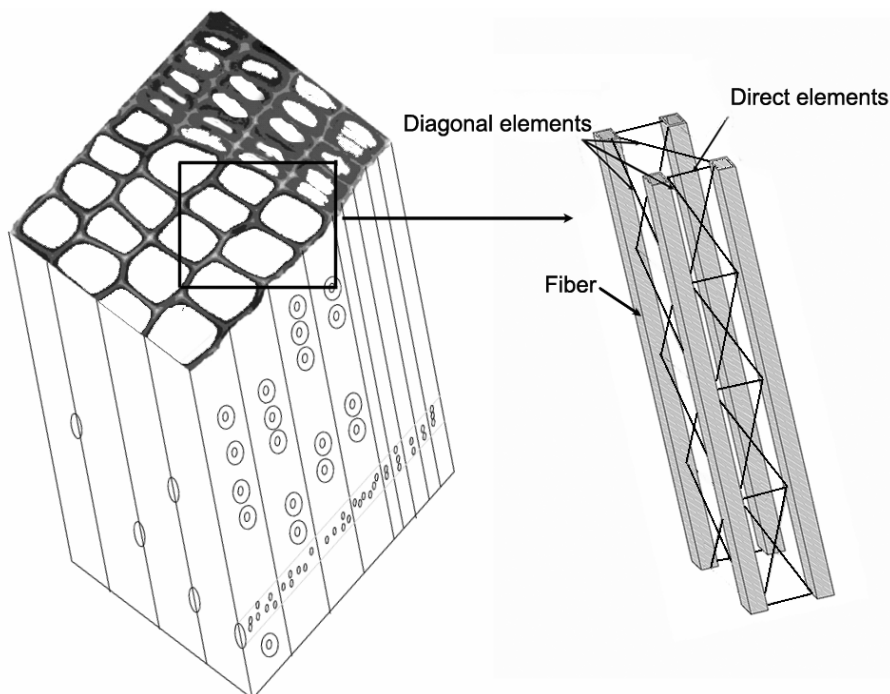
Figure 6-6 Lattice geometry at cellular level is defined by beam elements which represent the wood fibers and are connected by diagonal and direct beam elements simulating the bonding medium

Earlywood and latewood growth rings are introduced in the model geometry by assigning different geometrical and mechanical properties to the elements which represent their fibers. In Figure 6-7, the perspective of a three-dimensional lattice with two growth rings of earlywood and latewood fibers is shown. To consider the other heterogeneities and defects in model, it is assumed that different lattice elements have different strengths. The method to assign different strengths (failure criteria) to elements is explained in section 6.5.
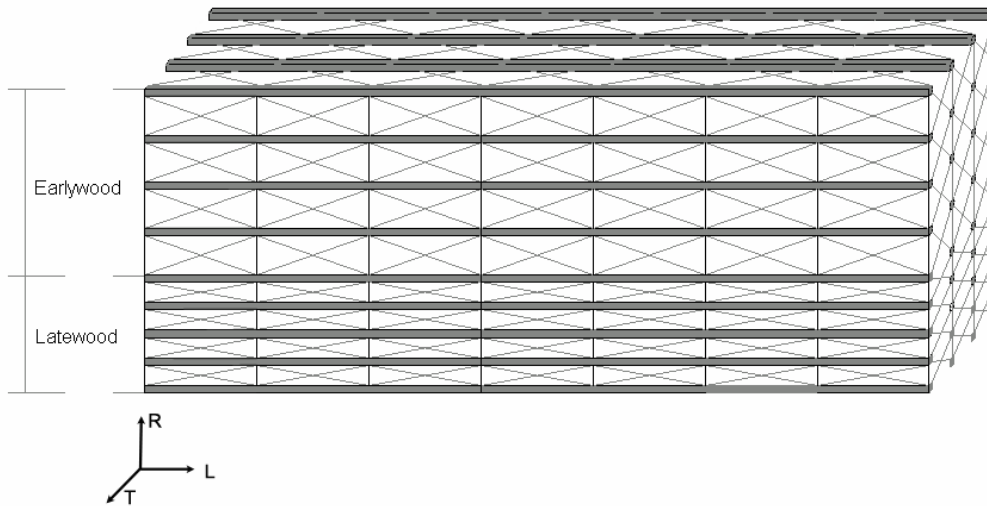
Figure 6-7 Three-dimensional lattice geometry; each horizontal element represents an earlywood or latewood fibers

6.2.1 Lattice elements type

The conventional basic elements in the lattice model are one-dimensional line elements such as beam, bar or spring. In Figure 6-8 these elements with their reaction forces are shown.

(a)   (b)
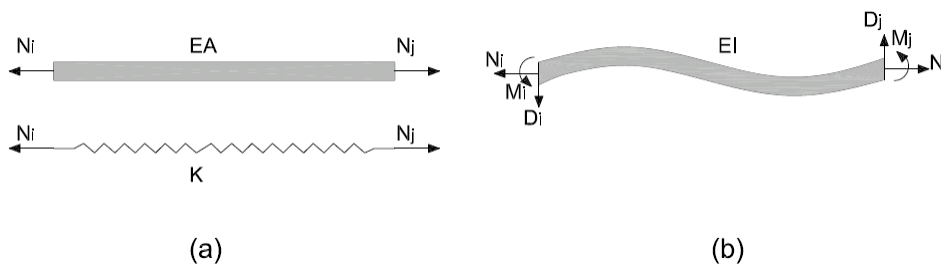
Figure 6-8 One-dimensional line elements which could be used in lattice model; (a) bar and spring elements with only normal force as reaction, (b) beam element with normal forces and moments

Beam elements are defined by their flexural stiffness (EI) whereas for the bar elements, the axial stiffness (EA) and for the spring elements, the spring constant (K) must be specified. Each type of element, depending on the number of degrees of freedom at its end points, gives different characteristics to the lattice.

84

Bar and spring elements with less degrees of freedom than beam elements are computationally less expensive and thus faster. Fracture simulations for the lattice of bar elements with our predefined geometry showed that the bar elements are not appropriate. The problem was the loss of the lattice coherence when elements were fractured (i.e. removed) during the simulation. The undesirable distortion of a part of the lattice in this case and matrix singularity after few loading steps made the lattice model inefficient.

On the other hand, a comparative study on a developed model for concrete has shown that the crack patterns in a lattice of beam elements are closer to the experimentally observed crack patterns than in a lattice of bar elements (Schlangen E. Garboczi E.J. 1996).

As a result, the *beam element*, as the basic element type in lattice, was chosen.

6.2.2 Mixing the lattice and continuum medium

To discretize a wood sample to a lattice with a mesh as fine as wood cellular structure, the number of used elements would be large. To reduce the model computational costs, for two dimensional models of concrete fracture, a mixed technique has been developed which is based on coupling the lattice and continuum medium (Bolander, Shiraishi et al. 1996; VanVliet 2000). This solution reduces the number of used elements and CPU time.

To use such a method, the crack path should be predicted at each step of analysis (as it advances) and the region close to the probable crack trajectory should be modeled as a lattice while the other parts are modeled as a continuum.

This method is more convenient in modeling the wood fracture, as the crack path in wood is approximately predictable. Wood microstructural formation, parallel fibrous structure connected by a bonding medium with considerably lower mechanical properties, makes natural weak planes in wood. It is confirmed by experiments, such as measurements of fracture toughness in different directions. Schniewind and Centen (1973) have shown that the fracture toughness in RL, TL, RT and TR fracture orientations is six or seven times less than LR and TL fracture orientations. From this, one can conclude that cracks have the tendency to propagate on these weak planes. For example as Figure 6-9 shows, in Mode I fracture in RL orientation, cracks propagate in the LT plane and it has been shown that the width of propagation of cracks, parallel to the fiber orientation, is predictable and does not exceed more than few growth rings (Mindess and Bentur 1986).

As the width of the region where crack trajectory is expected is quite predictable, this region in front of the notch could be modeled using lattice elements while the remaining parts are modeled as a continuum with a coarser mesh. It is assumed that no cracks exist in the continuum medium.
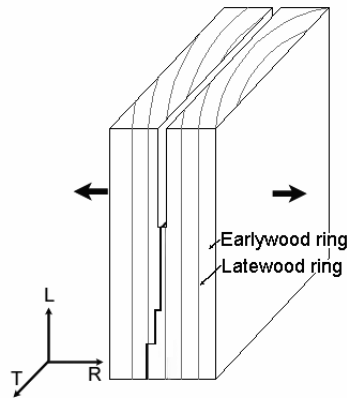
Figure 6-9 Crack trajectory in weak plane in Mode I fracture in RL orientation

6.3 Geometry of specimen and boundary conditions

The simulation results should be validated by comparing them with the results of experimental fracture tests. Consequently the model geometry should have the same dimensions as the tested specimens.

Direct tension fracture tests, comparing to the other fracture testing methods, could show the *real* material behavior as it eliminates the undesirable effect of bending moments due to boundary conditions (VanMier 1996). The problem of direct tension fracture testing is the difficulty of providing fracture stability (Vasic S. 2000).

Fracture stability:

The fracture test is unstable when the variation of energy release rate[4] for a given crack length is higher than variation of material resistance to crack extension (Anderson 1994). In Figure 6-10 the schematic representation of fracture instability is shown. As this sketch shows, in fracture instability, the load suddenly reduces from one value to another.
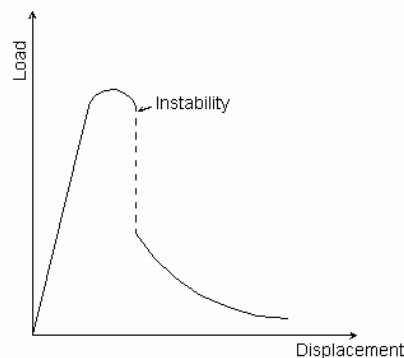
Figure 6-10 Schematic representation of fracture instability

---

[4] Measure of the energy available for an increment of crack extension

The conditions which prevent the fracture instability are discussed by many researchers. Stability of fracture test is affected by different parameters such as boundary conditions and experimental set up, specimen geometry and material properties (Boström L. 1992; Wang 1994).

In direct tension fracture test, an increase of the stored strain energy in the specimen during the test can lead to unstable fracture. In other words, the amount of internally stored energy should be minimized to provide the stability of the fracture test. One of the main controlling parameters to minimize the stored energy is the specimen geometry and size. Smaller wood specimens show more stable behavior in fracture tests. One of the successful stable direct tension fracture tests in literature are the presented result for a notched spruce specimen of 20 x 4 x 20 mm³ (length, width, thickness) by Vasic (2000).

The simulation results by mixed lattice-continuum fracture model are validated by comparing to Vasic's experimental results. For this purpose the width and height of the model geometry were defined similar to the dimensions of the tested specimens. Only the thickness (in the T direction) was reduced to 1 mm (from 20 mm) to reduce the computation time. The defined dimensions of the model geometry are shown in Figure 6-11.
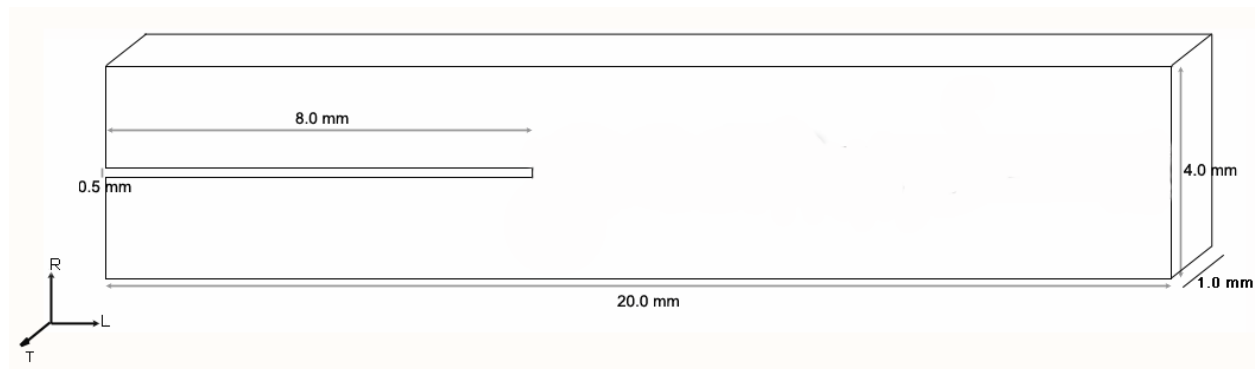
Figure 6-11 Chosen dimensions for model geometry

A volume of 12 x 1 x 1 mm³ (length, width, thickness) in front of the notched was modeled as a lattice of beam elements while the other parts were considered as a continuum and were meshed with solid elements. The length of the lattice was defined as 12 mm to cover all the length of the specimen minus the notched depth. A better solution for reducing the number of elements is modeling a volume with smaller length with lattice and updating the position of lattice in model geometry when the fracture advances. However in this model, for simplification, a fixed width was defined.

The defined lattice contained different beam elements which represent the alternations of earlywood and latewood fibers and bonding medium. Although the dimension of the model geometry in T direction is less than the experimental specimens, the number of elements

87

which represent the wood fibers in depth is sufficient to show the crack trajectory in RT plane. Figure 6-12 shows the model geometry in LR plane and the dimensions of the lattice in front of the notch.
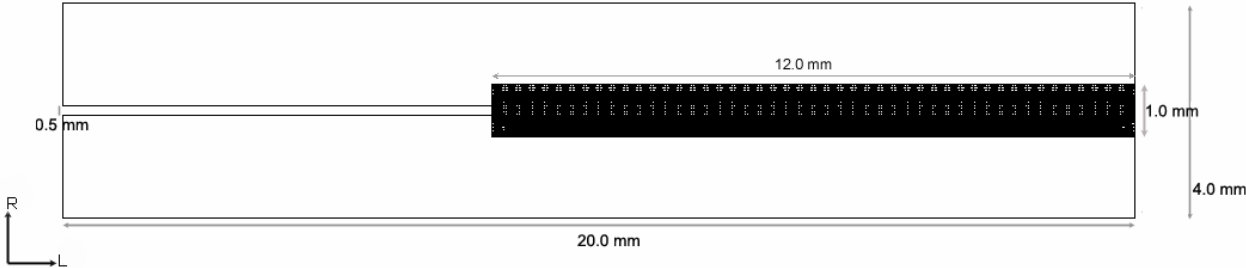
Figure 6-12 Mixed model geometry; a volume of 12 x 1 x 1 mm³ (length, width, thickness) in front of the notched is represented by lattice

The number of elements needed to construct the whole model geometry was 312750, of which 289550 of them were used for the lattice. In Figure 6-13 the three-dimensional view of the model geometry is shown.
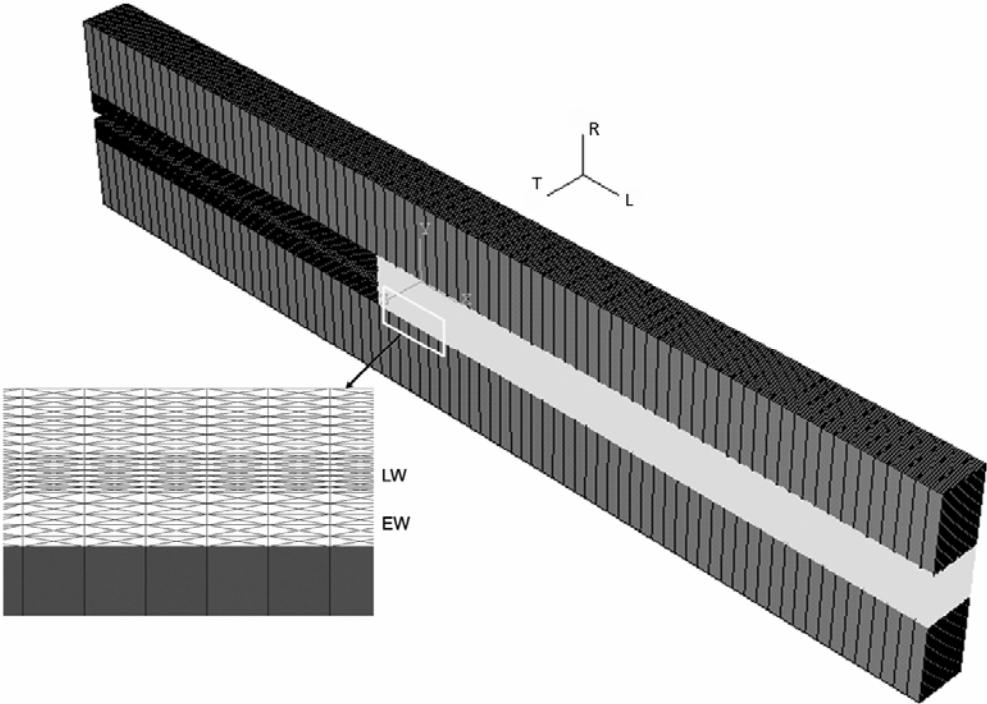
Figure 6-13 Perspective of the studied wood sample; LW and EW represent latewood and early-wood fibers band respectively

As this figure shows, beam and solid elements have common nodes at the interfaces between lattice and continuum. Beam elements have six degrees of freedom per node: translation in the nodal L, R, and T directions and rotation about the nodal L, R, and T axes. The

solid elements of the continuum mesh on the other hand have only three translational degrees of freedom at each node. To guaranty the compatibility of the interactions at the interface nodes between beam and solid elements, the work done at interfaces should be equated. For this purpose, it is easy to use the facilities of ABAQUS finite element code, which was used for numerical calculation of this model, to tie the degrees of freedom of the interfaces nodes between the lattice beam and continuum solid elements. For example Monaghan et al (1998) used the *EQUATION command of ABAQUS to equate the displacements of the three-dimensional continuum nodes on the interfaces to the twisting rotations and displacements of the beam nodes (Monaghan, Doherty et al. 1998; Hatfielda and Fukushimab 2005).

In this model, the Mode I fracture in direct tension fracture testing (uniaxial loading condition) is investigated and no rotation occurs in the beam interfaces nodes. Consequently the results remained the same whether the rotational degrees of freedom of beams were tied or not.

To compare the modeling and the experimental results, the prescribed boundary conditions of the model should reflect the experimental set up of the fracture tests. In direct tension fracture tests, the sample is mounted in the fracture test machine by gluing its sides to the stiff surface of steel clip gages, while the load is applied to the steel beam above the specimen. Thus the applied load on the surface of the specimen is a uniform tensile load.

To simulate this experimental set up, in each loading step a uniform vertical displacement (in R direction) is applied to the upper surface of the specimen while other displacements and rotations in both the upper and lower surfaces are fixed. In Figure 6-14, the boundary conditions applied to the model are shown.
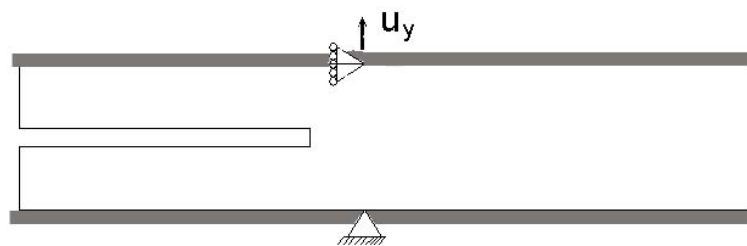
Figure 6-14 Defined boundary conditions, similar to the direct tension fracture test set up

6.4 Lattice mechanical properties

The defined lattice should represent the wood continuum and its effective mechanical properties should be similar to the experimentally obtained mechanical properties of wood. It allows comparing the results of the fracture tests and of the simulations. Moreover, to be

able to use the mixed lattice-continuum model, consistency between the effective properties of the lattice and the assigned mechanical properties to continuum is necessary.

In this part, the role of different sets of elements in lattice structure and method to calculate the properties of each lattice element set are explained. The aim is to adjust the calculated properties of the lattice to the experimentally obtained properties of wood by using an iterative approach. Different flexural stiffnesses are assigned to different beam element sets of the lattice to fit its calculated effective properties and the experimentally obtained mechanical properties of wood.

6.4.1 Different beam element sets of lattice

The three-dimensional lattice of beam elements in this model is defined by considering of five different element sets; *earlywood, latewood, direct, S-diagonal* and *L-diagonal* beams.

Earlywood and latewood beam sets:

Each wood fiber is represented by a beam element of length 1 mm which is placed in the center of the fiber lumen. To show the difference between earlywood and latewood fibers, different properties and cross sectional areas are assigned to the beam elements which represent earlywood or latewood fibers.

As the beams should be placed in the center of the fibers lumens, the distances between the longitudinal axes of the beams are dependent to the cross-sectional dimensions of the fibers. In this model as Figure 6-15 shows, the distance in the R direction is assumed to be 40 μm between the earlywood fibers and 20 μm between the latewood fibers. Also in the T direction this distance is assumed to be 40 μm.
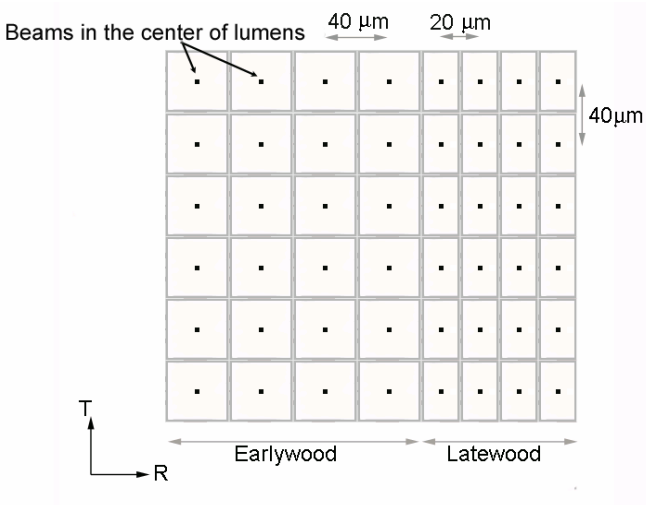
Figure 6-15 Distance between earlywood and latewood beams which are placed in the center of fiber lumen

The assigned cross sectional area of each earlywood and latewood beam set was defined based on the wood microstructure in Figure 6-16. The assigned cross sectional dimensions in latewood beams were considered to be 20 x 40 µm (in R and T directions respectively) with a thickness of 6µm. In earlywood beams, the assigned cross sectional dimensions were considered to be 40 x 40 µm with a thickness of 2µm.
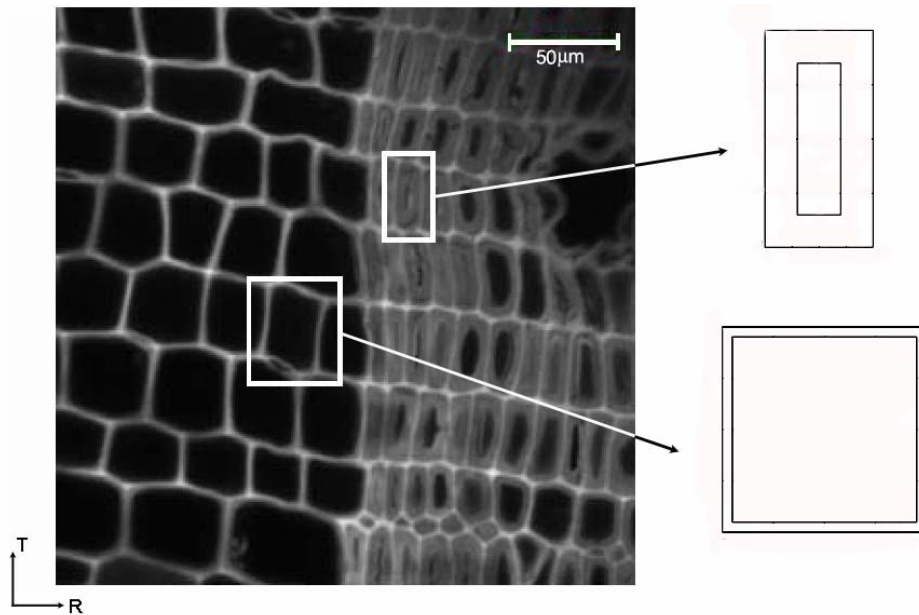
Figure 6-16 Cross sectional dimensions of earlywood and latewood beams which are used in the model are based on the wood microstructure

Diagonal and direct beam sets:

Series of diagonal and direct beam elements connect the earlywood and latewood beams together. These elements represent the bonding medium between the wood fibers. In Figure 6-17 the order of these elements in the prescribed lattice geometry is shown.
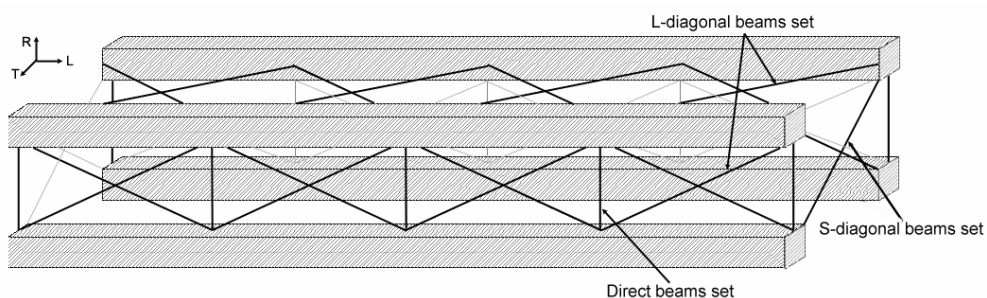
Figure 6-17 Diagonal and direct beams sets represent the bonding medium between the wood fibers

There are two series of diagonal beam elements in the lattice structure. One set includes those short diagonal elements which connect the fibers in the RT plane, the S-diagonal

beams set and the other the longer diagonal elements which connect the fibers in the LR and LT planes, the L-diagonal beams set. Direct beam elements are the vertical beams which connect the fibers in the R direction.

Each element set of lattice has a predefined function in its structure. Knowing the role of the different element sets helps the iterative process of section 6.4.2 to converge more quickly to the appropriate lattice properties. For example the role of earlywood and latewood beam sets is not critical in determining the transversal and shear properties of the lattice. On the other hand shear properties of the lattice are mainly provided by diagonal (S-diagonal and L-diagonal) beam elements. For example the shear moduli in LR and LT planes are mainly defined by the flexural stiffnesses and the orientation of the L-diagonal elements in relation to the axial direction of the fibers (L direction). Two element sets are involved in determining the lattice transversal property in the T direction: S-diagonal beam elements and L-diagonal beams in the LT plane. Also the lattice transversal property in the R direction is provided by direct beam elements (which could represent the ray cells) and L-diagonal beams in the RL plane.

ν, the Poisson's ratios of the lattice in general depends on the shape of the lattice structure, the cross section of the beams and the elastic properties of the beams (VanMier 1996). In a regular triangle lattice of beam elements (with unit thickness), which is elastically isotropic, Poisson's ratio can be analytically derived by evaluating the elastic energy of a unit cell of the lattice under a uniform strain (Schlangen and Garboczi 1997):

$$\nu = \frac{1-(h/l)^2}{3+(\frac{h}{l})^2} \qquad\qquad 6\text{-}1$$

where l is the chosen beam length and h is the beam height. In this model, as the defined structure for the lattice is heterogeneous, this analytical equation for Poisson's ratio is not adequate. In the following section, the procedure of calculating the Poisson's ratios of the lattice in different planes by numerical solution, as well as the other properties of lattice, is explained.

6.4.2 Calculation of lattice properties

An iterative approach is used to adjust the mechanical properties of the lattice elements as the calculated mechanical properties of the defined lattice fit to the experimentally obtained mechanical properties of wood. The steps of iteration are described in flowchart of Figure 6-18.
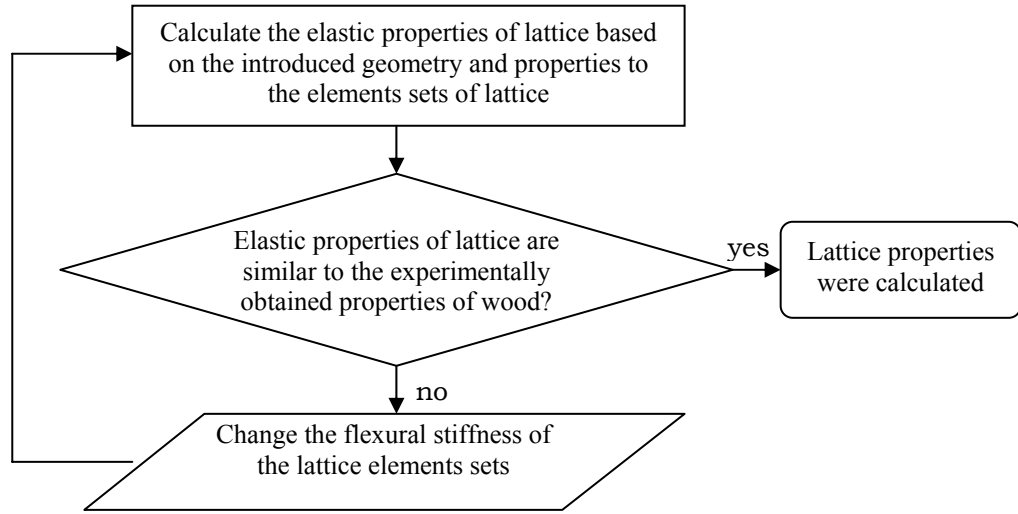
Figure 6-18 Steps of iteration to calculate the mechanical properties of lattice elements

The anisotropic elasticity tensor of the lattice, C_{ab} is defined through the following relationship between the average stress tensor, σ_a and the average strain tensor, ε_b:

$$\boldsymbol{\sigma}_a = C_{ab} \cdot \boldsymbol{\varepsilon}_b \qquad\qquad 6\text{-}2$$

or

$$\begin{bmatrix} \boldsymbol{\sigma}_{LL} \\ \boldsymbol{\sigma}_{RR} \\ \boldsymbol{\sigma}_{TT} \\ \boldsymbol{\sigma}_{LR} \\ \boldsymbol{\sigma}_{LT} \\ \boldsymbol{\sigma}_{RT} \end{bmatrix} = \begin{bmatrix} C_{LLLL} & C_{LLRR} & C_{LLTT} & C_{LLLR} & C_{LLTL} & C_{LLRT} \\ C_{RRLL} & C_{RRRR} & C_{RRTT} & C_{RRLR} & C_{RRTL} & C_{RRRT} \\ C_{TTLL} & C_{TTRR} & C_{TTTT} & C_{TTLR} & C_{TTTL} & C_{TTRT} \\ C_{LRLL} & C_{LRRR} & C_{LRTT} & C_{LRLR} & C_{LRTL} & C_{LRRT} \\ C_{TLLL} & C_{TLRR} & C_{TLTT} & C_{TLLR} & C_{TLTL} & C_{TLRT} \\ C_{RTLL} & C_{RTRR} & C_{RTTT} & C_{RTLR} & C_{RTTL} & C_{RTRT} \end{bmatrix} \begin{Bmatrix} \boldsymbol{\varepsilon}_{LL} \\ \boldsymbol{\varepsilon}_{RR} \\ \boldsymbol{\varepsilon}_{TT} \\ 2\boldsymbol{\varepsilon}_{LR} \\ 2\boldsymbol{\varepsilon}_{LT} \\ 2\boldsymbol{\varepsilon}_{RT} \end{Bmatrix} \qquad 6\text{-}3$$

In the first step of the iteration, for the first series of introduced properties to the lattice element sets, the equation (6-3) is solved. Dimensions of the lattice for calculating the mechanical properties were defined as 3 x 1x 1 mm³ (length, width, thickness). Six loading cases, one for each column of the elasticity matrix in Voigt representation are needed. For these six loading cases, the *uniform displacements* applied on the specific faces of lattice are shown in Figure 6-19.

For example in case (a) a uniform displacement in L direction is applied on a face of lattice which is in RT plane, while in all other faces the boundary conditions are defined as fix the displacements in R and T directions. In this case, by calculating the stress in different faces, σ_{LL}, σ_{RR}, σ_{TT}, σ_{LR}, σ_{LT} and σ_{RT} for the applied strain, (ε_{LL}= 0.01, $\varepsilon_{RR}=\varepsilon_{TT}=\varepsilon_{LR}=\varepsilon_{LT}=\varepsilon_{RT}=0$), C_{LLLL}, C_{RRLL}, C_{TTLL}, C_{LRLL}, C_{TLLL} and C_{RTLL} of the anisotropic elasticity matrix are calculated. Continu-

ing this process in other loading cases, a first calculated matrix of elasticity for the lattice is obtained. Numerical solutions were performed by using the ABAQUS finite element code.
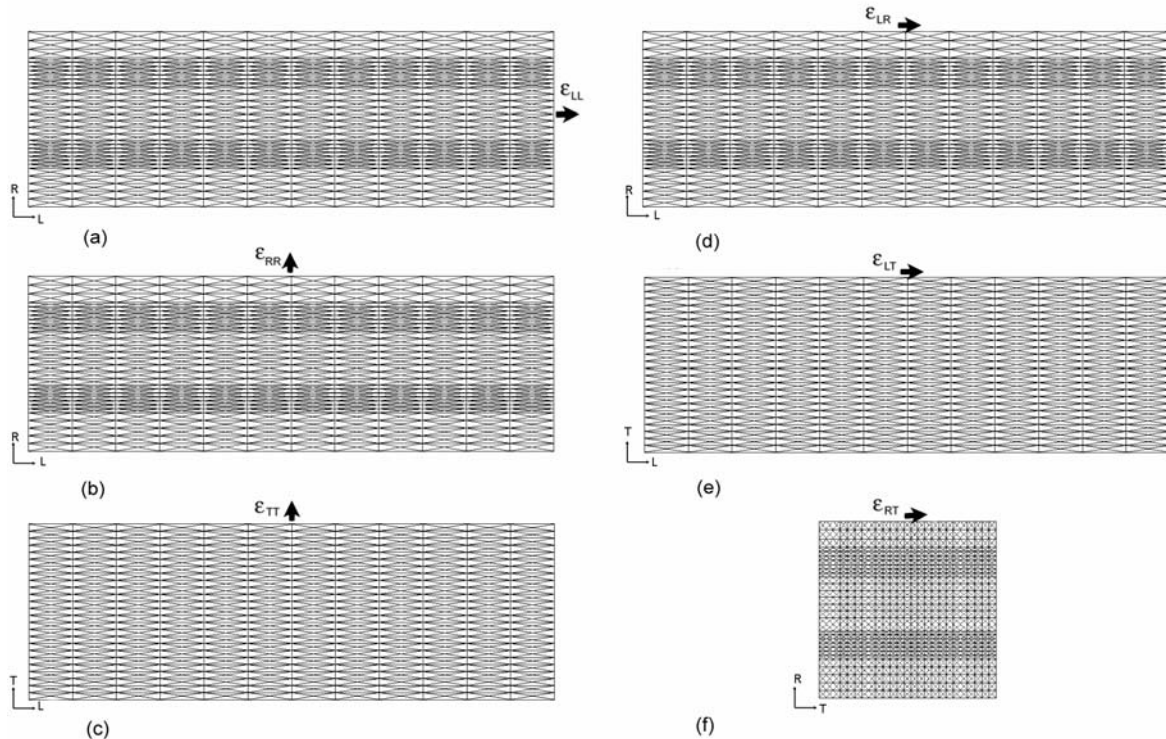
Figure 6-19 Schematic representation of 6 different loading cases, uniform displacements applied on the lattice faces, ε_{LL}, ε_{RR}, ε_{TT}, ε_{LR}, ε_{LT} and ε_{RT}

Uniform boundary conditions:

The defined three-dimensional lattice geometry for calculating the properties is periodic across the wood material. Figure 6-20 shows the periodicity of the lattice geometry in RL plane. To avoid the boundary effects on the calculated elasticity matrix, the defined boundaries in calculation should be uniform.
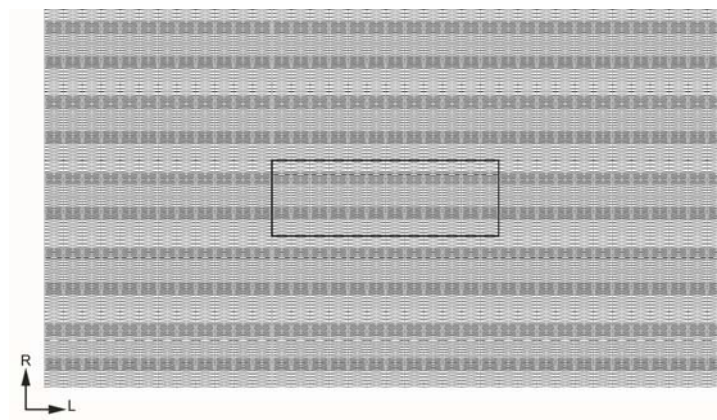
Figure 6-20 Illustration of periodicity of the defined lattice geometry

In the two-dimensional simple example of Figure 6-21, the method to implement the uniform boundary conditions in the numerical simulation is explained. Section A is periodic across the assumed infinite plate shown in Figure 6-21-a. The influence of an applied displacement in L direction on the right edge of the infinite plate could be represented by a uniform displacement in the same direction on the corresponding edge of the section A, when displacements in R direction on other edges are fixed (see Figure 6-21-b). This condition simulates the links between deformation of the upper and lower edges of section A and deformation of the corresponding edges in its adjacent sections. In Figure 6-21-c & d, the other boundary conditions and the applied uniform displacements in the other directions to simulate the periodicity of section A are shown.
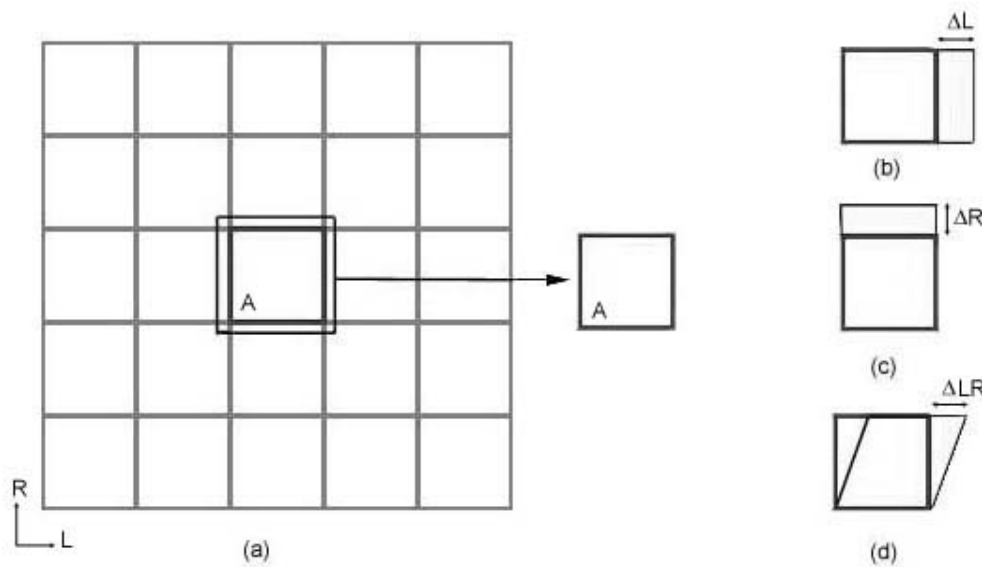
Figure 6-21 A uniform displacement on the each edge of the section simulates its periodicity across the given plate

In the next step of the iteration, the lattice compliance matrix is calculated by inverting the calculated matrix of elasticity of lattice:

$$S_{abl} = C_{abl}^{-1} \qquad\qquad 6\text{-}4$$

As the calculated matrix of elasticity of lattice is orthotropic, comparing the calculated compliance matrix of lattice by equation (6-6) could give the orthotropic elastic properties of lattice.

The calculated lattice properties are compared to the experimentally obtained properties of wood. If the effective properties of the lattice differ from the wood properties, the flexural stiffnesses (EI) is changed and the process is repeated as long as these properties need to be adjusted.

$$S_{ij} = \begin{bmatrix} \dfrac{1}{E_L} & \dfrac{-\nu_{RL}}{E_R} & \dfrac{-\nu_{TL}}{E_T} & 0 & 0 & 0 \\[2ex] \dfrac{-\nu_{LR}}{E_L} & \dfrac{1}{E_R} & \dfrac{-\nu_{TR}}{E_T} & 0 & 0 & 0 \\[2ex] \dfrac{-\nu_{LT}}{E_L} & \dfrac{-\nu_{RT}}{E_R} & \dfrac{1}{E_T} & 0 & 0 & 0 \\[2ex] 0 & 0 & 0 & \dfrac{1}{G_{LR}} & 0 & 0 \\[2ex] 0 & 0 & 0 & 0 & \dfrac{1}{G_{LT}} & 0 \\[2ex] 0 & 0 & 0 & 0 & 0 & \dfrac{1}{G_{RT}} \end{bmatrix} \qquad \text{6-5}$$

It was explained in section 6.3 that the resulting stress-strain curves from simulation are validated by comparing with the experimentally obtained stress-displacement curves by Vasic (2000); Mode I fracture test of notched spruce sample in RL orientation. The calculated E_R (mechanical property in R direction) of that tested specimen, considering the reducing effect of notch on the secant modulus of stress-displacement curve in her fracture test (from Figure 6-5-a), is 280 MPa. Properties of this tested spruce specimen, in other directions, are not available, while to adjust the properties of lattice, all orthotropic properties of wood are needed.

Orthotropic properties of wood can be found in literature. These properties have been measured since a long time ago (Hearmon 1948; Bodig and Goodman 1973; Bodig and Jayne 1982) and the high range of variation of the reported mechanical properties showed that the wood properties are affected by many variables. Table 6-1 shows a summary of the experimentally obtained properties of spruce from the existing literature, by Persson (2000).

Coefficient	Minimum	Maximum
E_L (MPa)	6000	25000
E_R (MPa)	**700**	**1200**
E_T (MPa)	400	900
G_{LR} (MPa)	600	700
G_{LT} (MPa)	500	600
G_{RT} (MPa)	20	70
ν_{RL}	0.02	0.05
ν_{TL}	0.01	0.025
ν_{TR}	0.2	0.35

Table 6-1 Suggested range of variation of experimentally obtained mechanical properties of spruce, Persson (2000)

The calculated E_R from the secant modulus of stress-displacement curve in the mentioned fracture test, 280 MPa, is 60 % less than the minimum reported values for E_R in Table 6-1 (700 MPa). This property is the most important mechanical property of the wood in direct

tension fracture test in Mode I and RL orientation. To be able to compare the simulation and experimental results, it was assumed that the lattice properties should be adjusted to 60 % reduced minimum values of Table 6-1, which are shown in Table 6-2. It was assumed that this reduction does not include the Poisson's ratios.

Coefficient	Minimum
E_L (MPa)	2400
E_R (MPa)	**280**
E_T (MPa)	160
G_{LR} (MPa)	240
G_{LT} (MPa)	200
G_{RT} (MPa)	8

Table 6-2 60 % reduced minimum values of Table 6-1 are assumed as the properties of tested specimen by Vasic

In this way, the lattice elastic properties in the R direction, E_R would be similar to the mechanical property of the tested specimen in R direction.

Characteristics of different beam element sets of the lattice which give the closest lattice properties to these reduced values (obtained by the mentioned iterative procedure) are presented in Table 6-3.

Element set	Area (mm^2)	Young's modulus (MPa)	Poisson's ratio
Earlywood beams	0.000304	2350	0.3
Latewood beams	0.000576	3400	0.3
Direct beams	0.000384	6400	0.3
S-diagonal beams	0.0025	450	0.3
L-diagonal beams	0.0025	5020	0.3

Table 6-3 Characteristic of different beam element sets of lattice

The calculated effective properties of the lattice based on the defined order and characteristic for different elements sets are:

E_L= 12586 Mpa , E_R= 280 Mpa , E_T= 170 Mpa

G_{LR}= 203 Mpa , G_{LT}=266 Mpa , G_{RT}=53 MPa

v_{RL}=0.015 , v_{TL}=0.03 , v_{TR}=0.17

There are some differences between these calculated properties and the reduced properties of wood in Table 6-2, which arise from the defined structure of lattice. For example the highest difference is between the properties in L direction, E_L, which causes from the large

97

stiffness of the L-diagonal beams. In fact, with the defined lattice geometry, these elements are necessary to represent (simulate) the shear properties of wood material, but also have a high influence on the property of material in the L direction.

The defined order of element sets in the lattice geometry does not allow to get a closer E_L to the value presented in Table 6-2, when E_R and E_T are adjusted (although it is still between the introduced range of variation of E_L for wood in Table 6-1). As the most important mechanical properties in our simulation are properties across the grain (E_R and E_T) and as these properties fit well to the parameters in Table 6-2, it was assumed this approximation is not to be critical.

6.5 *Failure criterion for beam elements*

In lattice of beam elements, fracture is simulated by removing the elements during the analysis when their internal reactions exceed a certain criterion. This predefined fracture criterion could be based on energy or strength criteria.

A strength based fracture criterion should be a function of internal forces in the lattice elements. Beam elements transmit the normal forces, shear forces and bending moments. So the fracture criterion in the lattice of the beam elements is a function of these internal force components or their effective value and the contribution of bending moments (Herrmann, Hansen et al. 1989; VanMier 1996).

$$\sigma = \frac{F}{A} + \alpha \frac{\sqrt{M_L^2 + M_R^2 + M_T^2}}{W} < f_t \qquad\qquad 6\text{-}6$$

where A and W are the area and section modulus of the beam cross-section, F, M_L, M_R and M_T are the internal axial force and bending moments and f_t is the beam tensile strength. The coefficient α defines the contribution of beam bending moments in the failure criteria and consequently the material fracture behavior. It has been shown that choosing a small value for α gives a longer tail to the stress-displacement response (Schlangen 1993). But in three-dimensional simulation, the variation of α in the range 0-0.05 does not change the crack pattern. Consequently the contribution of bending moment can be ignored in fracture analysis (Lilliu and VanMier 2003).

In this model, a tensile strength criterion was adopted which is based on the *maximum normal strain* in a beam element. After solving the lattice for a given displacement, normal strain of all lattice elements are calculated. When the normal tensile strain of each element exceeds a *predefined strain limit*, the element is removed.

In the defined lattice geometry, different beam sets have different roles. Assigning different predefined strain limits (failure limits) to different element sets can show the importance of the strength of each element set in the fracture behavior of the material.

The chosen failure limit for the elements represents the strength of wood microstructural elements: the fibers and the bonding medium. Contrary to wood fibers, there is not much information about the strength of the bonding medium in literature. On the other hand, the strength of the bonding medium is the most influential parameter in investigating the wood fracture in Mode I, RL orientation. In this model, to find the failure limit of the bonding medium elements, the obtained stress-strain curves after simulation of fracture with different failure limits are compared to the experimental stress-stain curves and the appropriate failure limit (which gives the best fit to the experimental results) is chosen.

The strength of wood microstructural elements is affected by microstructural defects and heterogeneities. Choosing one constant value for the failure limit, when the strength of each element could be affected by different defects, is far from reality. The influence of microstructural defects on the fracture behavior could be simulated by randomly choosing the failure limit of each element set from a set of normal distribution. The mean of this normal distribution represents the assigned mean strength to the element set while the standard deviation represents the spread or variability in the strength value. In this model the size of the standard deviation (which is assumed as a percentage of the mean value), shows the influence of defects on the strength of elements. For example, assuming a large standard deviation indicates the more influential defects which have a large influence on the strength of the elements.

6.6 Fracture analyses

In this study the behavior of a small notched wood specimen in Mode I direct tension fracture test in RL orientation, is investigated. Steps for solving the problem are as in the flowchart of Figure 6-22.

In each step, the model is solved for the applied displacement. Normal strain of all lattice elements are calculated, the elements with tensile strain above the failure limit are removed from the lattice mesh and the model is solved for the applied displacement at the next step. This process is repeated until the boundary reaction force in the direction of the applied displacement reaches zero, meaning that the model is completely fractured. By calculating the reaction force on the model boundaries at each step (each applied displacement), the stress-displacement response of the model can be plotted.
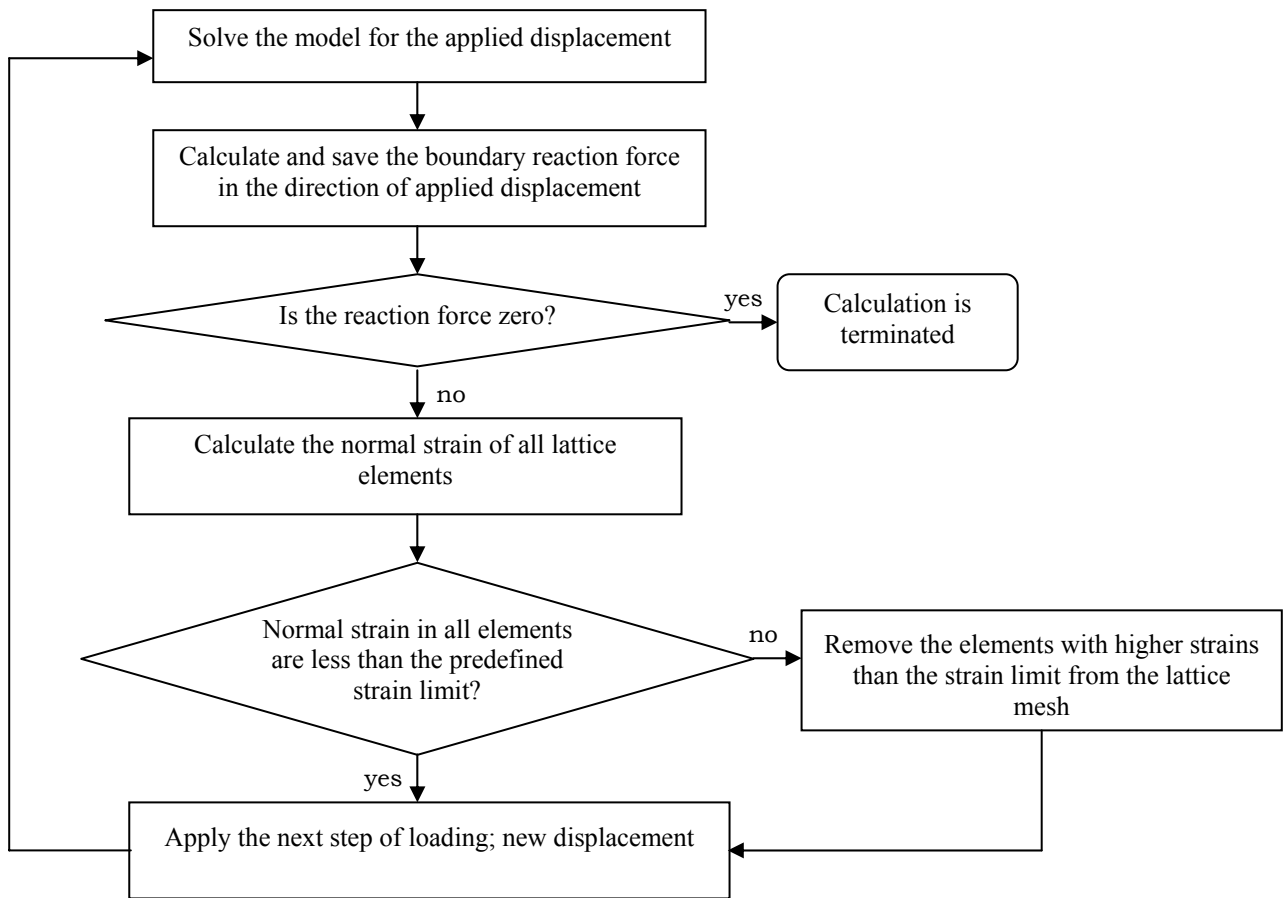
Figure 6-22 Steps of solution of the problem

Numerical solutions were obtained by using the ABAQUS finite element code. Also the loop of automatically calculating the internal strains, removing the critical elements and resolving the problem, was performed by writing an additional program in Python language.

This model has the potential of simulating the behavior of wood samples with a given microstructure, before and during crack propagation in fracture tests. Therefore, it enables the study of the influence of parameters such as the strength of the bonding medium, fiber heterogeneities and defects on wood fracture behavior.

Using this model, the pre-peak behavior, peak load, post-peak behavior, crack pattern and the fracture stability are discussed. The obtained stress-displacement responses from simulation are compared with the experimental evidence found in the literature, direct tension fracture tests of same size samples.

6.7 Concluding remarks

In this chapter, a method to develop a lattice fracture model for studying the fracture process at cellular level of a small notched wood samples was explained.

In Mode I fracture, parallel to the fibers, the crack propagation occurs in the natural cleavage planes, which are made by the wood' special structure. Knowing that in this fracture condition, the width of the crack zone is predictable and does not exceed more than few growth rings, a mixed lattice-continuum model was developed. The advantage of mixed lattice-continuum models is reducing the computational costs by modeling the less critical part of the structure with a coarser mesh while the probable crack width is modeled by a lattice. Using this method, the fracture process of larger wood samples at cellular level can be investigated.

The defined lattice has a heterogeneous structure with alternation of earlywood and latewood fibers. Other heterogeneities were introduced by randomly choosing the element failure limit through a normal set with a given mean and standard deviation. Studying the problem with different ranges of chosen mean and standard deviation, could show the dependency of wood fracture behavior to the strength of different microstructural elements and their defects. The performed comparative investigation using the parametric study on the simulation results is presented in the next chapter.

Chapter 7 Application of the model and interpretation of results

7.1 Introduction

In this chapter the model developed in chapter 6 is used for investigating the fracture process in a notched wood sample in Mode I, RL orientation.

Using the mixed lattice-continuum model, the stress-displacement response of the specimen in direct tension fracture test is investigated and compared to the experimental result. After model validation, a parametric study is made to understand the role of different elements and parameters in the fracture behavior.

In the lattice model, the structure and mechanical properties of wood material are simulated by the network of interconnected beam elements. Each set of elements in the defined lattice has a specific role in providing the characteristics and properties of lattice. Consequently the assigned strength to different element set could show their contribution in the response and fracture behavior of whole material. In this study, by introducing different strengths to different lattice element sets, this contribution is investigated.

It was assumed that the step by step removing of the critical elements (reached elements to their failure limit) from the lattice mesh shows the process of development of microcracks and crack propagation during the simulation of fracture test. Using this advantage, the crack patterns in longitudinal-sections (RL plane) and cross-sections (RT plane) of lattice were studied and compared to the experimental evidences, microscopic observation of crack surface by CLSM (Job L. Navi P. 1996).

7.2 Stress-displacement response

In each step of simulation, the reaction force in the direction of the applied displacement is calculated and used to plot the stress-displacement curve of the specimen in fracture. Comparing the obtained stress-displacement curves and the experimental results in pre-peak behavior and post-peak branch and also investigating the influences of variation of strength of different element sets on these responses are useful in understanding the mechanism of wood fracture.

7.2.1 Failure limit

The first step of simulating the fracture test is choosing the appropriate failure limit. The failure limit has an important influence of the obtained stress-displacement curve results; the peak stress and the post-peak softening behavior. In our problem, Mode I fracture in the RL orientation, the failure limit of three element sets are more critical; direct, S-diagonal and L-diagonal beams sets. In Figure 7-1, these elements and their corresponding lengths in model are shown.
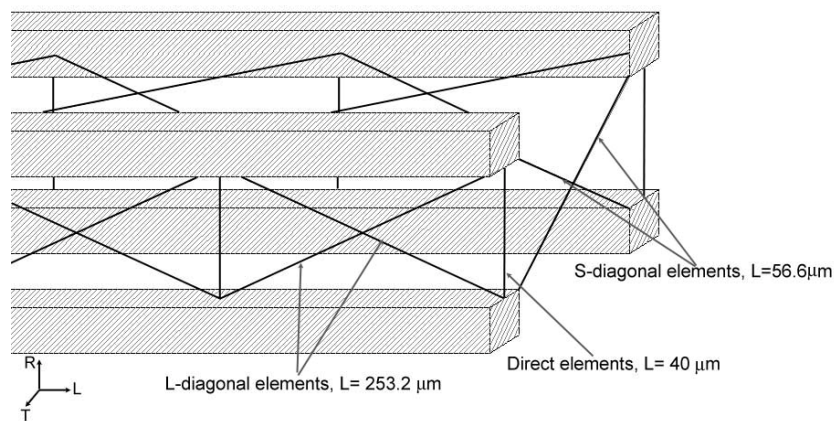
Figure 7-1 Length of the different element sets in the defined geometry

In this model, as was explained in section 6.5, the failure limit of each element is randomly selected from a normal distribution, while the mean is a prescribed strain limit and the standard deviation is a percentage of the mean value. The prescribed strain limit for each element set is calculated by dividing an assumed ultimate deformation (failure deformation) to the element length. Standard deviation represents the variability of strain limit due to defects. In fact, comparing between the obtained results from simulation with large and small standard deviations could show the different behavior of specimens with more and less influential defects.

To find the failure limit of the element sets which represent the bonding medium, fracture tests are simulated with different failure limits and the appropriate failure limit is selected by comparing between the resulted stress-displacement curves and the experimental results. For example in the Figure 7-2, the stress-displacement curves for different mean strain values (failure limit) and a constant standard deviation (assumed as 16.7% mean) are presented. The mean strains were calculated based on the assumption that in different cases (a), (b) and (c), the ultimate deformations for S-diagonal and L-diagonal elements are 1.36, 1.7 and 2 μm respectively. Consequently the mean strains for each case were calculated by dividing these deformations to the element lengths. Table 7-1 is a summary of the failure limits used to obtain Figure 7-2.

Element	Length μm	(a) ultimate deformation=1.36 μm		(b) ultimate deformation=1.7 μm		(c) ultimate deformation=2.0 μm	
		Mean strain	Standard deviation	Mean strain	Standard deviation	Mean strain	Standard deviation
S-diagonal and direct beams	56.6 & 40	0.0240	0.004	0.0300	0.005	0.0353	0.006
L-diagonal beams	253.2	0.0054	0.0009	0.0067	0.0011	0.0079	0.0013

Table 7-1 Mean values and standard deviations for three cases in Figure 7-2
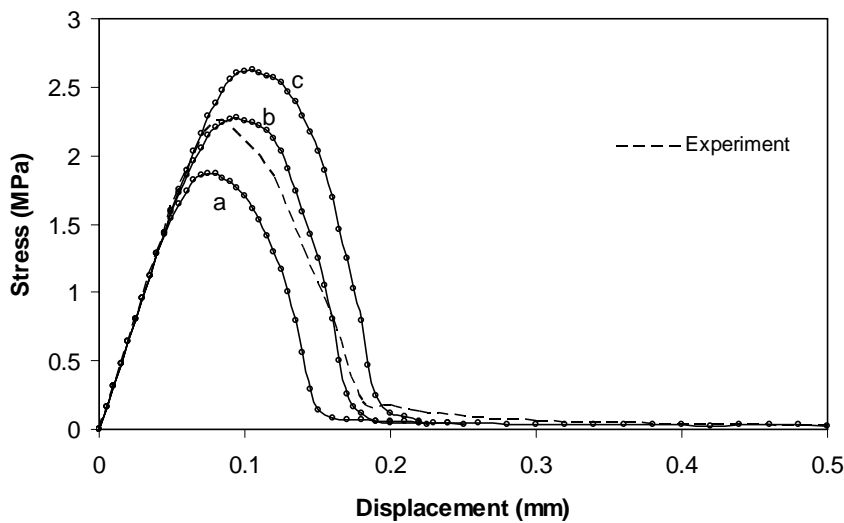
Figure 7-2 Comparison between the obtained stress-displacement curves with different failure limits and experimental curve

Figure 7-2 shows that the failure limit has a large influence on the peak stress. Comparing between the obtained stress-strain curves and the experimental curve for a 20 x 20 x 4 mm³ notched sample in Mode I, RL orientation (Vasic S. 2000) shows that for the defined geometry and modeling set-up, the failure limit of case (b) should be considred. For the appropriate failure limit, the agreement between the initial properties, peak stress and softening response of fracture tests and simulation results shows the model works properly.

In this study, it was assumed that only the three mentioned element sets (L-diagonal, S-diagonal and direct beams) might fail and the earlywood and latewood fibers remain intact. Comparison between the results of simulation with different assigned strain limits to the fiber elements shows that this assumption has little influence on the simulation results and the fiber elements do not play an important role in the results of fracture test in RL orientation. Figure 7-3, shows the result of simulation for different assigned strain limit to the fibers, while the failure limit of the other elements are as the cased (b) in Table 7-1. As this

figure shows, assigning a small strain limit to the fiber elements (0.01 in third case) reduces the tail of the stress-strain curve.
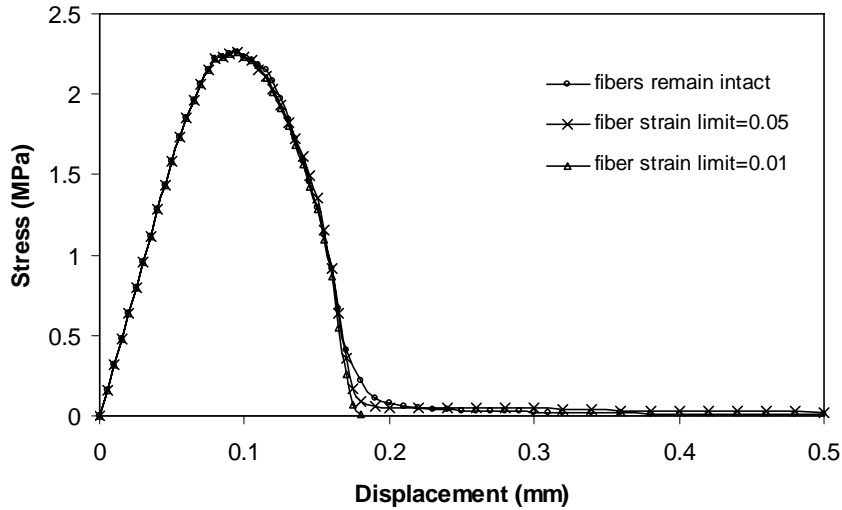
Figure 7-3 Comparison between the simulation results for different strain limit of the fiber elements

7.2.2 Fracture stability in model

The obtained stress-displacement curves by simulation with different random or constant failure limits show the stable fracture responses (see Figure 7-4). In Table 7-2, a summary of the used failure limits for this study is shown.

The curves marked with (a) and (b) were obtained based on a similar ultimate deformation (1.7 μm), but for different standard deviations to represent the fracture responses of two specimens with and without defects. Consequently, in case (b) (specimen without defects) the peak stress was higher.

Element	Length μm	(a) ultimate deformation=1.7 μm		(b) ultimate deformation=1.7 μm	
		Mean strain	**Standard deviation**	Mean strain	**Standard deviation**
S-diagonal and direct beams	56.6 & 40	0.0300	**0.005**	.0300	**0.00**
L-diagonal beams	253.2	0.0067	**0.0011**	0.0067	**0.00**

Table 7-2 Mean values and standard deviations for three cases in Figure 7-4
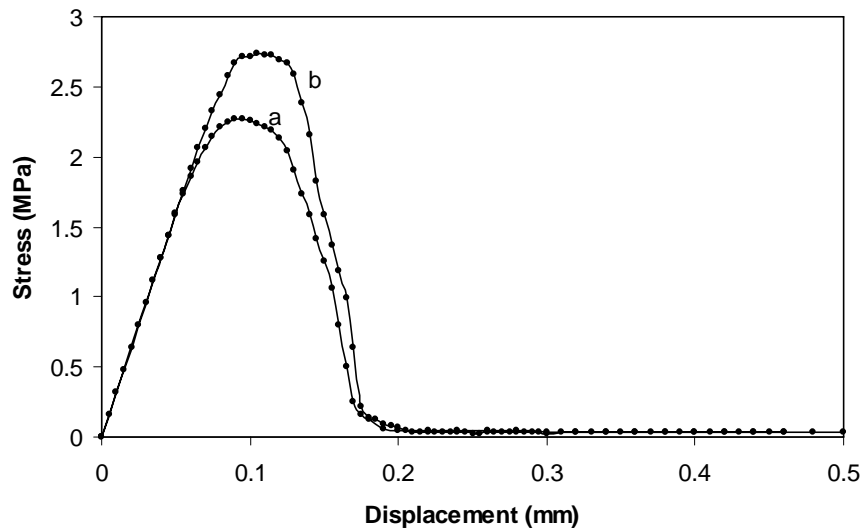
Figure 7-4 Obtained stress-displacement response for random and constant failure limits, the failure limits in cases (a) and (c) were constant

The stability of the simulated fracture test, even for a constant failure limit, shows that the constructed lattice, which represents the structure and mechanical properties of wood material, guarantees fracture stability in model. This stability is attributed to the specific *three-dimensional heterogeneous* geometry of the lattice, composed of different element sets with different geometries, properties and settlement orders (horizontal, vertical and diagonal orders).

7.2.3 The role of different element sets of lattice in fracture behavior

Comparison between the results of simulation with different failure limits showed the importance of this criterion in the stress-displacement response of the sample in fracture test. On one hand, mean and standard deviation of the normal distribution, which represent the failure limit, have their own special influences on the fracture behavior. On the other hand, the lattice is constructed by different element sets while each of them has a special role in the mechanical behavior of whole lattice. Consequently, assigning different failure limits to different element sets of lattice could show the contribution of different elements in the response and fracture behavior of the modeled specimen.

In this part the influence of assigning different strain limits to different element sets and also variation of the standard deviation on the lattice fracture are studied.

(a) Mean of normal distribution as a representation of the microstructural strength:

The mean value of the normal distribution represents the assigned average strength to the microstructural elements of the material. In the presented simulation results in Figure 7-2, for all elements which represent the bonding medium, the assigned mean value to the normal distribution was the calculated strains based on *one* predefined deformation. For example in case (b) of Figure 7-2, the ultimate deformation for all elements which represent the bonding medium was assumed as 1.7 μm. However, assigning different failure limits (based on different ultimate deformations) to different element sets, could show the role of different element sets in the fracture behavior.

To investigate the influence of considering different ultimate deformations for different elements sets, first the simulation results in three cases, with three different ultimate deformations for L-diagonal elements and similar ultimate deformation for direct and S-diagonal elements were compared. These inputs correspond to assuming different strength for L-diagonal elements (which are the main providers of shear strength in lattice) comparing to the other elements of bonding medium. The used mean and standard deviations for three cases of this study are summarized in Table 7-3. The assigned ultimate deformation to L-diagonal elements was assumed as their strain limits in cases (a) and (c) are to be respectively 50% less and higher than case (b). For this purpose, the ultimate deformation to L-diagonal elements in cases (a), (b) and (c) are 0.76, 1.7 and 2.3 μm respectively, while the ultimate deformation of all S-diagonal and direct elements is 1.7 μm in all cases. Also the standard deviations in all cases were assumed as 16.7% mean values. Figure 7-5 shows the result of simulation. Different shapes of the softening branches for different strengths of the L-diagonal beams shows the important role of these elements in the post-peak behavior. On the other hand, changing the failure limit of L-diagonal beam elements did not considerably affect the peak stresses. It shows that the peak stress is mainly defined by the failure of S-diagonal and direct beam element. A comparative study on the failure limits of S-diagonal and direct beam elements, could confirm this dependency.

Element	Length μm	(a)		(b)		(c)	
		Mean strain	Standard deviation	Mean strain	Standard deviation	Mean strain	Standard deviation
S-diagonal and direct beams	56.6 & 40	0.03	0.005	0.03	0.005	0.03	0.005
L-diagonal beams	**253.2**	**0.003**	**0.0005**	**0.006**	**0.001**	**0.009**	**0.0015**

Table 7-3 Mean values and standard deviations for three cases in Figure 7-5
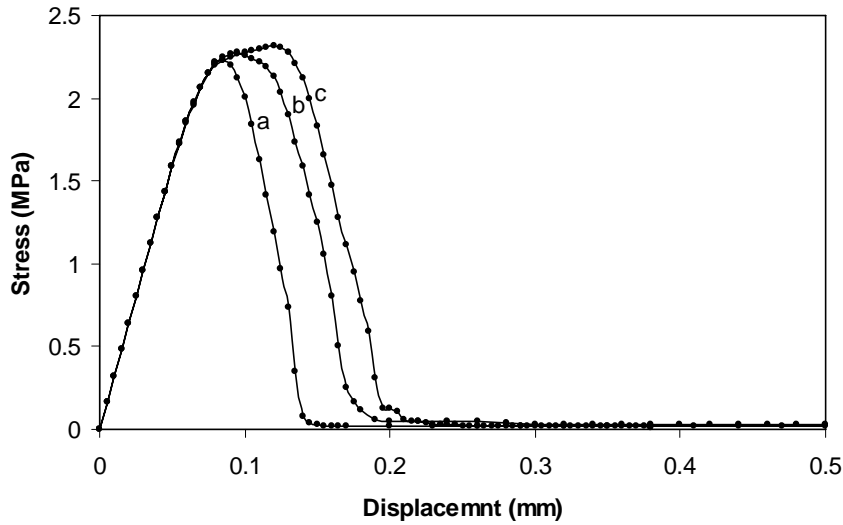
Figure 7-5 Dependency of stress-displacement curve on the failure limit of L-diagonal elements; in simulation (a) and (c) the mean strains of L-diagonal beam elements are 50% less and higher that in simulation (b)

The results of simulation for three cases with three different ultimate deformations for S-diagonal and direct beam elements and similar ultimate deformation for the L-diagonal elements are shown in Figure 7-6. The inputs correspond to assuming different strength for S-diagonal and direct beam elements comparing to the L-diagonal elements. Detail of mean strains and standard deviations for these cases are given in Table 7-4. The assigned ultimate deformation to S-diagonal and direct beam elements was assumed as their strain limits in cases (a) and (c) are respectively 16% less and higher than case (b). For this purpose, the assigned ultimate deformations to these elements in cases (a), (b) and (c) are 1.4, 1.7 and 2 μm respectively, while the ultimate deformation of all L-diagonal elements is 1.7 μm in all cases. Also the standard deviations in all cases were assumed as 16.7% mean values. Comparison between the obtained stress-displacement curves show the importance of S-diagonal and direct beam elements in defining the peak stresses of simulation, although they do not have an important influence of the slope of the post-peak softening branch.

Element	Length μm	(a)		(b)		(c)	
		Mean strain	Standard deviation	Mean strain	Standard deviation	Mean strain	Standard deviation
S-diagonal and direct beams	**56.6 & 40**	**0.025**	**0.0042**	**0.03**	**0.005**	**0.035**	**0.0058**
L-diagonal beams	253.2	0.006	0.001	0.006	0.001	0.006	0.001

Table 7-4 Mean values and standard deviations for three cases in Figure 7-6
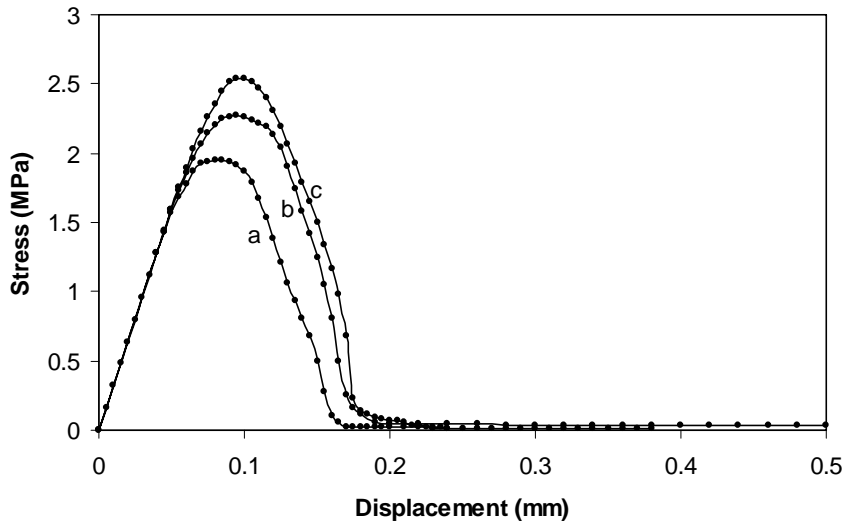
Figure 7-6 Dependency of peak stress to the failure limit of direct and S-diagonal beam elements; in simulations (a) and (c) the mean values are 0.16% lower and higher than simulation (b)

(b) Standard deviation of normal distribution as a representation of the natural defects:

To consider the role of microstructural defects in the fracture model, the failure criterion adopted as the failure stain limit was randomly selected from a normal distribution. The standard deviation of normal distribution reflects the influence of defects on the strength of microstructural elements. For a given mean strain, considering a larger standard deviation represents a material with more influential defects which have a large influence on the strength of the elements and vice versa.

Figure 7-7 shows the simulation results for three different cases with similar mean strain and different standard deviations. The used mean strains and standard deviations are given in Table 7-5. Standard deviations in cases (a) and (c) were assumed 40% higher and lower than in case (b), respectively. It means that in cases (a) and (c) of Figure 7-7, the standard deviations were 23.3% and 10% of the mean strain while in case (b) it was 16.7% of it.

Element	Length µm	(a)		(b)		(c)	
		Mean strain	**Standard deviation**	Mean strain	**Standard deviation**	Mean strain	**Standard deviation**
S-diagonal and direct beams	56.6 & 40	0.03	**0.007**	0.03	**0.005**	0.03	**0.003**
L-diagonal beams	253.2	0.006	**0.0014**	0.006	**0.001**	0.006	**0.0006**

Table 7-5 Mean values and standard deviations for three cases in Figure 7-7
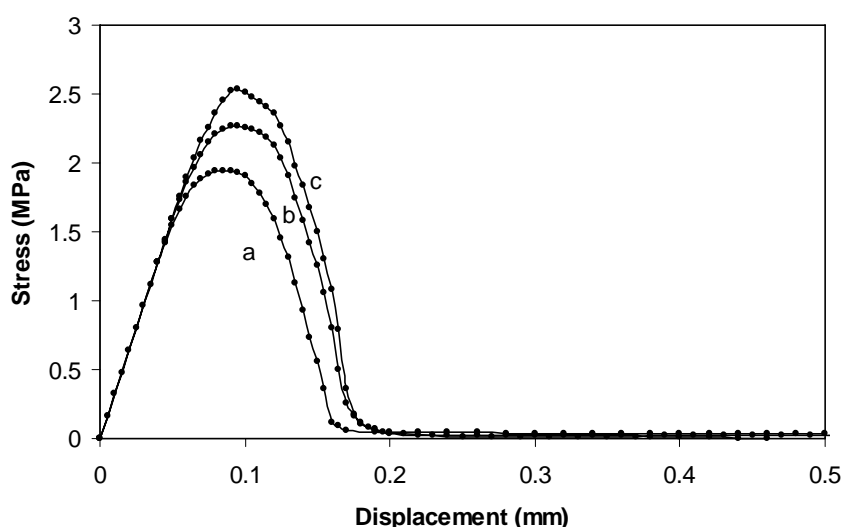
Figure 7-7 Dependency of stress-displacement curve to the variation of standard deviations; in simulation (a) and (c) standard deviations are 40% higher and lower than in simulation (b)

Comparison of these curves shows that the variation of standard deviation can change the peak stress of stress-displacement curves and the slope of softening branch. Increase of the standard deviation (more influential defects) reduces the peak stress while its reduction (less influential defects) increases its level.

7.2.4 Lattice dimensions

Knowing that the width of the fracture process zone in our problem is limited to a few growth rings (as explained in section 6.2.2), the mixed lattice-continuum model, with a limited width for lattice was developed. In the main geometry of model which was used in the above simulations, the width of the lattice in R direction was 1 mm, composed of two latewood and three earlywood rings (31 wood fibers). However, to insure that this lattice width is enough, the stress-displacement responses of two new geometries with different lattice width were compared. Fracture was simulated in two notched specimens of 5 x 5 x 1 mm^3 (length, width, thickness), while the lattice dimensions are 3 x 1.5 x 1 mm^3 in case (a) and 3 x 1 x 1 mm^3 in case (b). Lattice with the width of 1.5 mm covers three latewood and four earlywood rings (45 wood fibers).

The obtained stress-displacement curves from simulations are presented in Figure 7-8. As this figure shows these curves are similar except at the toe of stress-displacement curve (marked in the black rectangular). The resulting toe of stress-displacement curve in a lattice with a larger width is closer to the experimental results. It could be attributed to existence of a wider band of intact lattice which could participate in branching mechanism.
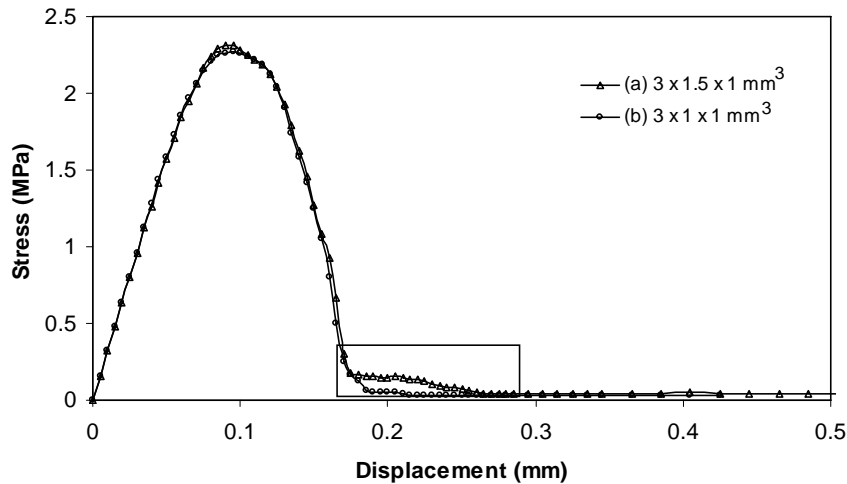
Figure 7-8 Stress-displacement of two specimens with different lattice dimensions

Although the result of the simulation with the wider lattice was closer to experimental results, the number of lattice elements and calculation time increased progressively. On the other hand the differences between the results of two simulations cannot have a significant effect on the fracture energies (275.8 N.m and 266.9 in lattices (a) and (b), respectively). The similarities between the results of two simulations such as the pre-peak behaviors, peak stresses and post-peak softening branches and also the small difference between the fracture energies shows that in our problem, 1mm width of the lattice would be enough.

7.2.5 Loading steps

Simulations with similar failure limit and different sizes of loading steps result in different stress-displacement responses. To show the importance of load steps on the simulation results, simulation with three loading step sizes, 0.0025mm, 0.005 and 0.01 mm was repeated when other parameters remained unchanged. Figure 7-9 shows results of the three simulations, with the constant failure limit which had been applied before for curve (b) in Figure 7-2 (case (b) in Table 7-1).

Different stress-displacement responses when the size of loading steps in different simulations is different, shows its importance. This factor could change the peak stress, fracture energy and stress level in the toe of stress-displacement curve. This dependency of the stress-displacement response to the size of the loading step is the main negative point of model. The problem arises from the fact that removing a large number of elements from the model geometry in each step prevents the gradual redistribution of stress in the adapted mesh during the simulation. For the most accurate simulation, the size of the loading steps of the analysis should be set as in each step only one element is removed. The problem is

that with the defined lattice size and the large number of involved elements in analysis, a simulation with such loading step set-up would be very time consuming. Consequently the number of removed elements in each step should be as small as possible.
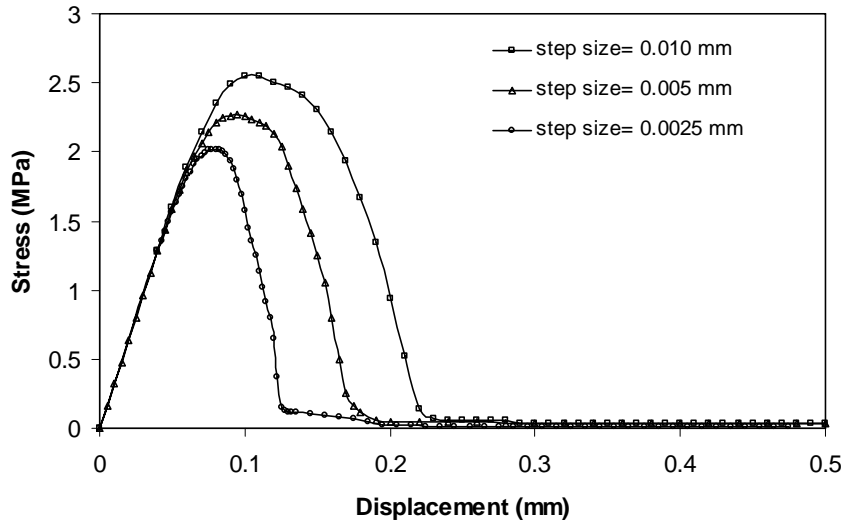
Figure 7-9 Effect of the size of the loading steps on stress-displacement response of the model

7.3 Three-dimensional detecting the crack trajectory

In the lattice fracture model, it has been assumed that removal of the critical elements from the lattice mesh during the simulation shows the propagation of crack in model geometry. This is used to investigate the development of microcracks and the pattern of crack propagation in the cross-section and longitudinal-section of the specimen during the simulation of the fracture test.

With the defined three-dimensional structure of the lattice with its large number of elements, observation of developed crack in a particular section, because of interference of other elements is difficult. Consequently the location of microcracks and the crack trajectory were investigated in the cut-sections (cross-section in RT plane and longitudinal-section in RL plane). As Figure 7-10 shows, to present a cross-section or longitudinal-section, only the elements of the selected cut-section are shown and the other lattice elements out of cut-section are hidden. Dimensions of the selected cross-sections are 0.25 x 1 x 1 mm³ (length, width, thickness) and dimensions of the selected longitudinal-sections are 20 x 4 x 0.04 mm³ (length, width, thickness).
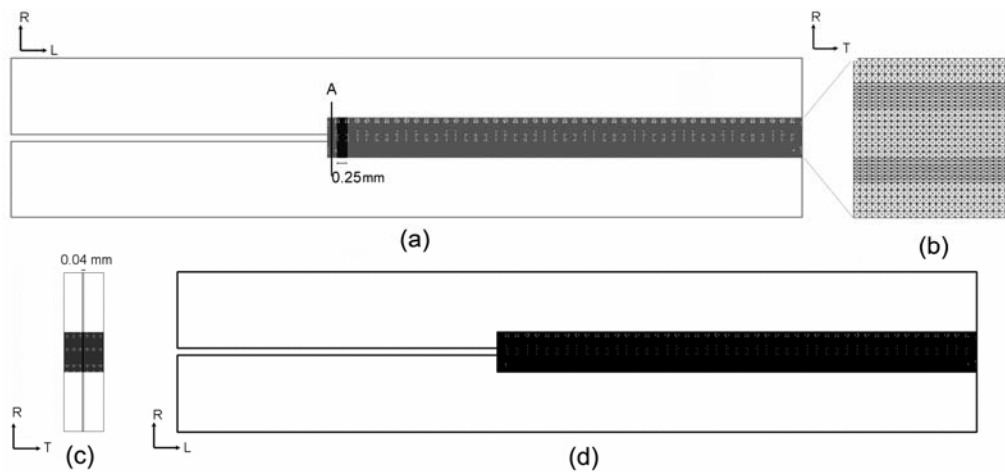
Figure 7-10 (a) Location of the selected cross-section A, (b) cross-section A in RT plane, (c) location of the selected longitudinal-section, (d) central longitudinal-section in RL plane

Figure 7-11 illustrates the cross-section of the model geometry (RT plane). The rectangles and diagonal elements which are visible in Figure 7-11-a are the elements which represent the bonding medium. In this view the beams which represent the wood fibers are the nodes in the intersections of the rectangles. Figure 7-11-b gives a better image of the fiber beam elements; shown by solid nodes in the intersections of rectangles. Each of these nodes represent a wood fiber whose cross-sectional dimensions are as the marked rectangular with dashed lines.
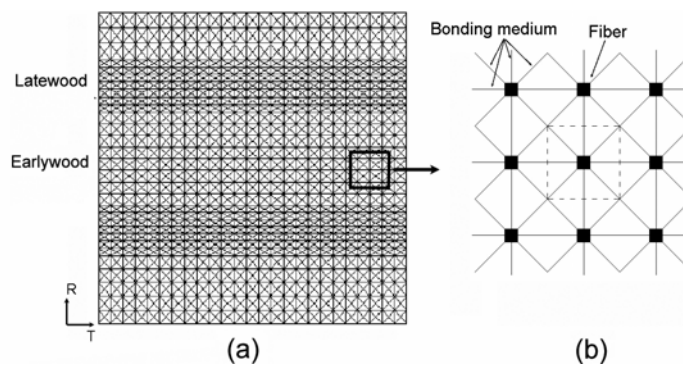
Figure 7-11 (a) lattice cross-section in RT plane, (b) the solid nodes show the wood fibers in RT plane while the diagonal and direct lines show the bonding medium between the fibers

7.3.1 Development of microcracks in cross-section

The importance of microcrack is their contribution in propagation of main crack trajectory. The lattice fracture model has the advantage of showing the probable position of micro-cracks and considering their influences on the material fracture.

To study the location of developed microcracks, lattice cross-sections (RT plane) for different steps of fracture simulation were monitored. Summary of the used failure limits for this study is given in Table 7-6.

Element	Length (µm)	Mean strain	Standard deviation
S-diagonal and direct beams	56.6 & 40	0.0300	0.005
L-diagonal beams	253.2	0.0067	0.0011
Earlywood and latewood fibers	253	.0500	.01

Table 7-6 Failure limits of different element sets in simulation for crack pattern studies

In Figure 7-12, location of microcracks in two different cross-sections of lattice after applying of 0.06 mm displacement (before peak stress) is shown. Figure 7-12-b & c show the two cross-sections of lattice which are marked with (A) and (B) in Figure 7-12-a. Comparing between the cross-sections (A) and (B) shows that in the same loading states, the microcracks in the close cross-section to the notch tip have already initiated while in a far section from it, no microcracks have developed.
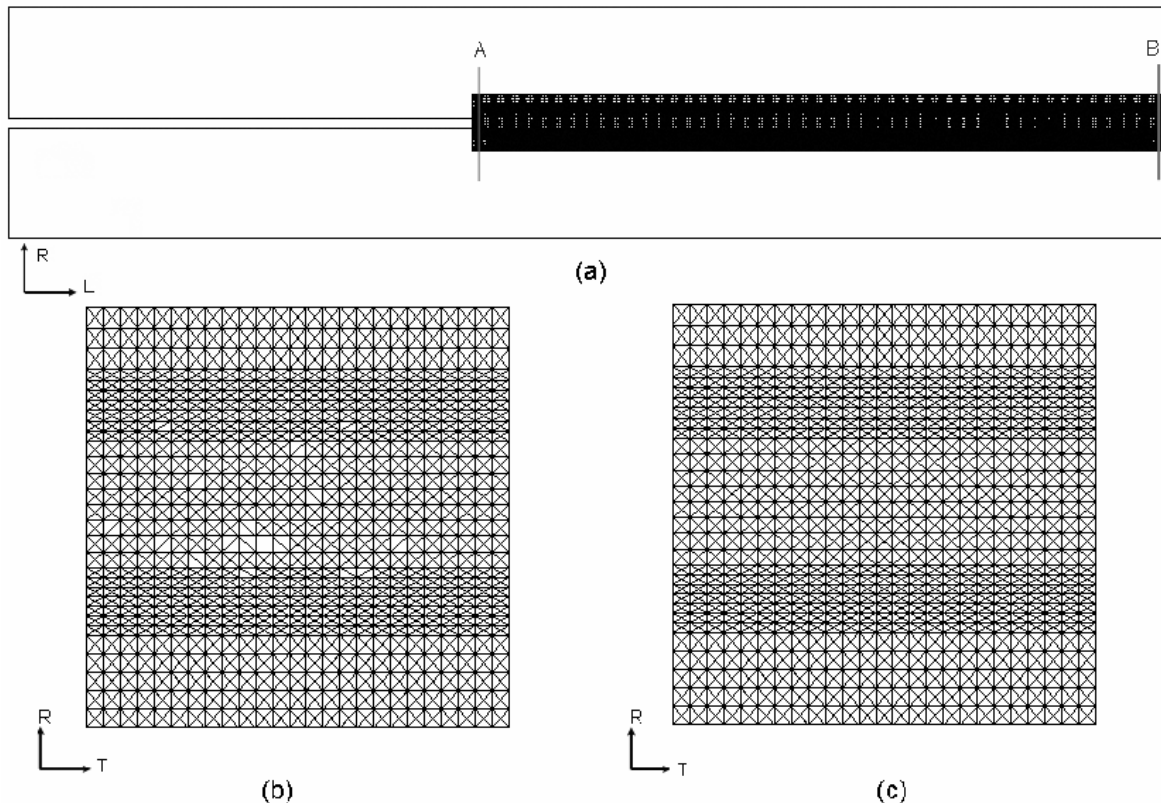
Figure 7-12 Comparing the two cross-sections shows that microcracks develop first in the areas close to the notch tip; (b) and (c) are the marked cross-sections with (A) and (B) in (a)

This study showed that early microcracks are mainly developed in the areas close to notch tip, which is obviously attributed to the high stress concentration close to the notch tip with the defined geometry and loading condition.

The propagated microcracks in the cross-section close to the notch tip (section (A) in Figure 7-12-a), in different loading states before peak stress are shown in Figure 7-13. Microcracks states in Figure 7-13-a, b & c corresponded to 0.06mm, 0.07mm and 0.08 mm displacement in direct tension fracture test (for 20 x 4 x 1 mm³ notched specimen). This comparison shows that the process of microcrack development begins before the peak stress of the stress-displacement curve and participates in forming the non-linear part of the curve before peak. Also the first microcracks have been developed in the central earlywood region.
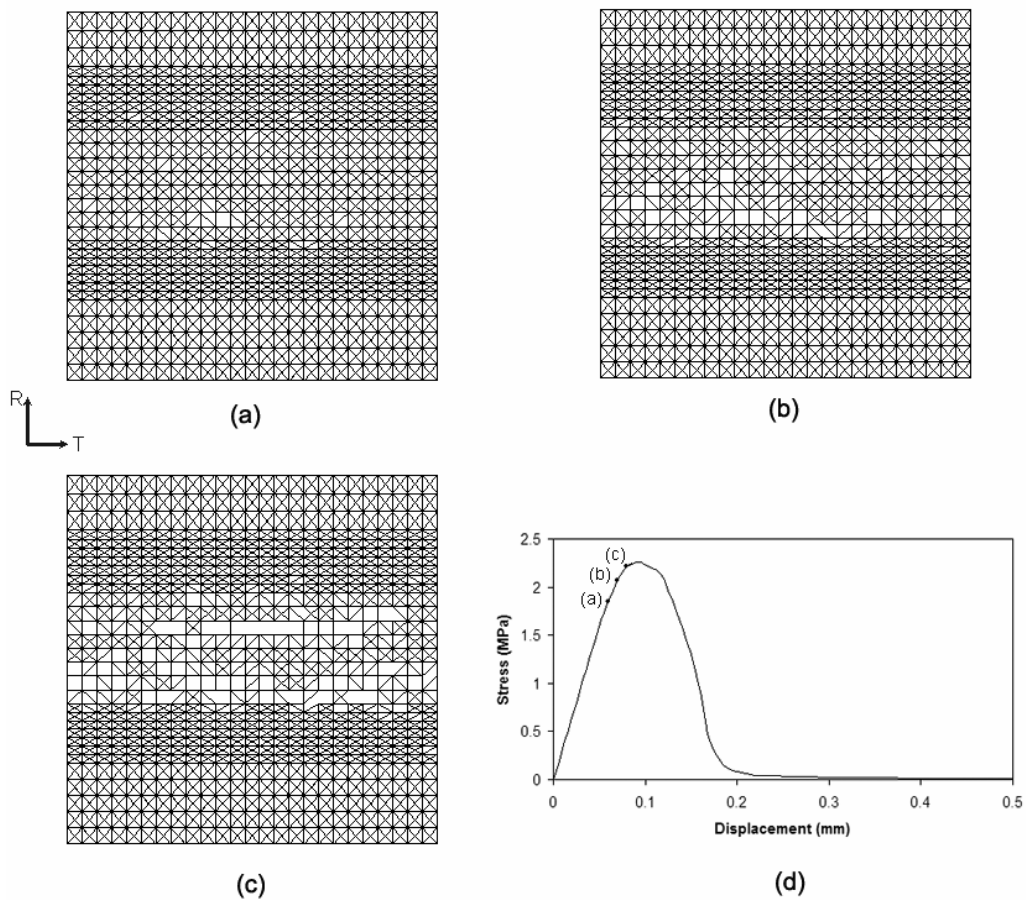
Figure 7-13 Developed microcracks before peak stress in the notch tip (section (A) in Figure 7-12-a); (a), (b), and (c) developed microcracks for different loading states marked with the same notations in (d) corresponding to 0.06mm, 0.07mm and 0.08 mm displacement, (e) stress-displacement response

7.3.2 Main cracks in cross-section

To investigate the mechanism of propagation of main crack through the different sections of lattice, four cross-sections close to the crack tip (for a known loading state, 0.11 mm applied displacement) were studied. The selected cross-sections and the crack profile are shown in Figure 7-14. These cross-sections show that for a given load state, in the cross-sections

close to the crack tip, crack propagates mainly in earlywood and in the cross-sections farther from the crack tip secondary cracks might start to propagate.
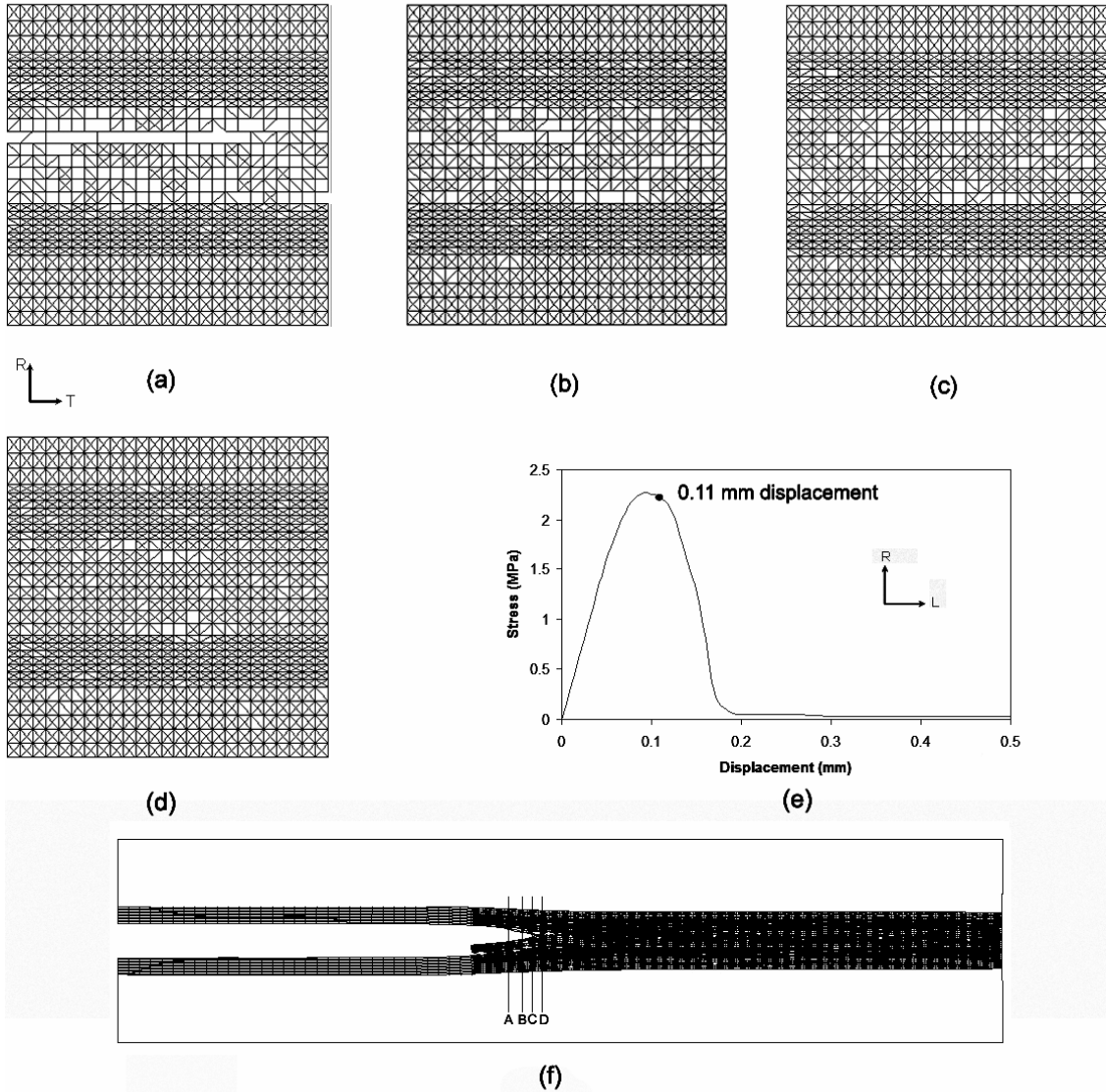
Figure 7-14 Crack pattern in the close cross-sections to the crack tip; (a), (b), (c) and (d) are the cross-sections of the lattice in different locations shown by (A), (B), (C) and (D) in the central longitudinal-section(f), for the shown fracture state in(e)

In Figure 7-15, the crack advance process in a specific cross-section (section A in Figure 7-12-a) and in different states of loading are shown. This figure shows that the initiation of the first crack and also the main separation band are in the earlywood ring. However, after the development of main crack in this cross-section (see Figure 7-15-d) the rate of failure of elements is considerably decreased.

117
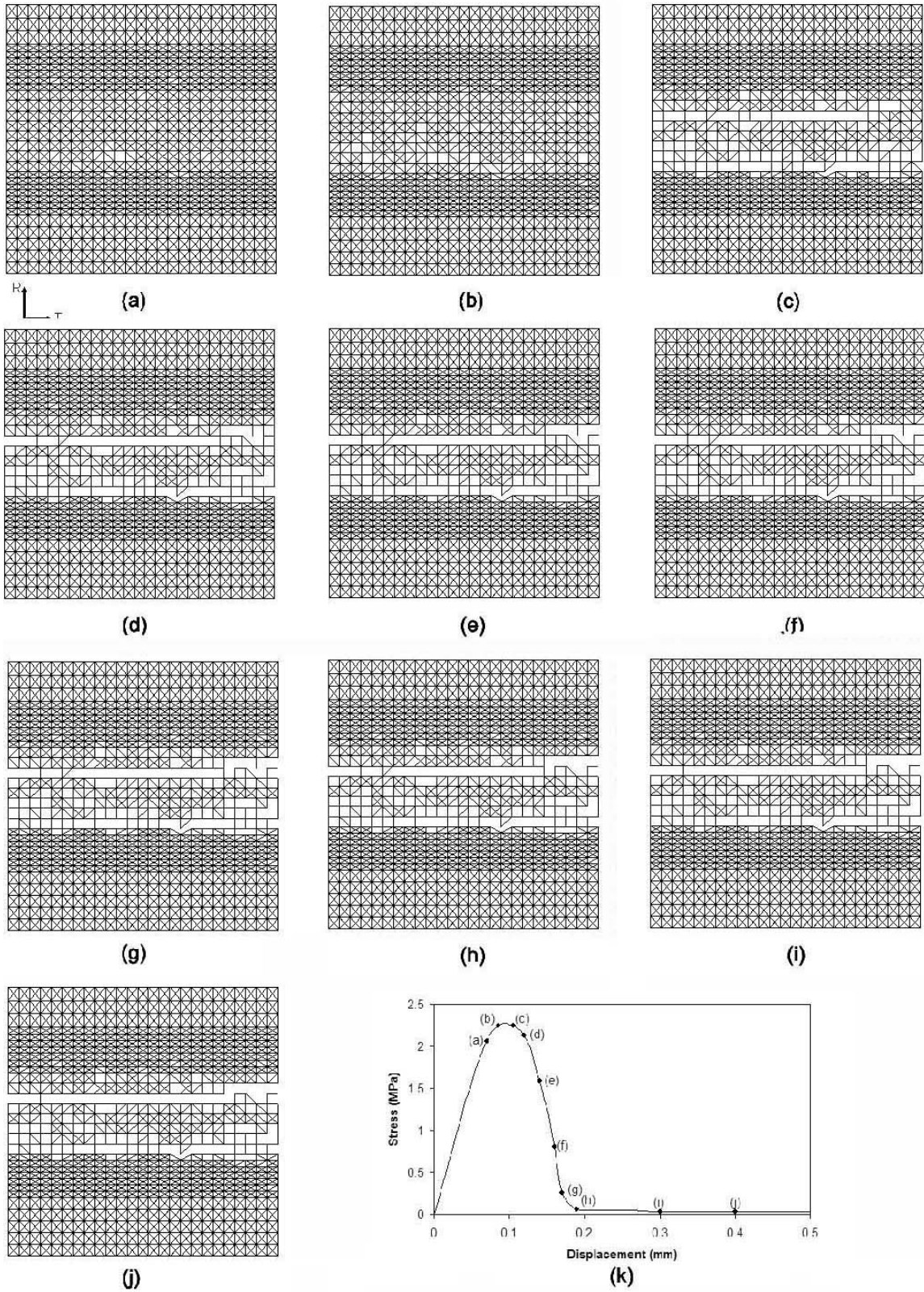
Figure 7-15 (a) to (j) crack advance in a specific cross-section (section A in Figure 7-12-a) in different loading states of fracture shown in (k)

118

Crack pattern in the lattice with a larger width:

For the main model geometry, with a lattice of 1 mm width (two latewood and three early-wood rings), the initiation of the first microcracks and the main separation band was in the earlywood ring. With this defined geometry, an earlywood ring is in front of the notch and it might be the reason of crack propagation in earlywood ring. However when the crack trajectory in the simulations of section 7.2.4 (lattice of 1.5 mm width) were studied, the same result is obtained. Crack pattern in two different geometries was studied: notched specimens of 5 x 5 x 1 mm³ (length, width, thickness), while the lattice dimensions are 3 x 1.5 x 1 mm³ in case (a) and 3 x 1 x 1 mm³ in case (b). In case (a), lattice covers three latewood and four earlywood rings while a latewood ring was in front of the notched. In Figure 7-16, geometries of two cases and the location of selected cross-section (section A and B) for investigating the crack advance process are shown.
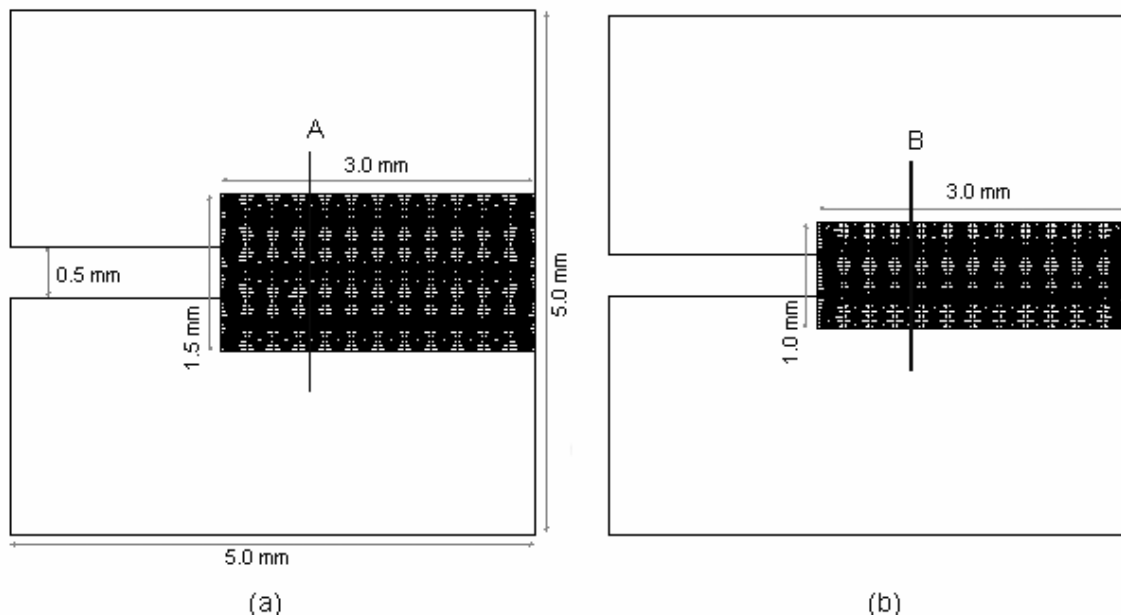
Figure 7-16 Geometry of the 5 x 5 x 1 mm³ (length, width, thickness) specimen with lattice of (a) 3 x 1.5 x 1 mm³ and (b) 3 x 1 x 1 mm³

Cross-sections (A) and (B) after 0.14 mm applied displacement are shown in Figure 7-17. In both cases, the main crack has been propagated in the earlywood ring, although in case (a), a latewood ring is in front of the notch.

Occurrence of this phenomenon; propagation of crack in Mode I, RL orientation in earlywood is confirmed by the results of CLSM observation on the fractured spruce specimens in wedge splitting tests (Job L. Navi P. 1996)
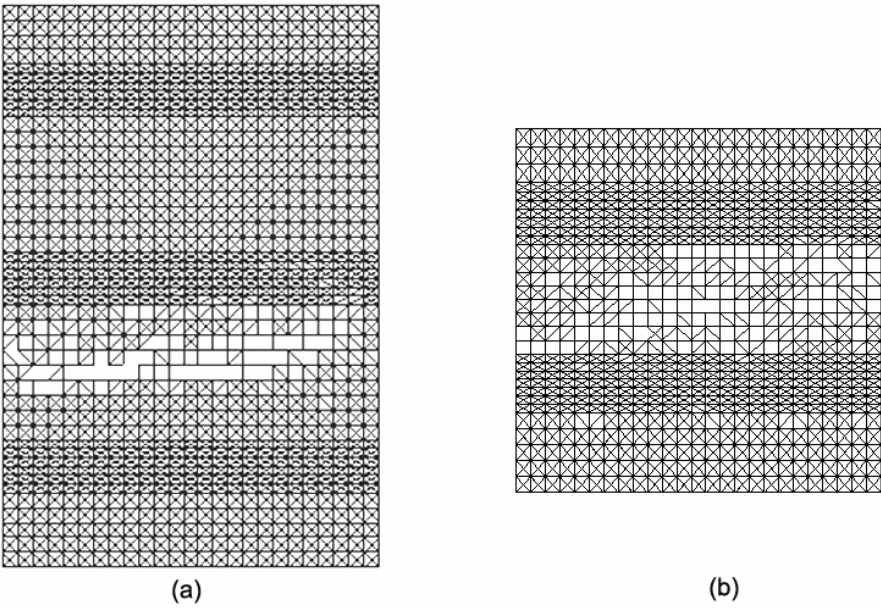
Figure 7-17 Crack pattern in the shown cross-sections in Figure 7-16, after 0.14 mm displacements, (a) cross-section (A), (a) cross-section (B)

As Figure 7-18 shows, in Mode I fracture in RL orientation, crack propagates in earlywood. Both intercellular and intracellular separations occur, although the intercellular separations are more predominant. In the presented model, as each fiber is represented by one beam element, observation of intracellular crack development is not possible.

Figure 7-18 Spruce in Mode I, RL orientation fracture test, the developed crack in *earlywood* has more intercellular form than intracellular one (Job L. Navi P. 1996)

7.3.3 Main cracks in longitudinal-section

In Figure 7-19 and Figure 7-20 the central longitudinal-section of sample in different states of crack opening are shown.

(a)

(b)

(c)

(d)

(e)

(f)
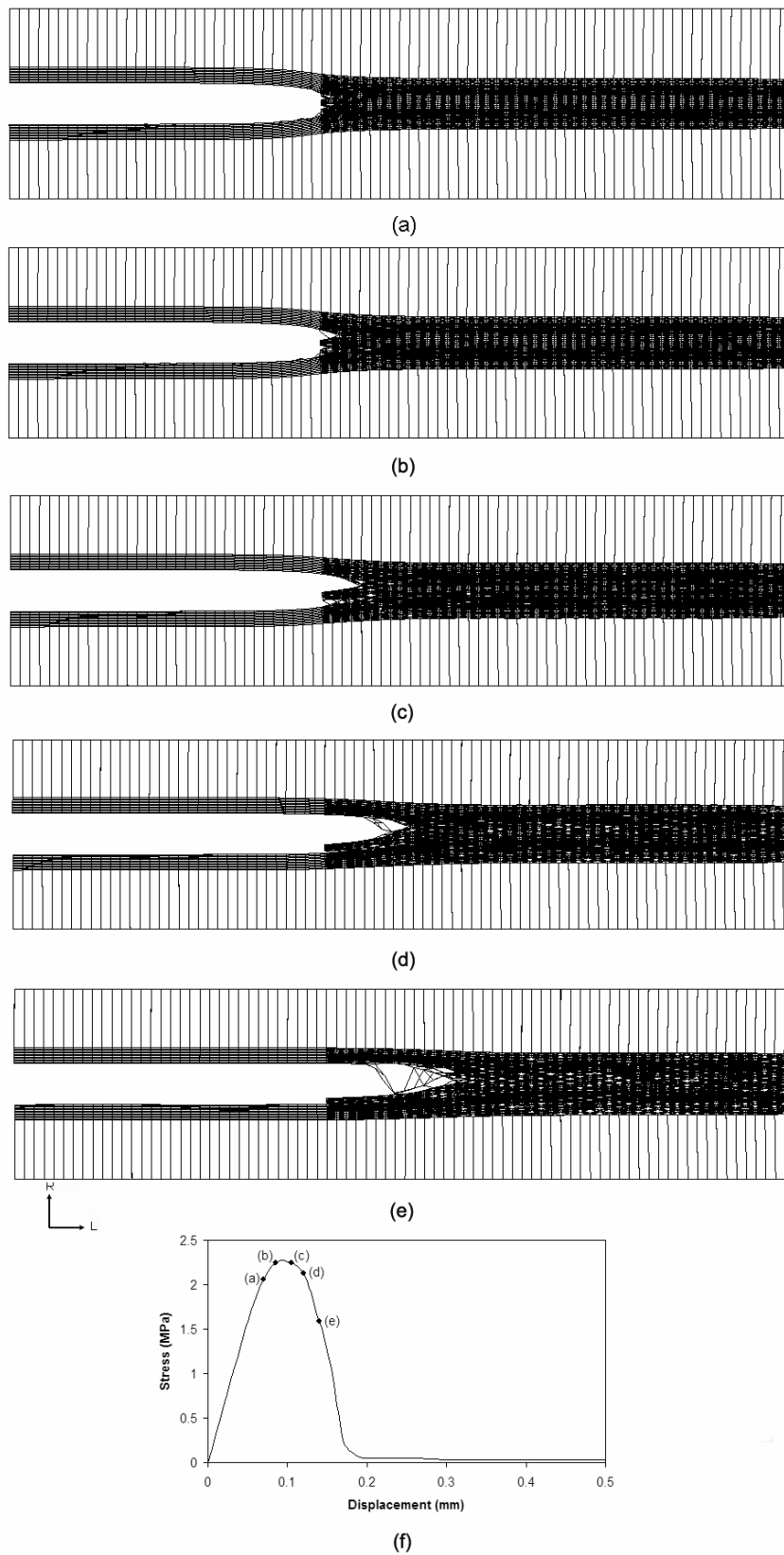
Figure 7-19(a) to (e) crack advance process in the central longitudinal-section of specimen in different loading states of fracture shown in (f)
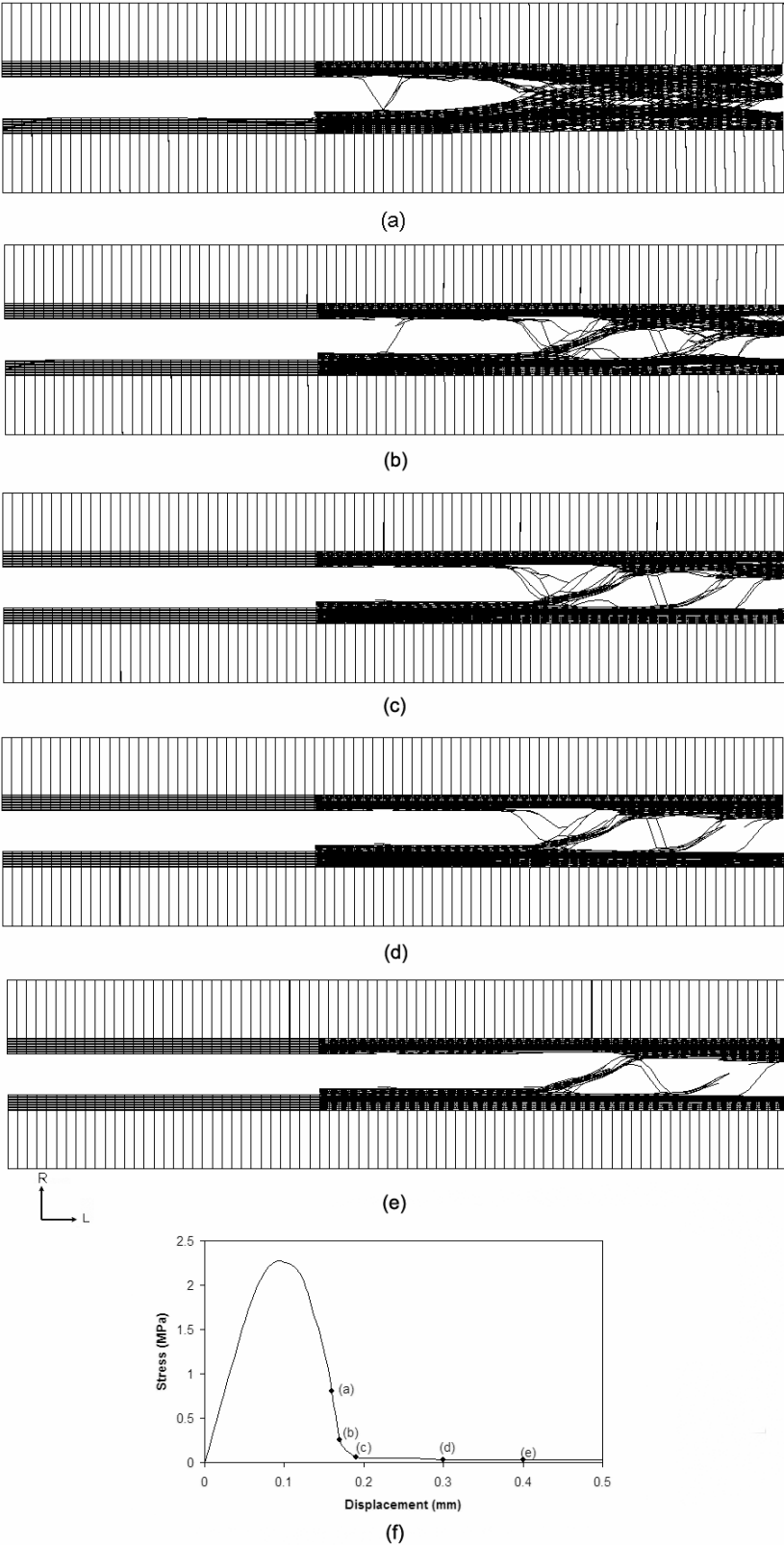
Figure 7-20 (a) to (e) Crack advance process in the central longitudinal-section of specimen in different loading states of fracture shown in (f)

122

Because of the three-dimensional structure of the lattice and the large number of elements, observation of the developed crack in the whole lattice geometry is difficult and confusing. For better visibility, cracking was monitored in the central longitudinal-section, while the elements out of the selected section are hidden (explained in section 7.3).

After the state of development of microcracks (see Figure 7-19-a), the main crack started to open and propagate through the sample (see Figure 7-19-b). As Figures 7-19-c to d show, the main crack grew until a certain state of fracture when secondary cracks started to appear (see Figure 7-19-e). As Figure 7-20-a to e show, after this state branching mechanism become the more influential mechanism of stress transferring from one part of the material to the other one until reaching to the state when specimen show a small resistance to the applied displacements (tail of softening branch in stress-displacement curve).

As in Figure 7-20, this crack is shown in the central longitudinal-section of the specimen, very few elements remain around the main crack and the branching phenomenon is not clearly visible. This phenomenon can be better observed if the whole three-dimensional fractured geometry is shown. Figure 7-21 shows the whole fractured geometry of the specimen, after 0.199 mm displacement, corresponding to the fracture state in Figure 7-20-c. The elements which still work in branching mechanism could be seen around the main crack.
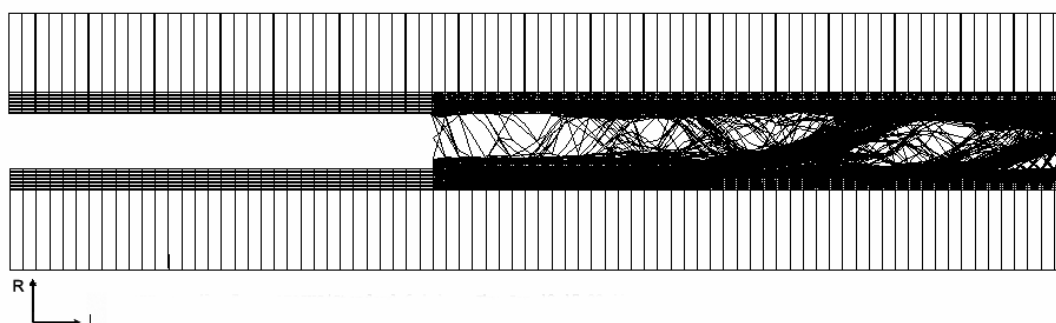
Figure 7-21 Branching phenomenon around the localized crack in whole fracture geometry

7.4 Concluding remarks

In this chapter, by using the developed model in chapter 6, the Mode I fracture of a small wood specimen in RL orientation (at fiber level) was investigated.

The obtained stress-displacement response and crack opening profile had a good agreement with the experimental results in direct tension fracture test. Detecting the crack propagation in both cross-sections and longitudinal-sections of the lattice showed that in Mode I fracture and RL orientation, the main trajectory of crack propagates in earlywood ring. The defined three-dimensional and heterogeneous structure of lattice provides the stability of simulated

fracture, agreement between the slope of the softening branches of the numerically obtained stress-displacement curves and experimental results. Fracture of the specimen in relation to different parameters was studied and model was used in characterization of the role of different parts of the defined lattice (each element set) in the fracture behavior.

The main advantages of model could be summarized as:

-Considering the main aspects of wood microstructure; heterogeneous and porous structure, in a three-dimensional model.

-Determining the non-linearity of stress-displacement curve before peak stress and giving the location of developed microcracks.

-Simulating a stable fracture test; agreeing slope of the post-peak softening branch of the stress-displacement curve with the experimental results.

-Giving the crack pattern in both longitudinal-section and cross-section in different fracture states.

These advantages make the lattice fracture model an appropriate tool for investigating the mechanism of crack propagation at micro-scale as well as other scales in a porous, heterogeneous material. This model could be modified by introducing a model geometry which shows the intracellular fracture of the cell wall in simulation. However, the dependence of the stress-displacement curves on the size of the loading step is considered as a disadvantage of lattice fracture model.

Chapter 8   Conclusions

8.1 Summary and concluding remarks

In this thesis, research concerning the mechanical and fracture behaviors of wood fibers and wood from the micromechanical point of view was undertaken. Both Experimentation and modeling tools were applied to investigate the tensile behavior of single wood fibers together with the fracture behavior of small wood specimens at the fiber level. Experiments involved studying the pattern of the distribution of cellulose microfibril angles within a wood fiber and also the tensile behavior of the single fibers by using simple and cyclic tensile tests. The aim was to investigate the behavior of single wood fibers in tension and to understand the influence of microfibril angle non-uniformities and other microstructural heterogeneities. In the modeling part, a simple micromechanical model was proposed to explain the observed non-linearity in the tensile and cyclic tensile behavior of wood fibers in relation to their heterogeneous microstructure. Also the mechanism of wood fracture at fiber level was investigated by using a three-dimensional mixed lattice-continuum model.

A study was carried out to determine the pattern of variation of MFA in different wood fibers: earlywood and latewood fibers of compression wood and normal wood by using the CLSM method. It was found that MFA is highly variable within the radial wall of earlywood fibers. Between the bordered pits, inside the border of the pits and cross-field zones are named the special zones, where MFA was found more variable. MFA in latewood fibers and tangential wall of earlywood fibers, though less than earlywood fibers, was still non-uniform. Measurements of MFA in different growth rings from pith to bark showed that MFA decreases from juvenile wood to mature wood. In compression wood fibers, the measured MFA in many cases shows a good agreement with the orientation of natural helical cavities.

The behavior of different single spruce fibers under tensile test and under cyclic tensile test was investigated. Among the different stress-strain curves, which were affected by the range of MFA non-uniformities and other defects, three different types of behaviors were recognized: linear, concave and segmented stress-strain curves. It was shown that MFA non-uniformities affect the linearity of the stress-strain curves and fibers with defects such as the cross-filed zones have considerably lower strength to failure. The obtained stress-strain curves from the cyclic tensile tests showed the force-history dependency of the fibers'

125

behavior. After a certain state of loading, wood fiber undergoes irreversible strains and the elastic limit as well as the Young's modulus of the fiber increases during tensile loading. Different positions of opening of the early crack and final failure, which were found by in-situ observation of the fiber under tensile test, showed the possibility of non-localized damage of the fiber in tension.

A micromechanical model was proposed to explain the mechanism involved in the tensile behavior of wood fibers. In this model, the influence of local degradation of the matrix (while microfibrils are assumed intact) on the longitudinal Young's modulus of the fiber wall was calculated and different probable mechanisms, which might occur during damage, were discussed. Experimental evidence, such as non-localized damage and increasing slope of the unloading-loading cycles in cyclic tensile test, led to suggestions that the reduction of MFA and multi-damaging are main governing phenomena in tensile behavior of wood fibers. Evolution of microfibrils and multi-damage were proposed, based on the fact that the microfibrils have a *helical* and *non-uniform* distribution in a wood fiber. Based on this model, the linear stress-strain domain for a fiber with non-uniform MFA is governed by the lowest force level corresponding to the highest MFA. Beyond this level, local damage initiates in the matrix of the weakest segment and allows simultaneously the local MFA to reduce. This evolution in the fiber structure is accompanied by recovery and increase of the stiffness in damaged segment and leads to the possibility of damage initiation in other weak segments and to multi-damaging phenomenon. Using this model, the experimental observations such as irreversible strains after yielding, non-localized damage, increasing slope of the loading-unloading cycles and the high slope of the stress-strain curve before failure, were explained.

A three-dimensional mixed lattice-continuum fracture model was proposed to investigate the fracture behavior of a small wood specimen taking in to account its porous and heterogeneous structure. The mixed model reduces the computational costs by modeling the less critical parts of the structure with a coarse continuum mesh while the probable crack width is modeled by lattice. This model is particularly compatible with the studied case; Mode I fracture of a notched wood specimen in RL orientation in direct tension fracture test, because the width of the cracked zone is predictable and does not exceed more than a few growth rings. The defined lattice to represent the wood material has a heterogeneous structure with alternation of earlywood and latewood fibers while the influences of other defects are introduced by a random failure limit criteria.

Results of the numerical study, pre-peak and post-peak of the obtained stress-displacement curve and also the crack opening trajectory in cross-section and longitudinal-section, have a good agreement with the experimental evidences evidence found in current literature.

Detecting the crack propagation in both cross-sections and longitudinal-sections of the lattice showed that in Mode I fracture and RL orientation, the crack propagates mainly in earlywood. The defined three-dimensional and heterogeneous structure of lattice provides the stability of simulated fracture and agreement between the slope of the softening branches of the numerically obtained stress-displacement curves and experimental results.

8.2 Future outlook

Though being commonly used, wood is still a complicated material with properties that have not been studied in detail, as is the case for other materials. Consequently, extending other developed theories and models used for materials other than wood, would accelerate steps to better understand it. This study was a preliminary step in using the micromechanical approach to wood problems which could be continued in many ways.

In the experimental part, difficulties of manipulation of the small fiber specimens did not let us perform more systematic tests. For example in tensile tests, MFAs in few points along the tested fibers were measured, while performing tensile tests on fibers with more detailed insight about the morphology of microfibrils in them is still necessary. In fact the three obtained types of stress-strain curve during tensile tests should be categorized based on more information about the variation of MFA in the fibers and other defects. Also an accurate method in order to measure the variation of local MFAs in the fibers during the tensile test should be developed.

Although the proposed model for explaining the tensile behavior of wood fibers is one of the first models that link between the heterogeneous structure of fibers and their non-linear behavior, it has many simplifying assumptions. This model should be modified by complementary assumptions such as considering a more realistic damage model (instead of the assumed isotropic damage), multilayered structure of cell walls, the influences of pits and cross-field zones and variation of properties of constituent with humidity and temperature changes. Solving this problem with finite element methods as damage and possibility of variation of MFAs in tension are considered, would be a further important step.

Developed lattice model could be used in investigating the fracture in other facture orientations. One important modification of the model is using an adaptive movable mesh for lattice to reduce the number of elements and computing costs. For this purpose, a volume with a smaller length in front of the crack tip is modeled with lattice and its position is updated across the model geometry, as the fracture advances. Microscopic observation of the cracked surface has shown that in RL crack orientation, both intercellular and intracellular separations occur, although the intercellular separation is more predominant. In the presented model, each wood fiber is represented by one beam element and the intracellular separa-

tions of the fiber cannot be shown. Other further step of the model is modifying the introduced geometry as both the intercellular separation and breaking of the cell wall during fracture process could be shown.

Bibliography

Anagnost, S., R. Mark, et al. (2005). "S-2 orientation of microfibrils in softwood tracheids and hardwood fibers." IAWA Journal 26(3): 325-338.

Anagnost, S. E., R. E. Mark, et al. (2000). "Utilization of soft-rot cavity orientation for the determination of microfibril angle. Part I." Wood and Fiber Science 32(1): 81-87.

Anagnost, S. E., R. E. Mark, et al. (2002). "Variation of microfibril angle within individual tracheids." Wood and Fiber Science 34(2): 337-349.

Ander, P. and K. Nyholm (2000). Deformation in wood and spruce pulp fibres: their importance for wood and pulp properties. International symposium on wood machining, properties of wood and wood composite related to wood machining, Vienna, Austria.

Anderson, T. L. (1994). Fracture Mechanics, CRC Press.

Andersson, S., R. Serimaa, et al. (2005). "X-ray scattering studies of thermally modified Scots pine (Pinus sylvestris L.)." Holzforschung 59 (4): 422-427.

Bailey, I. W. and M. R. Vestal (1937). "The orientation of cellulose in the secondary wall of tracheids cells." Arnold Arbo 18: 185-195.

Barnett, J. R. and V. A. Bonham (2004). "Cellulose microfibril angle in the cell wall of wood fibres." Biological Reviews 79(2): 461-472.

Batchelor, W. J., A. B. Conn, et al. (1997). "Measuring the fibril angle of fibers using confocal microscopy." Appita Journal 50: 377-380.

Bergander, A., J. Bränström, et al. (2002). "Fibril angle variability in earlywood of Norway spruce using soft rot cavities and polarization confocal microscopy." Journal of Wood Science 48(4): 255-263.

Bergander, A. and L. Salmén (2002). "Cell wall properties and their effects on the mechanical properties of fibers." Journal of Materials Science 37 (1): 151-156.

Boatright, S. W. J. and G. G. Garrett (1983). "The Effect of Microstructure and Stress State on the Fracture Behaviour of Wood." Journal of Materials Science 18(7): 2181-2199.

Bodig, J. and J. Goodman (1973). "Prediction of elastic parameters for wood." Wood Science 5(4): 249-264.

Bodig, J. and B. Jayne (1982). Mechanics of wood and wood composites. New York, USA, Van No Reinhold Company.

Bibliography

Bolander, J. E., T. Shiraishi, et al. (1996). "An adaptive procedure for fracture simulation in extensive lattice networks." Journal of Engineering Fracture Mechanics 54(3): 325-334.

Boström L. (1992). Method for determination of the softening behavior of wood and the applicability of a nonlinear fracture mechanics model., Lund, Sweden: 132.

Brändström, J., G. Daniel, et al. (2002). "Use of soft rot cavities to determine microfibril angles in wood; Advantages, disadvantages and." Holzforschung 56 (5): 468-472

Brändström J. (2001). "Micro-and ultra-structural aspects of Norway spruce tracheids, a review." LAWA Journal 22(4): 333-353.

Burgert, I., K. Fruhmann, et al. (2004). "Structure-function relationships of four compression wood types: micromechanical properties at the tissue and fibre level." Trees-Structure And Function 18(4): 480-485.

Burgert, I., K. Fruhmann, et al. (2005). "Properties of chemically and mechanically isolated fibres of spruce (Picea abies [L.] Karst.). Part 2: Twisting phenomena." Holzforschung 59(2): 247-251.

Burgert, I., N. Gierlinger, et al. (2005). "Properties of chemically and mechanically isolated fibres of spruce (Picea abies [L.] Karst.). Part 1: Structural and chemical characterisation." Holzforschung 59(2): 240-246.

Burgert, I., J. Keckes, et al. (2002). "A comparison of two techniques for wood fiber isolation-evaluation by tensile tests on single fibers with different microfibril angle." Plant Biology 4: 9-12.

Cave, I. (1978). "Modelling moisture related mechanical properties of wood-Part II, coputation of properties of a model of wood and comparison with experimental data." Wood Science and Technology 12: 127-139.

Cave, I. D. (1968). "The anisotropic elasticity of the plant cell wall." Wood Science and Technology 2(4): 268-278.

Cave, I. D. (1969). "The longitudinal young's modulus of Pinus radiata." Wood Science and Technology 3(1): 40-48.

Cho, P. C., J. Carleone, et al. (1972). "Elastic constants of layered media." Journal of Composite Materials 6: 80-93.

Cockrell, R. A. (1974). "A comparison of latewood pits, fibril orientation and shrinkage of normal and compression wood of Giant Sequoia." Wood Science and Technology 8: 197-206.

Côte, W. A. and A. C. Day (1965). Anatomy and ultrastructure of ueaction wood. WA Côte (ed) Cellular ultrastructure of woody plants. Syracuse University, N.Y.: 391-418.

Cousins, W. (1978). "Young's modulus of hemicellulose as related to moisture content." Wood Science and Technology 12: 161-167.

Cramer, S. M. and W. B. Fohrell (1990). "Method for simulating tension performance of lumber members." Journal of Structural Engineering 116(10): 2729-2747.

Cramer, S. M. and J. R. Goodman (1986). "Failure modelling : a basis for strength prediction of lumber." Wood and Fiber Science 18(3): 446-459.

Dadswell, H. and J. Nicholls (1960). "Some aspects of wood anatomy in ralation to pulping quality and tree breeding." Appita 13(5): 161-172.

Dill-Langer, G., S. Lütye, et al. (2002). "Microfracture in wood monitored by confocal laser scanning microscopy." wood science and technology 36: 487-499.

Donaldson, L. A. (1992). "Within- and between-tree variation in microfibril angle in Pinus radiata " New Zealand Journal of Forestry Science 22(1): 77-86.

El-Hosseiny, F. and D. H. Page (1973). "The measurement of fibril angle of wood fibers using polarized light." Wood Fiber 5: 208-214.

Evans, R. (1999). "A variation approach to the X-ray diffractometry estimation of microfibril angle in wood." Appita Journal 52: 283-294.

Färber, J., H. Lichtenegger, et al. (2001). "Cellulose microfibril angles in a spruce branch and mechanical implications." Journal of Materials Science 36: 5087-5092.

Fengel, D. (1969). "The ultrastructure of cellulose from wood, Part I:Wood as the basic material for the isolation of cellulose." Wood Science and Technology 3: 203-217.

Fengel, D. and M. Stoll (1973). "Variation in cell cross-sectional area, cell wall thickness and wall layers of spruce tracheids within an annual ring." Holzforschung 27: 1-7.

Fioravanti, M. and N. Sodini (2005). Personal communication. DISTAF-University of Florence-Italy.

Fratzl, P., I. Burgert, et al. (2004). "Mechanical model for the deformation of the wood cell wall." Zeitschrift Fur Metallkunde 95(7): 579-584.

Gassan, J., A. Chate, et al. (2001). "Calculation of elastic properties of natural fibers." Journal of Materials Science 36 (15): 3715-3720.

Groom, L., S. Shaler, et al. (2002). "Mechanical properties of individual southern pine fibers. part III: Global relationships between fiber properties and fiber location within an individual tree." Wood and Fiber Science 34(2): 238-250.

Harada H. (1965). "Ultrastructure and organization of gymnosperm cell walls." Côté WA Jr (ed) Cellular ultrastructure of woody plants. Syracuse University Press, Syracuse: 215-233

Harrington, J. J., R. Booker, et al. (1998). "Modeling the elastic properties of softwood. Part I: the cell-wall lamellae." Holz als Roh- und Werkstoff 56: 37-41.

Hatfielda, R. and R. Fukushimab (2005). "Can lignin be accuratly measured? ." Crop Science Society of America 45: 832-839.

Hearmon, R. (1948). The elasticity of wood and plywood. Special Report on Forest Products Research. HMSO London, No. 7: p. 87.

Bibliography

Herrmann, H., H. Hansen, et al. (1989). "Fracture of disordered, elastic lattices in two dimensions." Physical Review B 39(1): 637-648.

Hiller, C. H. (1964). "Correlation of fibril angle with wall thickness of tracheids in summerwood of slash and loblolly pine." Tappi 47(2): 125-128.

Holmberg, S., K. Persson, et al. (1999). "Nonlinear Mechanical Behaviour and Analysis of Wood and Fibre Materia." Computers and Structures 72: 459-480.

Hrennikoff, A. (1941). "Soution of problems of elasticity by the framework method." Journal of Applied Mechanics (Transactions of the ASME) 8: A169-A175.

Jakob, H., P. Fratzl, et al. (1994). "Size and arrangement of elementary cellulose fibers in wood cells- A small-angle X-ray scattering study of Picea-abies." Journal of Structural Biology 113 (1): 13-22.

Jang, H. F. (1998). "Measurement of fibril angle in wood fibres with polarization confocal microscopy." Journal of Pulp and Paper Science 24: 224-230.

Job L. Navi P. (1996). Microscopic analysis of crack propagation in softwood, model I and II. International COST 508 wood mechanics conference, Stuttgart, Germany.

Jung, H., V. Varel, et al. (1999). "Accuracy of Klason lignin and acid detergent lignin methods as assessed by bomb calorimetry." Journal of Agricultural and Food Chemistry 47(5): 2005-8.

Kachanov, L. M. (1986). Introduction to continuum damage mechanics. Dordrecht, Netherlands., Martinus Nijhoff

Keckes, J., I. Burgert, et al. (2003). "Cell-wall recovery after irreversible deformation of wood." Nature Materials 2: 810-814.

Kersavage, P. C. (1973). "Moisture content effects on tensile properties of individual Douglas-fir latewood tracheids." Wood and Fiber Science 5(2): 105-117.

Khalili, S. (1999). Microscopic studies on plant fiber structure. Department of wood science. Uppsala, Sweden, Swedish University of Agricultural Sciences: 33p.

Khalili, S., T. Nilsson, et al. (2001). "The use of rot fungi for determining the microfibrillar orientation in the S2 layer of pine tracheids." Holz als Roh- und Werkstoff 58: 439-447.

Koponen, S., T. Toratti, et al. (1989). "Modelling longitudinal elastic and shrinkage properties of wood." Wood Science and Technology 23: 55-63.

Koponen, S., T. Toratti, et al. (1991). "Modelling elastic and shrinkage properties of wood based on cell structure." Wood Science and Technology 25: 25-32.

Landis E. Davids W.G. Parrod P. Vasic S. (2003). Lattice models for wood fracture and failure. Second international conference of the European society for wood mechanics, Stockholm, Sweden.

Landis, E. N., S. Vasic, et al. (2002). "Coupled experiments and simulations of microstructural damage in wood." Experimental mechanics 42(4): 1-6.

Lichtenegger, H., A. Reiterer, et al. (1999). "Variation of cellulose microfibril angles in soft-woods and hardwoods- a possible strategy of mechanical optimization." Journal of Structural Biology 128: 257-269.

Lichtenegger, H. C., M. Müller, et al. (2003). "Microfibril angle inside and outside cross-fields of Norway spruce tracheids." Holzforschung: 13-20.

Lilliu, G. and J. VanMier (2003). "3D lattice type fracture model for concrete." Engineering Fracture Mechanics 70 (7-8): 927-941.

Lindstrom, H., J. W. Evans, et al. (1998). "Influence of cambial age and growth conditions on microfibril angle in young Norway spruce (Picea abies [L.] Karst.)." Holzforschung 52 (6): 573-581.

Macdonald, E. and J. Hubert (2002). "A review of the effects of silviculture on timber quality of Sitka spruce." Forestry 75 (2): 107-138.

Mark, R. (1967). Cell wall mechanics of tracheids. Yale University press, New Haven, Connecticut.

Mindess, S. and A. Bentur (1986). "Crack propagation in notched wood specimens with different grain orientations." Wood Science and Technology 20: 145-155.

Monaghan, D., I. Doherty, et al. (1998). Coupling 1D beams to 3D bodies. Sandia National Laboratory, 7 th International Meshing Roundtable, Dearborn, Michigan.

Mott, L., L. Groom, et al. (2002). "Mechanical Properties of Individual Southern Pine Fibers. Part II. Comparison of Earlywood and Latewood Fibers with Respect to Tree Height and Juvenility." Wood and Fiber Science 34(2): 221-237.

Mott, L., S. Shaler, et al. (1995). "The tensile testing of individual wood fibers using environmental scanning electron microscopy and video image." Tappi 78(5): 143-148.

Navi, P. (1998). The influence of microfibril angle on wood cell and wood mechanical properties, experimental and numerical study. IAWA/IUFRO, Microfibril angle in wood, New Zealand.

Navi, P. (2005). Comportement thermo-hydromécanique du bois. Lausanne, Presses polytechniques et universitaires romandes.

Navi, P. and C. Huet (1989). A three dimensional multilevel technique to study influence of the fiber microstructure on wood macroscopic elastic properties. Mechanics of Cellulosic and Polymeric Materials, New York, The American Society of Mechanical Engineers.

Navi, P., V. Pittet, et al. (2002). "Transient moisture effects on wood creep." Wood Science and Technology 36: 447–462.

Navi, P., P. Rastogi, et al. (1995). "Micromechanics of wood subjected to axial tension." Wood Science and Technology 29: 411-429.

Navi, P. and M. Sedighi-Gilani (2004). Modelling the influences of microfibril angles and natural defects on the force-extension behavior of single wood fibers. COST E20 book U. Schmitt, P. Ander, J. R. Barnettet al: 57-70.

133

Bibliography

Navi, P. and M. Sedighi-Gilani (2006). Mode I crack propagation in softwood, microanalyses and modeling. . 16th European conference of fracture, Greece.

Nishino, T., K. Takano, et al. (1995). "Elastic modulus of the crystalline regions of cellulose polymorphs." Journal of Polymer Science Part B- Polymer Physics 33(11): 1647-1651.

Nyholm, K., P. Ander, et al. (2001). "Dislocation in pulp fibers, their origin characteristic and importance-a review." Nordic Pulp Paper Research Journal 16: 376-384.

Page, D., F. EL-Hosseiny, et al. (1977). "Elastic modulus of single wood pulp fibers." Tappi 60: 114-117.

Page, D. H. (1969). "A method for determining the fibrillar angle in wood tracheids." Journal of Microscopy 90: 137-143.

Page, D. H. and F. El-Hosseiny (1983). "The mechanical properties of single wood pulp fibers. Part VI. Fibril angle and the shape of stress-strain curve." Journal of Pulp and Paper Science 9: 99-100.

Perez, L., V. Pittet, et al. (2000). Fiber behavior under tensile force, experimentation and modeling. International conference of wood and wood fiber composites, Stuttgart, Germany.

Persson, K. (2000). Micromechanical modeling of wood and wood fiber properties. department of mechanics and materials, structural mechanics, LUND University-Sweden: 223.

Peter, G. F., D. M. Benton, et al. (2003). "A simple, direct method for measurement of microfibril angle in single fibres using differential interference contrast microscopy." Journal of Pulp and Paper Science 29 (8): 274-280.

Peura, M., M. Muller, et al. (2005). "Structural studies of single wood cell walls by synchrotron X-ray microdiffraction and polarised light microscopy." Nuclear instruments and methods in physics research section B-Beam Interactions with materials and atoms 238((1-4)): 16-20

Plummer, C., V. Pittet, et al. (2002). Transient moisture effects on wood creep, molecular dynamics. Fist international conference of the European society for wood mechanics, Lausanne, Switzerland.

Prado, E. P. and J. G. M. VanMier (2003). "Effect of particle structure on mode I fracture process in concrete." Engineering Fracture Mechanics 70(14): 1793-1807.

Reiterer, A., H. Jakob, et al. (1998). "Spiral angle of elementary cellulose fibrils in cell walls of Picea abies determined by small-angle X-ray scattering " Wood Science and Technology 32(5): 335-345.

Sahlberg, U., L. Salmen, et al. (1997). "The fibrillar orientation in the S2-layer of wood fibres as determined by x-ray diffraction analysis " Wood Science and Technology 31(2): 77-86.
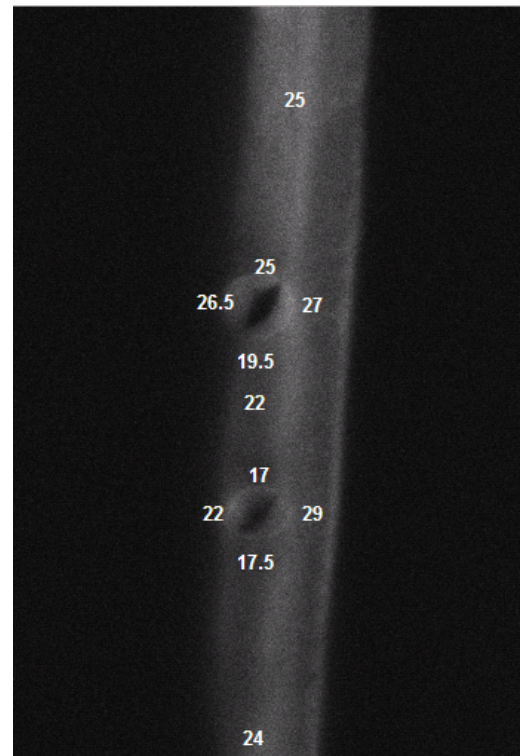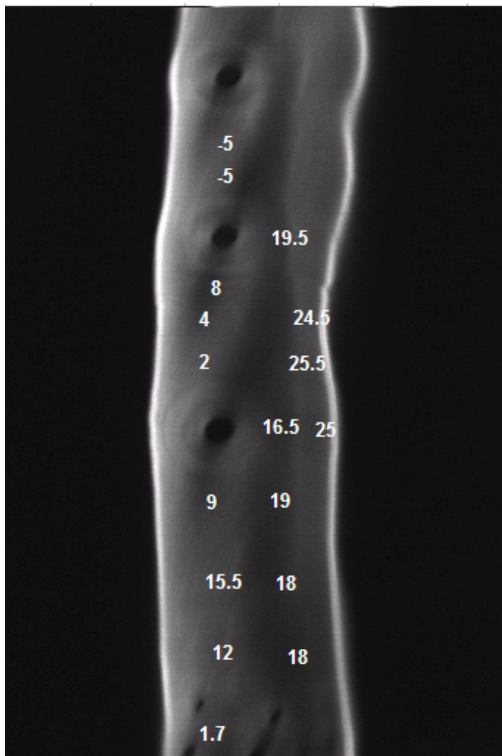
Sakurada, I., Y. Nukushina, et al. (1962). "Experimental determination of the elastic modulus of the crystalline region of oriented polymers." Journal of Polymer Science 57: 651-660.

Salmén, L. and A. de-Ruvo (1985). "A model for the prediction of fiber elasticity." Wood and Fiber Science 17(3): 336-350.

Salmén, L., P. Kolseth, et al. (1986). "Modelling of small strain properties and environmental effects on paper and cellulosic fibers." Composite Systems from Natural and Synthetic Polymers: 211-223.

Schlangen, E. (1993). Experimental and numerical analysis of fracture processes in concrete. Delft university of technology.

Schlangen, E. and E. J. Garboczi (1997). "Fracture simulations of concrete using lattice models : computational aspects." Engineering Fracture Mechanics 57(2/3): 319-332.

Schlangen, E. and E. J. Garboczi (1997). "Fracture simulations of concrete using lattice models: Computational aspects." Engineering Fracture Mechanics 57(2-3): 319-332.

Schlangen E. Garboczi E.J. (1996). "New method for simulating fracture using an elastically uniform random geometry lattice." International journal of engineering science 34(10): 1131-1144.

Schlangen E. Van Mier J.G.M. (1992). "Simple lattice model for numerical simulatiuon of fracture of concrete materials and structures." Materials and Structures 25: 534-542.

Schniewind, A. P. and J. D. Barrett (1969). "Cell wall model with complete shear restraint." wood fibre 1(3): 205-214.

Sedighi-Gilani, M. and P. Navi (2004). Influence of local variation of microfibril angle on tensile behavior of individual wood fibers. . Wood Machining conference, Vienna, Austria

Sedighi-Gilani, M. and P. Navi (2004). Influence of wood fibers morphology on their nonlinear behavior in axial tension. Third international conference of the European society for wood mechanics, Vila Real, Portugal.

Sedighi-Gilani, M. and P. Navi (in press). "Experimental observations and micromechanical modeling of successive-damaging phenomenon in wood cells tensile behavior." Accepted to be publishes in Wood Science and Technology.

Sedighi-Gilani, M., P. Pittet, et al. (2003). Modeling the wood fibers behavior under tensile force. Second international conference of the European society for wood mechanics, Stockholm, Sweden.

Sedighi-Gilani, M., H. Sunderland, et al. (2005). "Microfibril angle non-uniformities within normal and compression wood tracheids " Wood Science and Technology 39(6): 419-430

Sedighi-Gilani, M., H. Sunderland, et al. (2006). "Within-fiber nonuniformities of microfibril angle." Wood and Fiber Science 38(1): 132-138
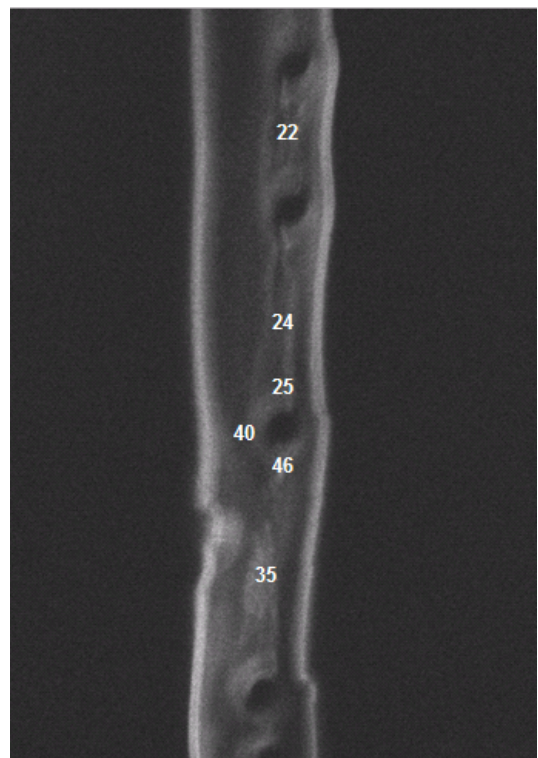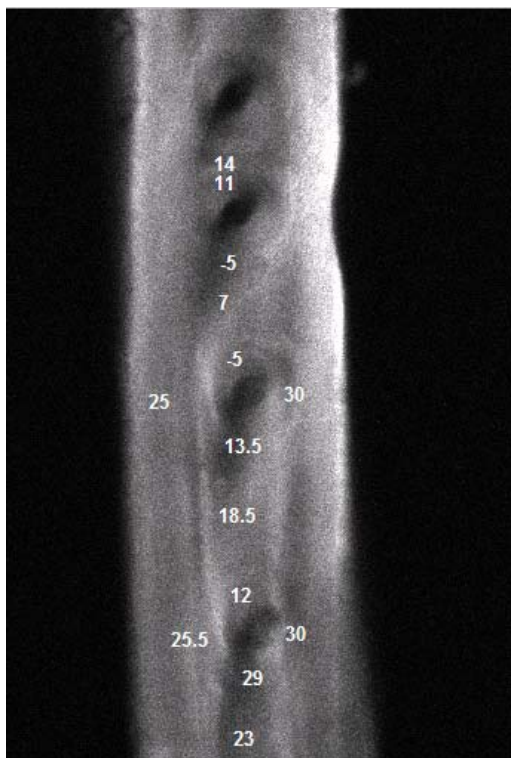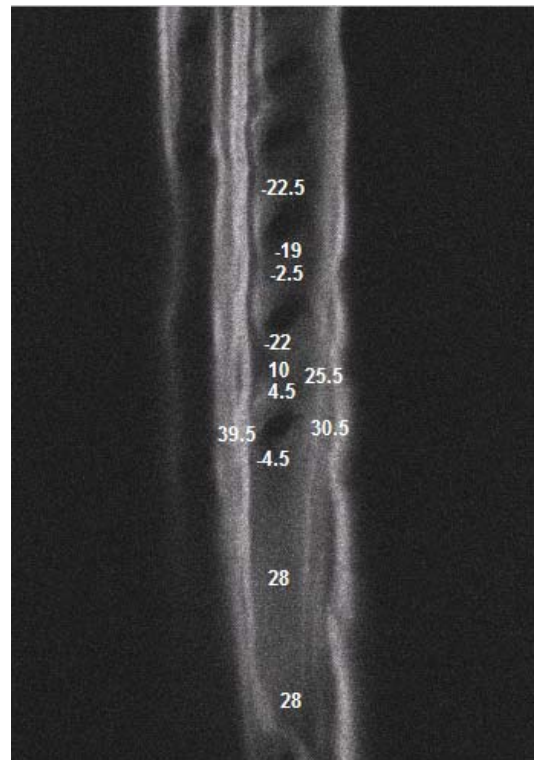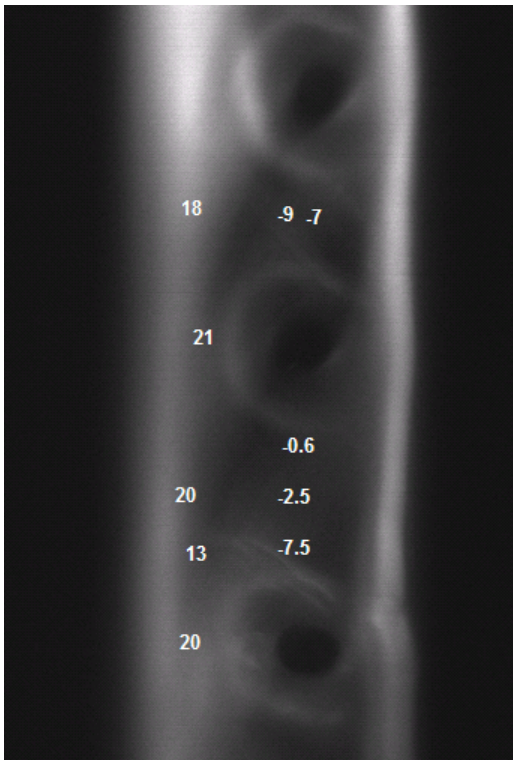
Bibliography

Senft, J. F. and A. B. Bendtsen (1985). "Measuring microfibrillar angles using light micros- copy." Wood and Fiber 17: 564-567.

Tappi (1998). Acid-insoluble lignin in wood and pulp. Technical Association of the Pulp and Paper Industry: T222 om-98.

Tashiro, K. and M. Kobayashi (1991). "Theoretical evaluation of three-dimensional elastic constants of native and regenerated cellulose." Polymer 32(8): 1516-1526.

Timell, T. (1978). "Ultrastructure of compression wood in Ginkgo biloba." Wood Science and Technology 12: 89.

Timell, T. (1983). "Origin and evolution of compression wood." Holzforschung(37): 1-10.

Tsai, S. (1992). Theory of composites design. USA, Think composites.

VanMier, J. G. (1996). Fracture Processes of Concrete: Assessment of Material Parameters for Fracture Models CRC Press.

VanVliet, M. R. A. (2000). Size effect in tensile fracture of concrete and rock. Delft University Press: 192

Vasic S. (2000). Applications of fracture mechanics to wood. Fredericton, N.B. Canada, University of New Brunswick.

Vasic S. Smith I. Landis E. (2002). "Fracture zone characterization- Micro- Mechanical study." wood and fiber science 34(1): 42-56.

Wang, H. H., J. G. Drummond, et al. (2001). "An improved fibril angle measurement method for wood fibers." Wood Science and Technology 34: 493-503.

Wang, J. (1994). Development and application of a micromechanics-based numerical ap- proach for the study of crack propagation in concrete, EPFL.

Wangaard, F. F. (1979). Wood : its structure and properties. Pennsylvania State University.

Wild, P. M., J. W. Provan, et al. (1999). "The effects of cyclic axial loading of single wood pulp fibers at elevated temperature and humidity." Tappi 82(4): 209-215.

Wittel, F., G. Dill-Langer, et al. (2005). "Modelling of damage evolution in soft-wood perpen- dicular to grain by means of a discrete element approach." Computational Materials Science 32: 594-603.

Yoshizawa, N. and T. Ideia (1987). "Some structural and evolutionary aspects of compres- sion wood tracheids." Wood and Fiber Science 19(4): 343-352.
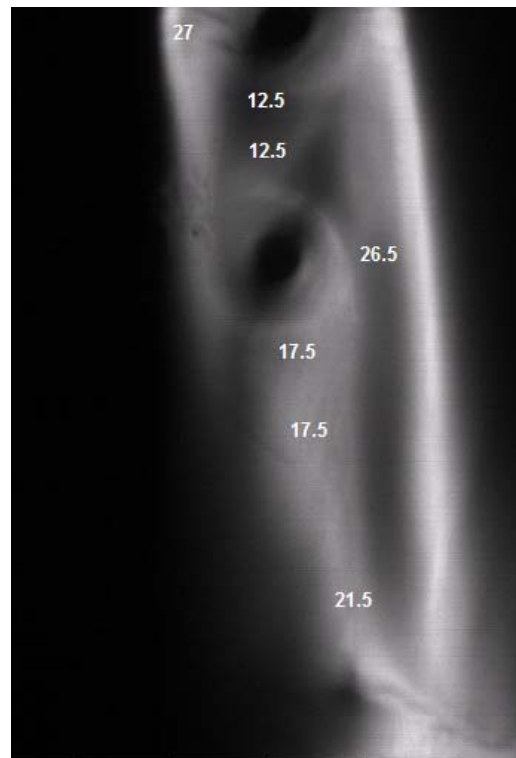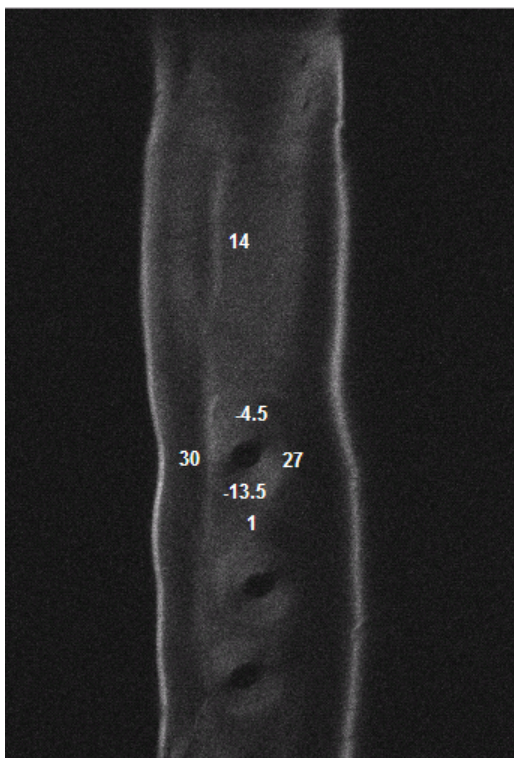
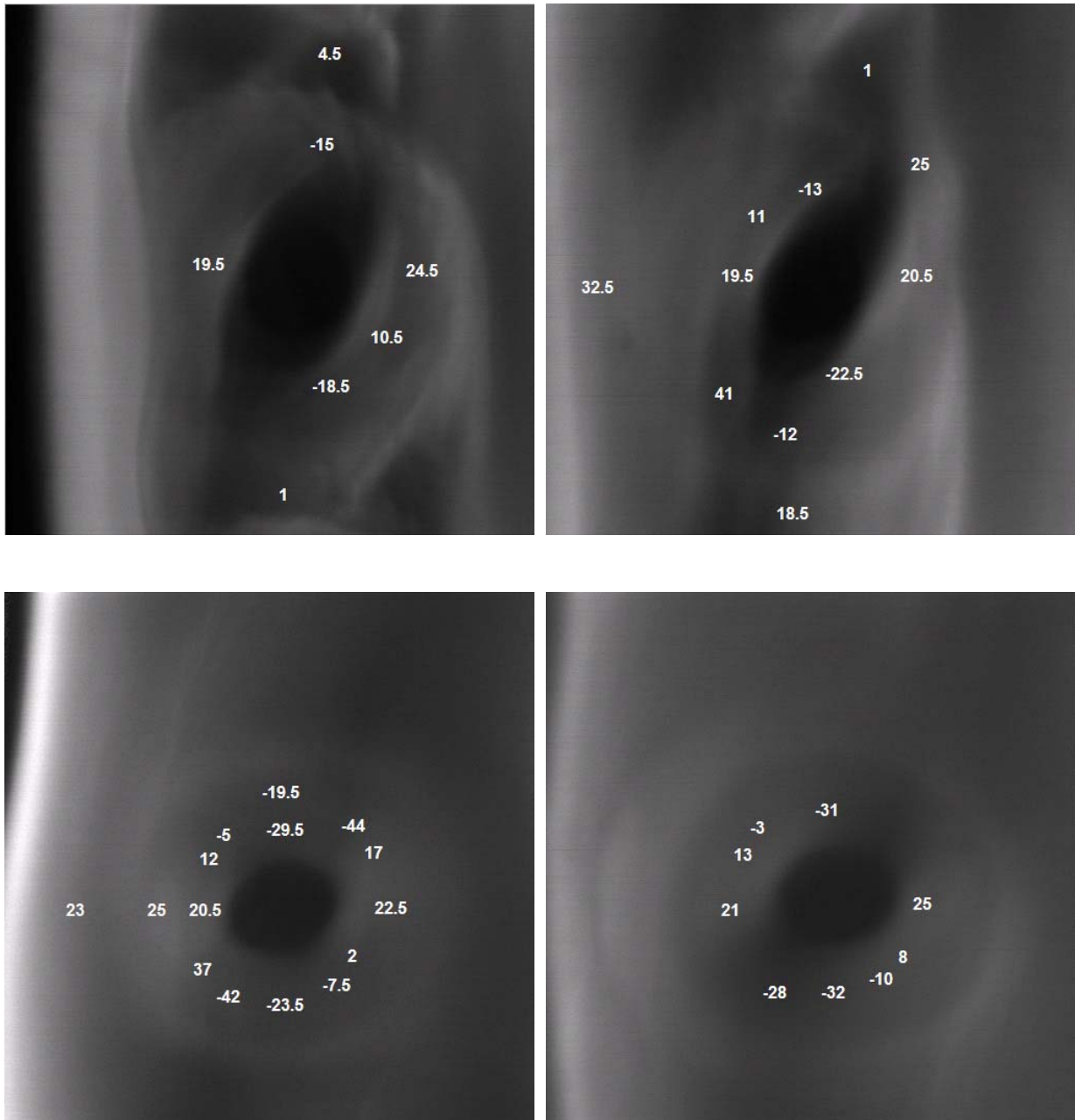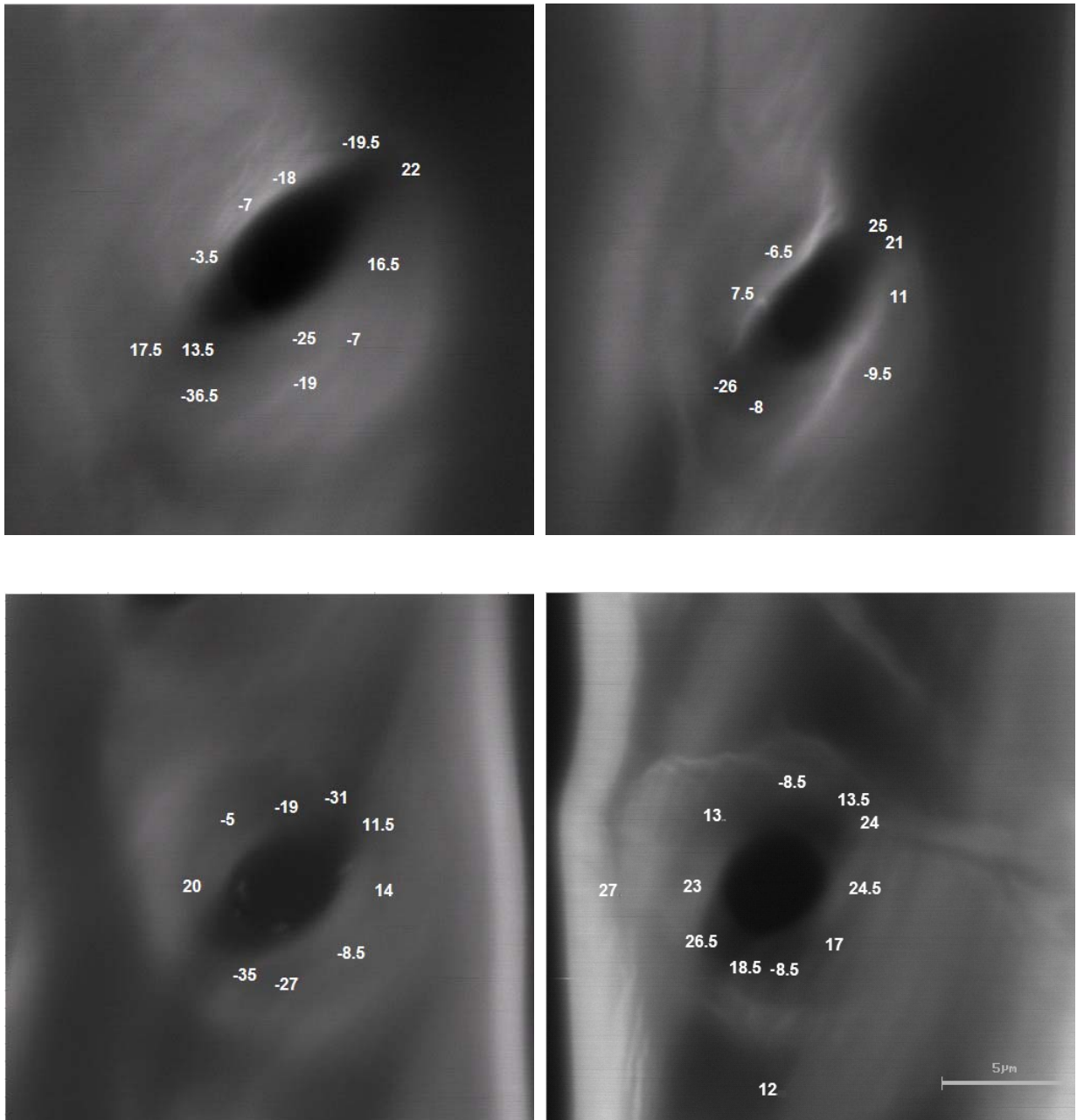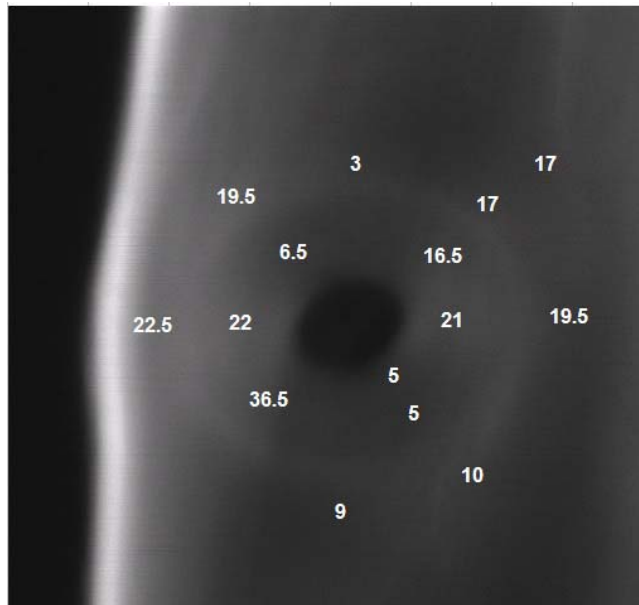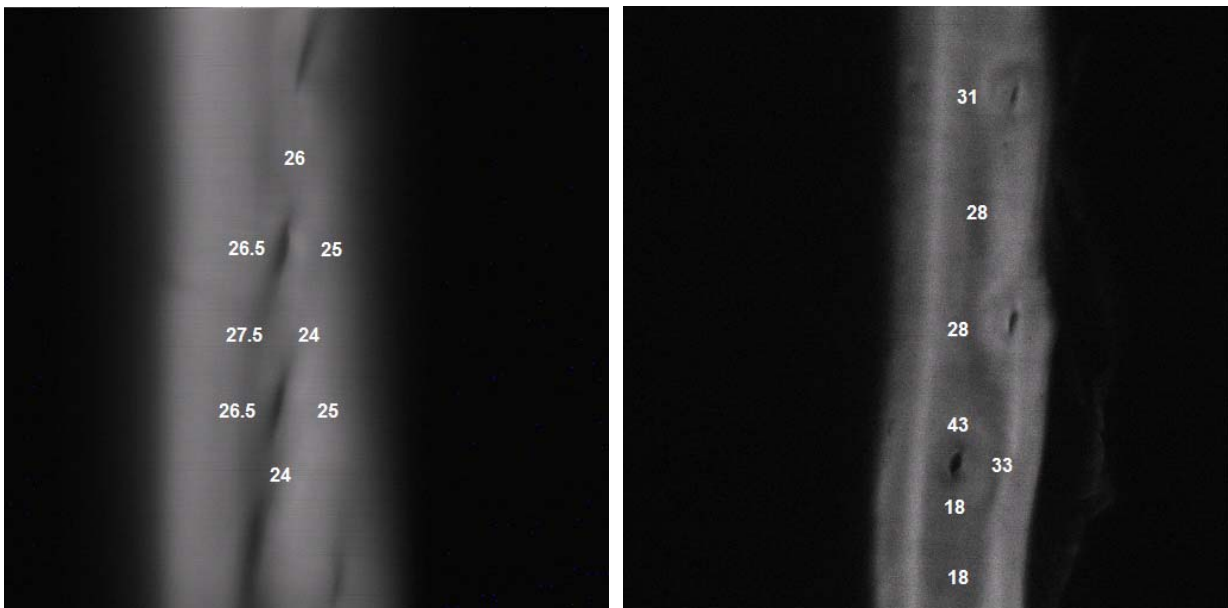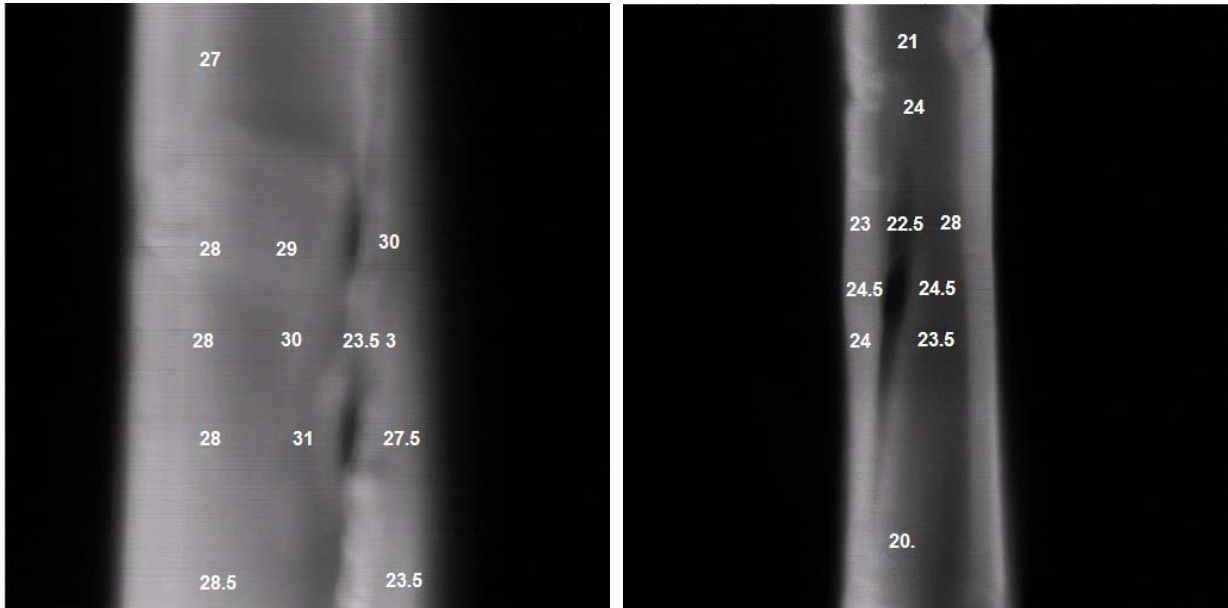# Appendix A

MFA variation in earlywood tracheids:

MFA variation in earlywood tracheids, inside the border of bordered pits:
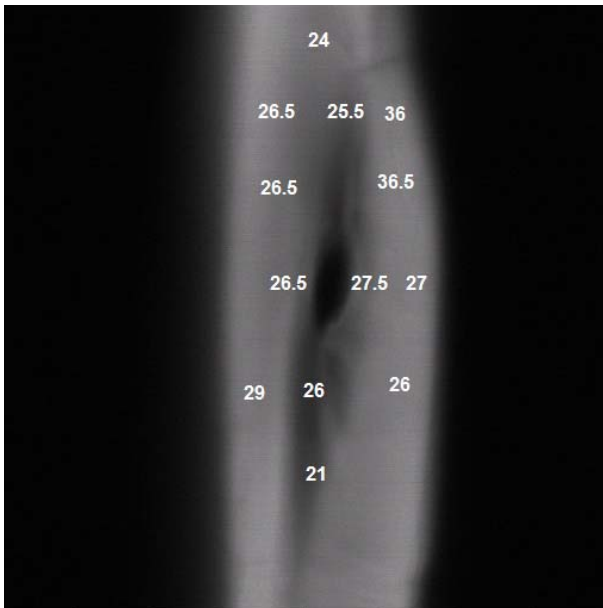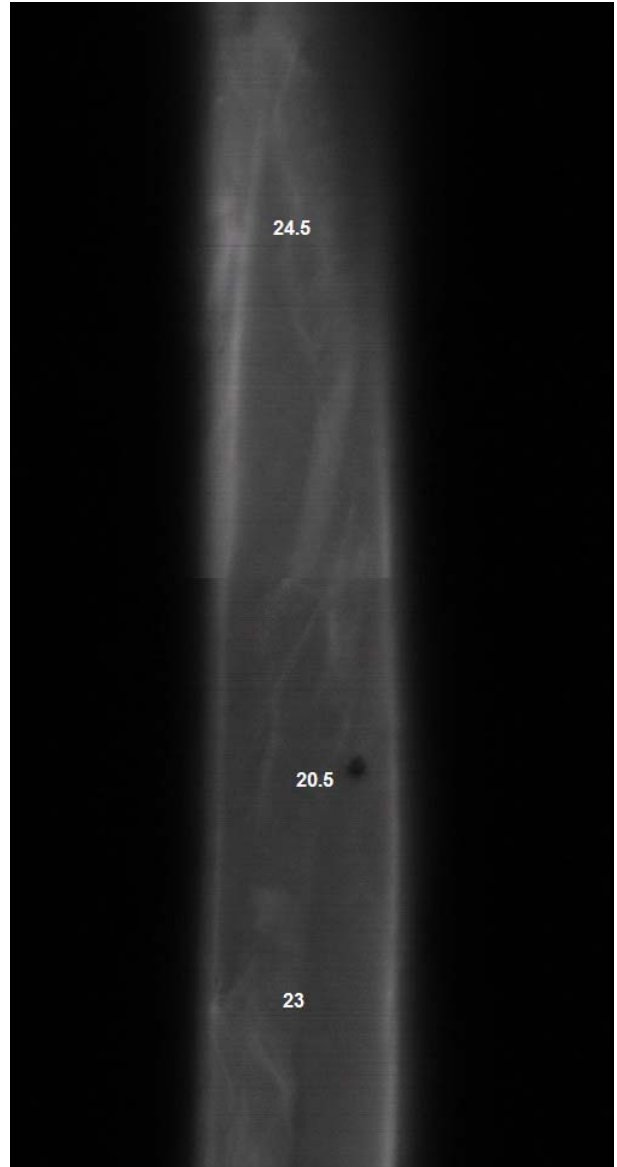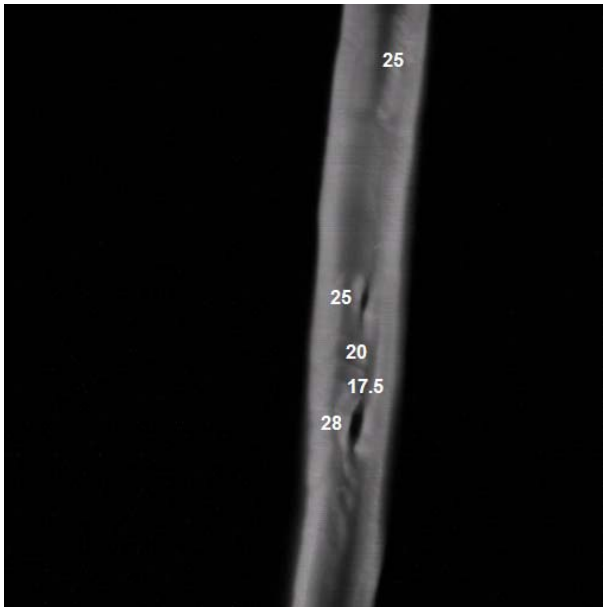
MFA variation in latewood tracheids:

Appendix B

MATLAB program for utilization of the developed formulation by Cho *et al (*1972) in calculating the elasticity matrix of the fiber wall from the elasticity matrices of its constituents:

```
clear
C(:,:,1)=[150.516 3.0103 3.0103 0 0 0;3.0103 23.393 11.727 0 0 0;3.0103 11.727 23.393 0 0 0;0 0 0 4.5 0 0;0 0 0 0 4.5 0;0 0 0 0 0 5.833];
C(:,:,2)=[18.876 3.146 3.146 0 0 0;3.146 4.691 2.191 0 0 0;3.146 2.191 4.691 0 0 0;0 0 0 1.5 0 0;0 0 0 0 1.5 0;0 0 0 0 0 1.25];
C(:,:,3)=[4.074 2.006 2.006 0 0 0;2.006 4.074 2.006 0 0 0;2.006 2.006 4.074 0 0 0;0 0 0 2.696 0 0;0 0 0 0 2.696 0;0 0 0 0 0 2.696];
V=[.445 .316 .239];
for i=[1,2,3,6]
   for j=[1,2,3,6]
     D(i,j) = 0;
     for k=1:3
       a = 0;
       for l=1:3
         a = a + V(l)*C(3,j,l)/C(3,3,l);
       end
       b = 0;
       for l=1:3
         b = b + V(l)/C(3,3,l);
       end
       D(i,j) = D(i,j) + V(k)*(C(i,j,k) - C(i,3,k)*C(3,j,k)/C(3,3,k) + C(i,3,k) * a/ (C(3,3,k)*b));
     end
   end
end

for i=4:5
   for j=4:5
     a = 0;
```

```
    for k=1:3
      a = a + V(k)*C(i,j,k)/det([C(4,4,k) C(4,5,k); C(5,4,k) C(5,5,k)]);
    end
    b = 0;
    for k=1:3
      for l=1:3
        b = b + V(k)*V(l)*(C(4,4,k)*C(5,5,l)-C(4,5,k)*C(5,4,l))/(det([C(4,4,k)  C(4,5,k);  C(5,4,k)
C(5,5,k)])*det([C(4,4,l) C(4,5,l); C(5,4,l) C(5,5,l)]));
      end
    end
    D(i,j) = a / b;
  end
end
```

Curriculum Vitae

Personal information

Name: Marjan Sedighi-Gilani

Date of birth: 24 December 1973

Place of birth: Tehran, Iran

Marital status: Married

Education

- 2002-2006: Ecole polytechnique fédéral de Lausanne (EPFL), Switzerland

Research Assistant and PhD Candidate in the laboratory of constructions materials

- 1997-2000: University of Tehran, Tehran, Iran

Master of Science in Civil Engineering, marine structures

Thesis: Analytical solution for stress and pore pressure distribution in a cross-anisotropic and multi-layer seabed

- 1992-1996: University of Tehran, Tehran, Iran

Bachelor of Science in Civil Engineering

Consulting and academic experiences

- 2002-2006: Laboratory of constructions materials in EPFL, Switzerland, Research assistant
- 1997-2002: Mahab-Ghods Consulting Engineering, Iran, Hydraulic structures engineer
- 1996-1997: Mandro Consulting Engineering, Iran, Soil mechanics engineer

Journal Publications and Book Articles

1. *Within-fiber nonuniformities of microfibril angle*, M. Sedighi-Gilani, H. Sunderland, P. Navi, Published in journal of wood and fiber science, 38 (1): 2006

2. *Microfibril angle nonuniformities within normal and compression wood tracheids*, M. Sedighi-Gilani, P. Navi, Published in Wood Science and Technology, 39 (6): 419-430 2005

3. *Modeling the influences of microfibril angles and natural defects on the force-extension behavior of single wood fibers*, P. Navi, M. Sedighi-Gilani, Published in COST Action E20 book, wood fiber cell wall structure 2004

4. *Experimental observations and micromechanical modeling of successive-damaging phenomenon in wood cells tensile behavior*, M. Sedighi-Gilani, P. Navi, Accepted for publication in Wood Science and Technology

5. *Three-dimensional modeling of wood fracture in mode I, parallel to the grain direction, at fiber level*, M. Sedighi-Gilani, L. Job, P. Navi, Accepted for publication in Wood Material Science and Engineering

Conferences and workshops

1. *Mode I crack propagation in softwood, microanalyses and modeling*, P. Navi, M. Sedighi-Gilani, Accepted to be published in 16th European conference of fracture, Greece, 2006

2. *Study of tensile behavior of single spruce fibers in tension by experiments and modeling*, M. Sedighi-Gilani, P. Navi, third international conference of the European society for wood mechanics, Vila Real, Portugal, 2004

3. *Influence of local variation of microfibril angle on tensile behavior of individual wood fibers*, M. Sedighi-Gilani, P. Navi, Wood Machining conference, Vienna, Austria, 2004

4. *Modeling of fibers behavior under tensile force,* M. Sedighi-Gilani, V. Pittet, P. Navi, second international conference of the European society for wood mechanics, Sweden, 2003

5. *Influences of microfibril angles and natural defects on the force-extension behavior of single wood fibers modeling*, M. Sedighi-Gilani, P. Navi, final workshop in building a cell wall E20, Helsinki, Finland, 2003

6. *Analytical solution for stress and pore pressure distribution in a cross-anisotropic and multi-layer seabed,* B. Gatmiri, M. Sedighi-Gilani, XVth international conference on soil mechanics and geotechnical engineering, 3, 2001